

UCLA

UCLA Electronic Theses and Dissertations

Title

A Disturbance Attenuation Controller Adaptive through a Nonlinear Modified Gain Observer

Permalink

<https://escholarship.org/uc/item/0cq3v08h>

Author

huang, wei

Publication Date

2021

Peer reviewed|Thesis/dissertation

UNIVERSITY OF CALIFORNIA
Los Angeles
Mechanical and Aerospace Engineering
Systems and Control

A Disturbance Attenuation Controller
Adaptive through a Nonlinear Modified Gain Observer

A dissertation submitted in partial satisfaction
of the requirements for the degree
Doctor of Philosophy in Mechanical Engineering

by

Wei Huang

2021

© Copyright by

Wei Huang

2021

ABSTRACT OF THE DISSERTATION

A Disturbance Attenuation Controller
Adaptive through a Nonlinear Modified Gain Observer
for
an Air Breathing Hypersonic Vehicle

by

Wei Huang

Doctor of Philosophy in Mechanical Engineering

University of California, Los Angeles, 2021

Professor Jason L. Speyer, Chair

This paper presents an adaptive robust control strategy for a class of uncertain linear systems with disturbance input. The uncertain linear system contains unknown parameters in both the system and the input matrices. The system makes perfect partial measurement of the state. A disturbance attenuation function is transformed into a minimax differential game where the disturbance and the unknown parameters act as the cooperative players that maximize the cost function, whereas the controller is the opposing player that minimizes the cost function. Having shown the existence of a saddle point in the cost function, the optimization yields a minimax controller coupled with a stable nonlinear modified gain observer, which estimates the state and the unknown parameters. By maximizing the cost function with respect to the uncertain parameters, the minimax controller takes the parameter estimation confidence level into account to generate the worst case input for a given instance of time. This leads to two sets of Riccati equations, one for the controller and one for the observer.

In this class of parameter estimation problem, the measurement function and the augmented system, which is composed of the state and the uncertain parameters, are modifiable functions or can be transformed into modifiable functions using an appropriate change of coordinate system, such as the observable canonical form. The essence of a modifiable function is that although the observer dynamics are nonlinear, the error in the observer's estimation error is linear. The existence of the saddle point in the performance index is presented. Under certain conditions, such as the observability and controllability of the system, the existence of the solution to the two Riccati equation and finiteness of the value function, the close loop system is stable and the estimation error is bounded, which demonstrates the disturbance attenuation properties of the observer.

We present an unstable single-input single-output (SISO) four state vector case example with four unknown system parameters, subject to worst case disturbance. The simulation demonstrates the applicability of the disturbance attenuation controller coupled with the nonlinear modified gain observer, and assess its performance against the linear quadratic regulator (LQR) coupled with a modified gain extended Kalman observer (MGEKO).

Furthermore, the derived disturbance attenuation controller is applied to an air breathing hypersonic flight vehicle with full state measurement. The nonlinear longitudinal dynamics of the aircraft, which is subject to large aerodynamic uncertainty, is linearized around a nominal trim condition to derive a nominal linearized perturbation model. The nonlinear modified gain observer estimates four system parameters to yield an estimated linearized perturbation model and the corresponding estimation error weightings for the worst case controller. The simulation result demonstrates the applicability of the worst case controller coupled with the nonlinear modified gain observer and its superior performance when compared against the Sum-of-Squares method shown in the previous literature.

The dissertation of Wei Huang is approved.

Tetsuya Iwasaki

James S. Gibson

Panagiotis D. Christofides

Jason L. Speyer, Committee Chair

University of California, Los Angeles

2021

To my beloved parents and my forever cheerful sister.

Contents

List of Figures	viii
List of Tables	x
1 Introduction	1
1.1 Robust Control	2
1.2 Adaptive Control	3
1.3 Dual Control	4
1.4 Background to the Current Research	5
1.5 Overview of the Current Research and Dissertation Layout	8
2 Disturbance Attenuation Control Adaptive Through a Modified Gain Observer	12
2.1 Problem Formulation	12
2.2 Performance Index	14
2.3 Dynamic Programming Solution	16
2.4 The Optimal Return Function	17
2.5 Modified Gain H_∞ Observer	19
2.6 The Connection Condition	26
3 Existence of Saddle-Point	30
4 Infinite-Time Problem: Stability of Close-Loop System	34

5	A Case Study: A Modifiable Nonlinear SISO Example	46
5.0.1	Application of the Modified Gain Observer	52
5.0.2	Application of Worst Case Control	54
5.0.3	Simulation Setup	55
5.0.4	Result	60
6	Application to Autonomous Hypersonic Flight Cruise Control	67
6.1	Background	68
6.2	Autonomous Hypersonic Flight Cruise Control	70
6.2.1	Aerodynamics of Hypersonic Flight	71
6.2.2	Simulation Setup	74
6.3	Linearization of the Nonlinear Longitudinal Dynamics	75
6.4	Defining the Augmented System and Weightings for Worst Case Controller	83
6.5	Simulation Result	85
6.5.1	Future Work	88
7	Conclusion and Future Work	95
	Bibliography	97

List of Figures

5.1	x_o , \hat{x}_o and x_o^* plots using disturbance attenuating controller (solid lines). x_o and \hat{x}_o plots using LQR controller (dash lines). The disturbance attenuation controller yields better performance than the LQR controller.	58
5.2	Various types of state estimation errors for both control algorithms.	59
5.3	Parameter estimates from nonlinear modified gain observer and MGEKO.	61
5.4	Worst case parameter estimation error.	62
5.5	Control gain and input for worst case control and LQR.	64
6.1	True state x , state estimate \hat{x} and worst-case state x^* are displayed in blue, red and green, respectively. Since V (6.4.7) is small, the three lines are very close to each other. The error in the nominal equilibrium point leads to the small steady state bias between the pitch rate estimate and the true pitch rate.	89
6.2	This is a close up look of the state history for the first 0.1 seconds. The initial worst case state is different than the initial state estimate as well as initial state. Since the system is assumed to have perfect measurement and V is very small, then the state estimate is very close to the true state. The initial differences between the worst case velocity and the initial velocity is about 65 ft/s. The initial differences between the worst case height and the initial height is about 950 feet.	90

6.3	$\hat{\zeta}$ and ζ^* are displayed in blue and green lines, respectively. Since initial error weighting in ζ is very small, $\hat{\zeta}$ and ζ^* is very close to each other, hence the blue and green lines are on top of each other. The large equilibrium change influences the linearization terms A_i and B_i , and mask the actual values of the unknown parameters, which are being estimated. Hence $\hat{\zeta}$ does not tend to actual ζ . However, the observer does yield a stable worst case controller, even though the linearization is violated.	91
6.4	The input history of 1000 seconds are displayed here. The thrust setting θ was saturated initially to increase velocity towards v_e . After velocity reaches past v_e , the thrust setting converges towards the true equilibrium setting of the aircraft. The deflection angle also saturated initially, but quickly converges towards the equilibrium deflection angle after the aircraft reaches sufficiently close to the target velocity v_e . .	92
6.5	The input history of 70 seconds are displayed here.	93
6.6	Worst case control input gain history for 1000 seconds. The blue lines represent the top row of the input gain, which is associated with the thrust. The red lines represent the bottom row of the input gain, which is associated with the deflection angle. . .	94

List of Tables

6.1	Constant and variable definition for hypersonic flight simulation.	72
6.2	The effect of κ on the perturbation model	80

NOTATIONS

x	State Vector, \mathbb{R}^n
u	Input Vector, \mathbb{R}^m
α	Unknown System Parameter Vector, \mathbb{R}^l
β	Unknown Control Parameter Vector, \mathbb{R}^k
ξ_r	Unknown Parameter Vector, Composed of Both α and β
ξ	Augmented State Vector, Composed of x , α , and β
$A(\alpha)$	System Matrix with Unknown System Parameters α
$B(\beta)$	Control Matrix with Unknown System Parameters β
G	Process Disturbance Coefficient Matrix, $\mathbb{R}^{n \times p}$
ω	State Process Disturbance Vector of Size p
z	Perfect Partial Measurement of State x
$(\cdot)^*$	Worst Case (\cdot) , for example u^* is the worst-case input generated using α^* and β^* .
$\hat{(\cdot)}$	Estimate of (\cdot)
$\ \cdot\ _Q^2$	$(\cdot)'Q(\cdot)$, Vector Norm Weighted by Symmetric Q .
$\mathbf{0}_n$	Zero Matrix of Size n
\mathbf{I}_n	Identity Matrix of Size n
τ	Running Variable for Time
T	Terminal Time

$(\cdot)_0$	(\cdot) at Initial Time
$(\cdot)_t$	(\cdot) at Current Time
$(\cdot)_T$	(\cdot) at Terminal Time
D_{af}	Disturbance Attenuation Function
$(\cdot)_0^t$	The Set of (\cdot) From Initial Time to Current Time t
$(\cdot)_t^T$	The Set of (\cdot) From Current Time t to Final Time T
R	Weighting on Input
W	Weighting on Process Disturbance
Q	Weighting on State
Q_T	Weighting on Terminal State
P_0	Weighting on Initial Estimate Error
J	Cost Function
U	Set of Possible Input
Ω	Set of Possible Process Disturbance
J_c	Return Function
J_f	Accumulation Function

ACKNOWLEDGEMENTS

First and foremost, I would like to extend my sincere gratitude to my advisor and mentor, Professor Speyer. I am extremely grateful for your patience, kindness, and insightful guidance throughout my academic journey. Thank you for your words of encouragement, immense support and confidence in my work, especially when I wanted to give up after the rejection of a paper. Thank you for all the long hours of discussion throughout the years. Without your encouragements and mentorship, I would not have made it this far. I would also like to thank Professor Yoneyama, for helping me understand his previous papers as well as the discussion on the existence of multiple optimal strategies for a different class of disturbance attenuation cost function.

I want to thank my friends at Sysense for all their help and support during my time there. Furthermore, Sung, thank you for assigning me to the aircraft cruise control project, which served as a motivation for this work. Thank you, Andre and Emmanuell, for all the technical discussions and guidances on various projects. I want to thank Tom and Jay for all their help in studying for the prelim.

I want to thank my family for all the emotional and financial support during my academic journey. Thank you Evelyn, for challenging me to do HIIT workouts every week, so that I can actually do push-ups. Thank you, Charles, for inspiring me towards the path of PhD.

This work was supported by the Ronald and Valerie Sugar Chair in Engineer Endowment.

VITA

2012-2016	Research Engineer, Sysense
2008-2010	M.S., Aeronautics, University of Southern California
2007-2011	Systems Engineer, Northrop Grumman
2003-2007	B.S., Mechanical Engineering, Caltech

PUBLICATIONS

1. W. Huang and J. L. Speyer, "Adaptive control based on disturbance attenuation and the modified gain observer for parameter uncertain linear systems.", *Proceedings of the 2021 American Control Conference*, New Orleans, LA, USA, 2021.
2. W. Huang and J. L. Speyer, "Disturbance attenuation controller for parameter uncertain linear systems adaptive through a modified gain observer", *IEEE Transaction on Automatic Control*, submitted.
3. W. Huang and J. L. Speyer, "Hypersonic cruise using a disturbance attenuation controller adaptive through a nonlinear modified gain observer", *AIAA Journal of Guidance, Control and Dynamics*, submitted.

Chapter 1

Introduction

Plant uncertainties and disturbances are inevitable hinderances in control design problem for many physical systems, as it is often difficult to obtain true system dynamics for physical systems, such as the aerodynamic tables of hypersonic flight vehicles. Uncertainties may enter the system through many channels. It can enter as an external plant disturbance such as unexpected wind gust in the case of hypersonic flight control, or it can enter as an internal disturbances such as sensor noise and actuator noise. Uncertainties can also enter the system through in system parameter error due to our limited understanding of the system parameters and system model. In the case of flight control, the nominal parameter identification of flight dynamic may be based on sub-scale dynamic wind tunnel experimentation as well as full-scale flight tests [1]. However, even the most thoroughly researched nominal parameter tables may be insufficient for the controller to guarantee close loop stability. For example, in the case of hypersonic flight, the wind-tunnel test may yield a set of nominal aerodynamic tables, but if the shape of the airfoil were changed during the flight test due to ablation, the nominal aerodynamic values might be drastically different than the true values, rendering the nominal controller useless in maintaining airplane stability. Therefore, besides a thorough investigation of plant dynamics, it is also important to estimate the system parameters online to accommodate for the parameter uncertainties.

The control of continuous-time linear systems with unknown constant parameters have been extensively studied in the past decades. Various approaches dealing with unknown disturbances ranges from robust control [2]-[6], adaptive control [7]-[14], dual control [15]-[17], to machine learning [18] [19] and many more. In this thesis, we present an adaptive disturbance attenuation controller adaptive through a nonlinear modified gain observer for a class of time-invariant linear systems with unknown system parameters in both system and control matrices. This control approach attempts to address the question of given the disturbances, such as process noise and uncertainties, play their worst case strategies in accordance to a disturbance attenuation based cost function, what is the optimal input strategy that can stabilize the uncertain plant?

1.1 Robust Control

Robust control methods are designed to guarantee desired system performance and system stability given the unknown parameters vary within a set of known bound. The controller is robust against a set of known bounded parameter uncertainties and modelling error [2] [3]. Robust controllers employ static gain policy, which means its control parameters do not change in spite of measurement history. Since robust controllers are designed to work without additional parameter estimation, as the uncertainties are assumed to be within a certain bounded compact set, then to guarantee robust performance and stability for a wide range of uncertainties, the resulting controller can be overly conservative. There are many types of robust controls, such as H_∞ loop-shaping and μ synthesis. The goal of the H_∞ control problem is to find all controller that yield the norm of the close-loop transfer function less than a positive given scalar. In 1988, [20] derived the results of the finite-horizon time varying H_∞ control problem with zero initial condition using the maximum principle. The state space solution to the standard H_∞ control problem is presented by Doyle *et al.* in 1989 [5].

H_∞ control are typically applied to plant with unstructured uncertainties, and μ synthesis extends H_∞ to systems with structured uncertainties, hence μ synthesis are typically less conservative than H_∞ controller [3] [2] [4] [5] [6]. However, both controllers does not consider the cases where the true uncertainty bounds might be bigger than expected. For example, going back to autonomous flight,

engineers can design the robust controller to handle disturbances such as wind gust up to a certain magnitude, as well as variations in aerodynamic tables. However, if the airplane wings ablated during mid-flight due to any reason, the disturbances from uncertain parameters may exceed what the controller is designed to handle, and the controller may eventually fail to stabilize the aircraft. Therefore, one control design approach is to estimate the uncertain parameters online, which is called adaptive controllers.

1.2 Adaptive Control

By the 1950s, the fixed gain controllers could no longer yield satisfying the tracking performance requirement for the pilot control command for the new classes of advanced manned aircrafts. These new advanced manned aircrafts operate in a wide range of flight envelope, various range of speeds and altitudes, wide range of center of gravity, different aircraft geometry, as well as a large range of control effectiveness. Adaptive control was one approach proposed to deal with the effect of unknown time-varying aerodynamic control effectiveness. By 1956, researchers had shown the theoretical feasibility of using adaptive control in aircrafts. The US government then proceed to test the practical implementation of the adaptive control in aircraft using F-94, the F-101 and eventually the X-15, which is a hypersonic rocket-powered aircraft [7] [21].

The basis of adaptive control is parameter estimation. Adaptive controller can automatically adjust its control parameters in response to system dynamics and disturbances, while satisfying certain performance criteria subject to the unknown plant dynamics. To update the control parameters, adaptive controllers require only the measurement history and *a priori* initial system information, such as initial parameter estimate and its covariance in the stochastic formulation or the initial parameter error weighting in the deterministic case [7] [8] [22]. Adaptive control can be classified into two catagories: direct versus indirect. Direct adaptive control methods will directly update the controller parameters, whereas the indirect adaptive controllers will first estimate the system parameters, then use those system parameter estimates to calculate for the controller parameters. Since the 1950s, various types of adaptive control came to existence. Examples of adaptive control are model reference adaptive control (MRAC), self-tuning regulators (STR), gain scheduling, adaptive

pole placement, extremum-seeking control, multiple model control [7] [22].

Adaptive control can also follow these two approaches, one approach is to solve the control problem and estimation problem separately via certainty equivalence principle, such as the self-tuning regulator [23]. This yields an adaptive control policy that treats the output of the parameter estimation as the truth without accounting for the uncertainties in the parameter estimation. Adaptive controllers obeying the certainty equivalence principle are typically easier to solve and are less complicated than the adaptive control schemes that abide by the non-certainty equivalence principle. However, by taking parameter estimation error variance or the confidence level of the parameter estimates into account, one can generate a controller that is less susceptible to stochastic variations. Examples of non-certainty equivalence adaptive controllers are the current disturbance attenuation control coupled with a nonlinear modified gain observer as shown in this thesis, as well as [17], [24], [25], [26] and [27].

1.3 Dual Control

The approach of taking into account the confidence level of the parameter estimation is also part of the central theme in dual control proposed by Feldbaum in 1960. Feldbaum addresses the question of generating a controller that stabilize the plant using information available at current time, while generating a probe signal to improve parameter estimation, which enhances future controller performance. These two objectives can have conflicting interests, as the better one controls the plant, the less observable the system parameters might be. If a probe is used on the system, then it may perturb the system away from optimal trajectory to gain observability of system parameter, thereby yielding a higher cost. Feldbaum has shown the optimal solution to the dual control can be derived using dynamic programming [15] [16]. Unfortunately, the solution is difficult to solve, and hence researchers have turned to sub-optimal dual controller, such as [17].

In [17], a stochastic discrete-time linear system with uncertain parameters is examined via the dual control approach. A cost-to-go expression is formulated base on quadratic functions of the state and the control, and included the cost of using the current control to improve future estimation and the

enhancement of the future estimation on future control. Hence, the cost function demonstrates the dual purpose of the control, which is to improve the estimation of the uncertain parameters and to enhance the control of the uncertain system. Once solved, according to the dual control cost function, the resulting controller can appropriately use a portion of the control input to improve estimation and the remaining input energy for control purpose. Unfortunately, the optimization of the dual control cost function is difficult to solve, the authors devised an ad-hoc scheme to perturb around a nominal certainty equivalent control and obtained an approximation of the optimal cost-to-go function using a second-order perturbation analysis. The derived control input is suboptimal and [17] does not prove stability of the controller.

1.4 Background to the Current Research

Various works formulate the H_∞ or disturbance attenuation control problem for linear systems based on the linear quadratic (LQ) game. Following the publication of [20] and [5], [28] extends these results by reformulating the standard finite-horizon time varying H_∞ control problem with zero initial condition using a game theoretic approach, and solving for the solution using the completion of squares method. The optimization yields two indefinite Riccati differential equations. The solution to the optimization exists if there exists solutions to the two Riccati equations.

Furthermore, [29] extended the results in [28] to a finite-time disturbance attenuation problem for time-varying systems with uncertain initial state and partial state measurement. A zero-sum LQ game is formulated, pitting the controller against the measurement noise, process noise and uncertainties in the initial state. The solution is found using calculus of variation technique. Around the same time frame, similar results were also shown in [30], [31] and [32]. [33] obtained a minimax controller for the discrete finite time linear system with hard bound on the disturbances subject to linear quadratic game cost function. The linear system is subject to a nonzero fixed initial conditions.

In [34], a minimax control problem is considered for a finite time nonlinear system subject to process and noise disturbance. The noise disturbances are square integrable. The optimization of the quadratic games cost function with respect to the input, the process disturbance and noise distur-

bance leads to a controller and an observer with a Kalman filter structure that satisfies the certainty equivalence principle. The control gain is a function of the estimated state.

Extending the results in [29], [35] conducted a game theoretic analysis of a linear compensator in the presence of process disturbance, measurement noise disturbance, as well as time-varying uncertain parameters in the system, input and measurement matrix. The system makes partial measurement of the state. The system is subject to a differential games cost function that pits the weighted norm of the terminal state, the state history and the input history against the process and the noise disturbances. The goal is to maximize the cost function with respect to the disturbances and initial state, and minimize with respect to the control input. Given the initial state and the parameters are contained within a certain region, the optimization yields a compensator that satisfies the saddle point inequality. Furthermore, the saddle point solutions might not be unique due to the uncertain parameters. The infinite-time problem were also presented for the time-invariant linear system.

In [36], a scalar system with a single unknown parameter in the control matrix is examined. The system has a zero coefficient as its system matrix, and is subject to no process noise. For such a simple plant, the resulting worst case solution is a fifth order polynomial, whose solution can only be solved numerically. For more complicated plants, one can expect the complexity of the worst case solution to increase, and the closed-form solution do not exist except for very specialized cases. To obtain the worst case solution, one would most likely employ the use of numerical methods.

Around the same time, [37] formulated a minimax adaptive control for a class of parameter uncertain linear systems subject to process disturbance. The system has full state information as well as full state derivative information. The system is also subject to a performance index that is quadratic in disturbance and the unknown constant parameters. For both finite time and infinite time cases, a set of necessary and sufficient conditions for the existence of the control strategy were presented. Since it is difficult to access the full state derivative information in practice, [38] formulates a worst-case parameter identifier in deterministic uncertain plants, which are linear with respect to the unknown parameters, with full state measurement.

Following the publication of [29], [35] and [36], [39], [26], and [40] derives a set of worst-case control

coupled with an estimator for linear systems with unknown parameters only in the input matrix using dynamic programming. This system is subject to process disturbance and measurement noise. Since the system matrix is known, then the estimator and the error dynamics are linear. A disturbance attenuation controller coupled with a linear estimator is derived using the dynamic programming method. The optimization yields a parameter connection condition that ties the worst case controller and estimator together. In [39], a minimax formulation and a dynamic programming approach are presented. It is shown that the control strategy from either approaches are equivalent to each other and the control strategy represent the saddle-point strategy of the game theoretic cost function. A generalized version of the example in [36] were also examined in [39], where the process disturbance is now included in the dynamics of the state. The resulting parameter connection condition, which is used to derive the optimality conditions, can be transformed into a fifth order polynomial in terms of the scalar worst case parameter.

The stability of the close loop sytem is presented in [26] by finding a value function that satisfies the Hamilton-Jacobi-Issac's equation. Furthermore, [26] also proved the disturbance attenuation properties of the estimator. The same example examined in [39] were also shown in [40], and it is demonstrated that at the initial time, the optimal return function can have two strategies which yields an equal optimal value. In [41], the adaptive robust controller derived in [26] and [40] is applied to the short period nonlinear longitudinal dynamics of the F-18 aircraft. The plant consists of two states, angle of attack and pitch rate, and is subject to elevator deflection and thrust vector command inputs. Linearizing the nonlinear dynamics yields a linear model of the aircraft. A single parameter is estimated in the input matrix associated with the control effectiveness of the elevator deflection, because the control effectiveness can vary at different flight conditions. The robust compensator stabilizes the aircraft by estimating the unknown parameters using the state measurements. Similar uncertain system was also studied in [42] with norm bound on the uncertainties in the input matrix.

Motivated by the results in [29], [39], [26] and [40], [27] considers a linear time-invariant stochastic system, subject to process and measurement noise, with constant uncertain parameters in both system and input matrix. A worst case control coupled with a linear estimator is presented in [27]. No stability results were discussed in [27]. Since the augmented system matrix \bar{A} used in

the estimator contains the noisy measurement of the state, the estimate of the unknown parameter might be biased, leading to a suboptimal or even an unstable controller. Furthermore, the stability of the estimator cannot be guaranteed, so the stability of the controller cannot be guaranteed. The only uncertainty in example [27] is the mass, which enters into both the system and input matrix. To the best of our knowledge, there has been no extension to the work in [27].

In contrast to previous work, this thesis presents a rigorous structure to the control of linear systems with partial state information in the presence of uncertain system parameters in both the system matrix and the input matrix. Rather than using a stochastic approach, a disturbance attenuation approach induces the structure of a stable controller. To avoid using ad-hoc parameter estimators, the nonlinear modified gain observer, which estimates both the state and system parameters, is formally introduced into the disturbance attenuation formulation. Given certain assumptions on controllability and observability, and the existence of control and estimation Riccati equations and value function, controller stability is assured.

1.5 Overview of the Current Research and Dissertation Layout

This thesis presents an adaptive control strategy for a class of parameter uncertain linear systems with disturbance input. The uncertain linear system contains unknown parameters in both the system and the input matrices. The system makes perfect partial measurement of the system states. The goal is to find the worst case control strategy assuming the system is perturbed by the worst case disturbances, the unknown parameters as well as the worst case state. The disturbance attenuation function, which often appears in H_∞ control, is the ratio between the norm of the output and the norm of input disturbance. In the standard H_∞ control, the goal is to find a feedback controller that can keep the disturbance attenuation function below a certain desired value for all possible input disturbances. In this thesis, the disturbance attenuation function is transformed into a minimax differential game where the disturbance, the unknown parameters and the unknown states act as the cooperative players that maximize the cost function, whereas the controller is the opposing player

that minimizes the cost function. Applying dynamic programming to the cost function naturally divides it into two sequential operations, one projected into the future forming the return function and the other related to the past yielding the accumulation function. Assuming the existence of a saddle point in the cost function, the optimization yields a minimax controller coupled with a stable nonlinear modified gain observer (MGO), which estimates the state and the unknown parameters.

In this class of parameter estimation problem, the measurement function and the augmented system, which is composed of the state and the uncertain parameters, are modifiable functions or can be transformed into modifiable functions using an appropriate change of coordinate system, such as the observable canonical form. The essence of a modifiable function is that although the observer dynamics are nonlinear, in this case the uncertain system matrix is multiplied by the uncertain state, the error in the observer's estimation error is linear. By maximizing the cost function with respect to the uncertain parameters, the minimax controller takes the parameter estimation confidence level into account to generate the worst case input for a given instance of time. A connection condition between the two sequential operations at current time t is derived, yielding the first order necessary condition and the second order sufficient condition. Chapter 2 presents the problem formulation, derivation of the performance index, and the dynamic programming solution, which is a disturbance attenuation controller coupled with nonlinear MGO. The derivation of the controller and observer can also be found in [43] [44].

Since the assumption of the existence of saddle point is used to derive the adaptive controller, Chapter 3 presents the proof for the existence of the saddle point in the cost function, demonstrating that the minimax decomposition in chapter 2 is valid. Given certain condition, such as the existence of the control and observer Riccati equations, the stability of the disturbance attenuation controller coupled with the nonlinear MGO is presented in Chapter 4. The close loop system is stable and the estimation error is bounded, which demonstrates the disturbance attenuation properties of the observer and the stability of the disturbance attenuation controller. The saddle point derivation can be found in [43] and [44]. The stability condition of the disturbance attenuation controller can be found in [44].

To illustrate the adaptive controller developed in this thesis, the adaptive controller is applied to an unstable single-input single-output (SISO) four state vector case example with four unknown system parameters subject to worst case disturbance. The unknown system parameters multiplies all elements of the state, but only one element of the state is measured perfectly. Hence, the system must be transformed to an observable canonical form such that only one measurement is required to estimate a different set of unknown system parameters. The new set of unknown parameters differs from the original set of unknown parameters due to the coordinate transformation of the original system into the observable canonical form. This is acceptable for control and close-loop system stability purposes, because once the observable canonical state tends to zero, so does the original state. The simulation demonstrates the applicability of the disturbance attenuation controller coupled with the nonlinear MGO, and assess its performance against the linear quadratic regulator (LQR) coupled with a modified gain extended Kalman observer (MGEKO). The MGEKO is chosen as a comparison strategy because MGEKO has similar observer structure as the current proposed MGO. Furthermore, MGEKO is proven to be globally convergent. This simulation is presented in chapter 5. The SISO example can also be found in [43] and [44].

In chapter 6, the disturbance attenuation controller coupled with a nonlinear modified gain observer (MGO) is proposed to stabilize the HFV with similar flight conditions and aerodynamic uncertainties as those in [45]. The nominal longitudinal dynamics model is linearized to yield a nominal linearized model at a certain trim condition. However, due to the large aerodynamic uncertainties, the derived nominal equilibrium point and the nominal linearized model deviates significantly from the true equilibrium point and the true linearized model of the true nonlinear longitudinal dynamics. Hence, certain parameters in the nominal linearized model need to be estimated to accommodate for the error contributed by the large aerodynamic uncertainties. This problem can be viewed as a linear system with unknown parameters in both the system matrix and the input matrix. An observer is used to estimate the unknown parameters in the system and input matrices to yield an estimated linearized model for the controller. Without additional parameter adaptations, controllers based on the nominal linearized model might not be able to stabilize the true plant or yield satisfactory tracking performance. The worst case controller coupled with the nonlinear MGO, derived based

on an estimated linear model, is applied to the true longitudinal dynamics with large aerodynamic uncertainties. The simulation demonstrates the stability of the close loop system and the tracking performance of the worst case control scheme. The performance of the disturbance controller is shown to perform better than the performance of the Sum-of-Squares method and the nonlinear dynamic inversion method in [45]. The application of the worst case controller to the hypersonic aircraft can be found in [46].

Chapter 7 is the summary of this work and possible future work.

Chapter 2

Disturbance Attenuation Control Adaptive Through a Modified Gain Observer

2.1 Problem Formulation

In this chapter, we consider the class of deterministic linear time-invariant systems with unknown parameters in both the system matrix and the input matrix. These constant, uncertain parameters are assumed to enter the plant linearly. We denote the unknown parameters in the system matrix as $\alpha \in \mathbb{R}^l$ and the unknown parameters in the control coefficient matrix as $\beta \in \mathbb{R}^k$. The state-space representation of the plant dynamics and measurement over the time interval $[0, T]$ is:

$$\dot{x} = A(\alpha)x + B(\beta)u + G\omega \tag{2.1.1}$$

$$z = Hx, \tag{2.1.2}$$

where $x \in \mathbb{R}^n$ is the state vector, $u \in \mathbb{R}^m$ is the input vector, and $\omega \in \mathbb{R}^p$ is the unknown square integrable process disturbance vector on the time interval $[0, T]$. The coefficient $G \in \mathbb{R}^{n \times p}$ is the process disturbance coefficient matrix. The system makes perfect partial measurement of the state x , as denoted by $z \in \mathbb{R}^r$. The system matrix $A(\alpha) \in \mathbb{R}^{n \times n}$ and input matrix $B(\beta) \in \mathbb{R}^{n \times m}$ are linear functions of the constant unknown parameter vectors α and β as defined below. Define $\mathbf{0}$ as a zero matrix of appropriate size:

$$\alpha = \begin{bmatrix} \alpha_1 & \alpha_2 & \cdots & \alpha_l \end{bmatrix}', \quad \dot{\alpha} = \mathbf{0} \quad (2.1.3)$$

$$\beta = \begin{bmatrix} \beta_1 & \beta_2 & \cdots & \beta_k \end{bmatrix}', \quad \dot{\beta} = \mathbf{0} \quad (2.1.4)$$

$$A(\alpha) = A_0 + \sum_{i=1}^l \alpha_i A_i, \quad 1 \leq i \leq l, \quad i \in \mathbb{Z}_+ \quad (2.1.5)$$

$$B(\beta) = B_0 + \sum_{i=1}^k \beta_i B_i, \quad 1 \leq i \leq k, \quad i \in \mathbb{Z}_+. \quad (2.1.6)$$

The coefficients A_i and B_i are known matrices. The goal is to find a controller $u \in U$ that minimizes a linear quadratic game cost function in the presence of $\omega \in \Omega$. U is the class of admissible controls. Ω is the class of admissible disturbances.

Since the unknown parameters α and β are linear in both the dynamic and the control matrices respectively, it can be estimated by concatenating α and β to the state x to define an augmented state:

$$\xi = \begin{bmatrix} x' & \alpha' & \beta' \end{bmatrix}'. \quad (2.1.7)$$

The respective augmented state dynamics is:

$$\dot{\xi} = \begin{bmatrix} \dot{x} \\ \dot{\alpha} \\ \dot{\beta} \end{bmatrix} = \underbrace{\begin{bmatrix} A(\alpha)x + B(\beta) \\ \mathbf{0}_{l \times 1} \\ \mathbf{0}_{k \times 1} \end{bmatrix}}_{F(\xi, u)} + \underbrace{\begin{bmatrix} G \\ \mathbf{0}_{l \times p} \\ \mathbf{0}_{k \times p} \end{bmatrix}}_{\Gamma} \omega = F(\xi, u) + \Gamma \omega. \quad (2.1.8)$$

The dynamics of ξ (2.1.8), which consists of x and α , is nonlinear due to the nonlinear term $A(\alpha)x$. In this class of nonlinear system, the augmented system and measurement functions can be transformed into modifiable functions (see definition 2.1), through appropriate coordinate system, such as the observable canonical form. The essence of a modifiable function is that although the observer dynamics are nonlinear, the observer's estimation error is linear. The discrete-time definition of a modifiable nonlinearity was defined in [47] and [48], whereas the continuous-time definition was defined in [49].

Definition 1. [47] [48] [49] *For any $x, \bar{x} \in \mathbb{R}^n$, \bar{x} a known vector, if there exists a time-varying matrix function $L : \mathbb{R}^p \times \mathbb{R}^n \rightarrow \mathbb{R}^{p \times n}$ such that the time-varying function $f : \mathbb{R}^n \rightarrow \mathbb{R}^p$ can be written as:*

$$f(x) - f(\bar{x}) = L(z, \bar{x})(x - \bar{x}), \quad z = Hx, \quad (2.1.9)$$

then f is a modifiable nonlinear system function.

2.2 Performance Index

This section aims to derive a disturbance attenuation controller that can stabilize the system in the presence of worst-case process noise and system parameter uncertainty. In the following, we derive the performance index from the disturbance attenuation function defined as $D_{af} = \frac{\|\bar{y}\|^2}{\|\underline{\omega}\|^2}$, where the norms $\|\bar{y}\|^2$ and $\|\underline{\omega}\|^2$ are defined as:

$$\|\bar{y}\|^2 = \|x_T\|_{Q_T}^2 + \int_0^T \|x\|_Q^2 + \|u\|_R^2 d\tau \quad (2.2.1)$$

$$\|\underline{\omega}\|^2 = \|\xi_0 - \bar{\xi}_0\|_{P_0^{-1}}^2 + \int_0^T \|\omega\|_{W^{-1}}^2 d\tau. \quad (2.2.2)$$

x_T is the terminal state. The initial estimate of the unknown system parameters α and β are denoted as $\bar{\alpha}_0$ and $\bar{\beta}_0$. $\bar{\xi}_0$ is defined as the initial estimate of ξ . The weightings in the disturbance attenuation

function are defined as follows, where the subscript of $\mathbf{0}$ indicates the size of the zero matrix:

$$\begin{aligned} R > \mathbf{0}_m, \quad W > \mathbf{0}_p, \quad Q \geq \mathbf{0}_n \\ Q_T \geq \mathbf{0}_n, \quad P_0 > \mathbf{0}_q, \end{aligned} \tag{2.2.3}$$

where $q = n + l + k$ is the length of the vector ξ . As in past literatures [39] and [26], the goal is typically to find an input such that $D_{af} \leq \frac{1}{\theta}$, where θ is a positive real number. Extending the results from [39] [26], uncertainties are also present in the system matrix. The D_{af} is rewritten in the differential game format to be used as the performance index. The cost function is multiplied by $\frac{1}{2}$ as a convenience for later analysis. Define the initial estimation error as:

$$e_0 = \xi_0 - \bar{\xi}_0. \tag{2.2.4}$$

The cost function is then defined as:

$$\begin{aligned} J &= \frac{1}{2} \{ \|\bar{y}\|^2 - \|\omega\|^2 \} \\ &= \frac{1}{2} \{ \|x_T\|_{Q_T}^2 - \|\xi_0 - \bar{\xi}_0\|_{P_0^{-1}}^2 + \int_0^T \|x\|_Q^2 + \|u\|_R^2 - \|\omega\|_{W^{-1}}^2 d\tau \}, \end{aligned} \tag{2.2.5}$$

where $\theta = 1$ for convenience. In this minimax game, the input is playing against four players. The unknown disturbance ω , the system uncertainties α and β , and the initial state x_0 are trying to maximize the cost function in (2.2.5), while the control u is trying to minimize the cost function.

The optimal cost function can be written as:

$$J^* = \min_{u \in U} \max_{x_0, \alpha, \beta, \omega \in \Omega} J, \tag{2.2.6}$$

where $(\cdot)^*$ represent the optimal value of (\cdot) . For now, assume J has a saddle point. The order of max and min operators is then irrelevant and will yield the same optimal cost. After optimization of all players, the optimal values are used to prove that J (2.2.6) indeed does have a saddle point. In the next section, the optimization of the cost function is derived via dynamic programming method.

2.3 Dynamic Programming Solution

At the current time t , the cost function (2.2.5) is split into two parts: an accumulation function $J_f(0, t)$ and a return function $J_c(t, T)$. The accumulation function contains the cost for the time interval $\tau \in (0, t)$, and the return cost function contains the cost for the time interval $\tau \in [t, T]$.

Dynamic programming is applied to the cost function (2.2.5). The cost function is then naturally divided into two sequential operations: a minimax of the $J_c(t, T)$ with respect to the controller and disturbances constructed going backwards in time followed by a maximization of the $J_f(0, t)$ with respect to the disturbance, the unknown parameters, and initial state processed going forwards in time. Using (2.2.4), the decoupled costs are:

$$J_f(0, t) = \frac{1}{2} \left\{ -\|e_0\|_{P_0^{-1}}^2 + \int_0^t \|x\|_Q^2 + \|u\|_R^2 - \|\omega\|_{W^{-1}}^2 d\tau \right\} \quad (2.3.1)$$

$$J_c(t, T) = \frac{1}{2} \left\{ \|x_T\|_{Q_T}^2 + \int_t^T \|x\|_Q^2 + \|u\|_R^2 - \|\omega\|_{W^{-1}}^2 d\tau \right\} \quad (2.3.2)$$

$$J = J_f(0, t) + J_c(t, T). \quad (2.3.3)$$

Let $(\cdot)_0^t$ and $(\cdot)_t^T$ represent the (\cdot) strategy for the time intervals $[0, t]$ and $[t, T]$, respectively. For $t \leq \tau \leq T$, both u_t^T and ω_t^T are optimized to yield their respective optimal strategies. Assuming there exists a saddle point, then the operations of min and max can be interchanged. The optimal cost function (2.2.6) can be written as:

$$\begin{aligned} J^* &= \min_{u \in U} \max_{\omega \in \Omega, \alpha \in \mathbb{R}^l, \beta \in \mathbb{R}^k, x_0} [J_f(0, t) + J_c(t, T)] \\ &= \max_{\alpha \in \mathbb{R}^l, \beta \in \mathbb{R}^k, x_0} \max_{\omega_0^t} [J_f(0, t) + \min_{u_t^T} \max_{\omega_t^T} J_c(t, T)]. \end{aligned} \quad (2.3.4)$$

For $0 < \tau < t$, the state x_0^t and the control input u_0^t have all occurred; hence, no minimization of u_0^t can be done for the accumulated cost function. Although ω has played its strategy in the past, ω_0^t is not available to the designer. The goal is to determine the worst strategy that ω_0^t could have played in the past to undermine the estimation of the initial state and the unknown parameters α and β ; therefore, the maximization of the disturbance ω_0^t is required in the optimization of the

accumulation function. The optimization of the return function is performed first followed by the optimization of the accumulation function.

2.4 The Optimal Return Function

In this section, the optimization of the $J_c(t, T)$, through maximizing $J_c(t, T)$ with respect to ω_t^T and minimizing with respect to u_t^T , is performed to yield a worst-case controller. The completion of squares method is applied to $J_c(t, T)$ to optimize (2.3.2) with respect to the future process disturbance and input. To accomplish this, the zero term $\frac{1}{2} \left\{ -x' \Pi x|_t^T + \int_t^T \frac{d}{d\tau} x' \Pi x d\tau \right\}$ is added to the return function (2.3.2). Note that:

$$\frac{1}{2} \left\{ -x' \Pi x|_t^T + \int_t^T \frac{d}{d\tau} x' \Pi x d\tau \right\} = \frac{1}{2} \left\{ -x'_T \Pi_T(\alpha, \beta) x_T + x'_t \Pi_t(\alpha, \beta) x_t + \int_t^T 2x' \Pi \dot{x} + x' \dot{\Pi} x d\tau \right\}, \quad (2.4.1)$$

where x_t is defined as x at current time t . $\Pi_t(\alpha, \beta)$ and $\Pi_T(\alpha, \beta)$ are defined as Π at current time t and terminal time T . respectively. Shown below, the system dynamic (2.1.1) is substituted into \dot{x} in the integrand of the return function to yield:

$$\begin{aligned} J_c(t, T) &= \frac{1}{2} \left\{ \|x_T\|_{Q_T}^2 - \|x\|_{\Pi}^2|_t^T + \int_t^T \|x\|_Q^2 + \|u\|_R^2 - \|\omega\|_{W^{-1}}^2 + \frac{d}{d\tau} \|x\|_{\Pi}^2 d\tau \right\} \\ &= \frac{1}{2} \left\{ \|x_T\|_{Q_T - \Pi_T(\alpha, \beta)}^2 + \|x_t\|_{\Pi_t(\alpha, \beta)}^2 + \int_t^T \|x\|_Q^2 + \|u\|_R^2 - \|\omega\|_{W^{-1}}^2 + 2x' \Pi \dot{x} + \|x\|_{\Pi}^2 d\tau \right\} \\ &= \frac{1}{2} \left\{ \|x_T\|_{Q_T - \Pi_T(\alpha, \beta)}^2 + \|x_t\|_{\Pi_t(\alpha, \beta)}^2 + \int_t^T \|x\|_Q^2 + \|u\|_R^2 - \|\omega\|_{W^{-1}}^2 \right. \\ &\quad \left. + 2x' \Pi (A(\alpha)x + B(\beta)u + G\omega) + \|x\|_{\Pi}^2 d\tau \right\}. \end{aligned} \quad (2.4.2)$$

Now the return function (2.4.2) is ready to be optimized with respect to ω and u . Applying the completion of the squares method to solve for the worst-case process disturbance ω^* that maximizes

the return function is shown as follows:

$$\begin{aligned} & -\|\omega\|_{W^{-1}}^2 + 2x'\Pi G\omega - \|WG'\Pi x\|_{W^{-1}}^2 + \|WG'\Pi x\|_{W^{-1}}^2 \\ & = -\|(\omega - WG'\Pi x)\|_{W^{-1}}^2 + \|WG'\Pi x\|_{W^{-1}}^2. \end{aligned}$$

Completion of the squares method is also used to solve for the worst-case input u^* that minimizes the return function (2.3.2):

$$\begin{aligned} & \|u\|_R^2 + 2x'\Pi B(\beta)u + \|R^{-1}B(\beta)'\Pi x\|_R^2 - \|R^{-1}B(\beta)'\Pi x\|_R^2 \\ & = \|u + R^{-1}B(\beta)'\Pi x\|_R^2 - \|R^{-1}B(\beta)'\Pi x\|_R^2. \end{aligned}$$

Simplify and rearrange some terms in $J_c(t, T)$ (2.4.2) yields:

$$\begin{aligned} J_c(t, T) &= \frac{1}{2}\{\|x_T\|_{Q_T - \Pi_T(\alpha, \beta)}^2 + \|x_t\|_{\Pi_t(\alpha, \beta)}^2 + \int_t^T \|x\|_{Q+A(\alpha)'\Pi + \Pi A(\alpha) + \dot{\Pi}}^2 + \|WG'\Pi x\|_{W^{-1}}^2 \\ & \quad + \|u + R^{-1}B(\beta)'\Pi x\|_R^2 - \|\omega - WG'\Pi x\|_{W^{-1}}^2 - \|R^{-1}B(\beta)'\Pi x\|_R^2 d\tau\} \\ &= \frac{1}{2}\{\|x_T\|_{Q_T - \Pi_T(\alpha, \beta)}^2 + \|x_t\|_{\Pi_t(\alpha, \beta)}^2 \\ & \quad + \int_t^T \|x\|_{Q+A(\alpha)'\Pi + \Pi A(\alpha) + \Pi(GWG' - B(\beta)R^{-1}B(\beta)')\Pi + \dot{\Pi}}^2 \\ & \quad + \|u + R^{-1}B(\beta)'\Pi x\|_R^2 - \|\omega - WG'\Pi x\|_{W^{-1}}^2 d\tau\}. \end{aligned} \tag{2.4.3}$$

The return function (2.4.3) is minimized by choosing:

$$u^* = -R^{-1}B(\beta)'\Pi x \tag{2.4.4}$$

$$\omega^* = WG'\Pi x \tag{2.4.5}$$

and by choosing Π as:

$$\begin{aligned} -\dot{\Pi} &= \Pi(GWG' - B(\beta)R^{-1}B(\beta)')\Pi + A(\alpha)'\Pi + \Pi A(\alpha) + Q \\ \Pi_T(\alpha, \beta) &= Q_T. \end{aligned} \tag{2.4.6}$$

As all other terms go to zero, only $\|x_t\|_{\Pi_t(\alpha,\beta)}^2$ remains in (2.4.3). Hence, the optimal return function (2.3.2) is:

$$J_c^*(t, T) = \min_{u_t^T} \max_{\omega_t^T} J_c(t, T) = \frac{1}{2} \|x_t\|_{\Pi_t(\alpha,\beta)}^2. \quad (2.4.7)$$

Using the derived $J_c^*(t, T)$ in (2.4.7), the optimal cost function can now be written as:

$$J^* = \max_{\omega_0^T, \xi_0} \frac{1}{2} \left\{ \|x_t\|_{\Pi_t(\alpha,\beta)}^2 - \|e_0\|_{P_0^{-1}}^2 + \int_0^t \|x\|_Q^2 + \|u\|_R^2 - \|\omega\|_{W^{-1}}^2 d\tau \right\}. \quad (2.4.8)$$

In the next section, the optimization of the accumulation function is performed to yield a modified gain estimator for ξ .

2.5 Modified Gain H_∞ Observer

A nonlinear observer will be derived through the optimization of the accumulation function. In [47], Song and Speyer derived a modified gain extended Kalman filter (MGEKF) for a class of modifiable nonlinear dynamics subject to nonlinear measurement function. Song applied the MGEKF to parameter identification in linear systems and proved that when used as a nonlinear observer (MGEKO) for a system with perfect partial measurement, MGEKO is globally exponentially convergent.

Motivated by the results in [47] and [48], a modifiable gain disturbance attenuation observer is developed for linear systems with unknown system parameters. By defining:

$$f(\xi, u) = A(\alpha)x + B(\beta)u, \quad (2.5.1)$$

the system dynamics in (2.1.1) can then be rewritten as:

$$\dot{x} = f(\xi, u) + G\omega. \quad (2.5.2)$$

Let us first introduce a pseudo measurement noise $\tilde{\nu}$ to the measurement:

$$z = \underbrace{\begin{bmatrix} H & \mathbf{0} \end{bmatrix}}_{\bar{H}} \xi + \tilde{\nu} = \bar{H}\xi + \tilde{\nu}. \quad (2.5.3)$$

The addition of this pseudo noise will be justified after the optimization of the accumulation function. Since z is a perfect partial measurement, $\tilde{\nu}$ is nominally zero. Adding the zero term $\|\tilde{\nu}\|_{V^{-1}}^2$, where $V > \mathbf{0}$, to the cost function (2.4.8) and rewriting the optimal cost function using the augmented state yields:

$$J^* = \max_{\omega_0^t, \xi_0} \frac{1}{2} \left\{ \|\xi_T\|_{Q_T}^2 - \|e_0\|_{P_0^{-1}}^2 + \int_0^T \left(\|\xi\|_Q^2 + \|u\|_R^2 - \|\omega\|_{W^{-1}}^2 - \|\tilde{\nu}\|_{V^{-1}}^2 \right) d\tau \right\}, \quad (2.5.4)$$

where the augmented weights are:

$$\bar{Q}_T = \begin{bmatrix} Q_T & \mathbf{0}_{n \times l} & \mathbf{0}_{n \times k} \\ \mathbf{0}_{l \times n} & \mathbf{0}_l & \mathbf{0}_{l \times k} \\ \mathbf{0}_{k \times n} & \mathbf{0}_{k \times l} & \mathbf{0}_k \end{bmatrix}, \quad \bar{Q} = \begin{bmatrix} Q & \mathbf{0}_{n \times l} & \mathbf{0}_{n \times k} \\ \mathbf{0}_{l \times n} & \mathbf{0}_l & \mathbf{0}_{l \times k} \\ \mathbf{0}_{k \times n} & \mathbf{0}_{k \times l} & \mathbf{0}_k \end{bmatrix}. \quad (2.5.5)$$

Remark 1. *The introduction of V into the cost function (2.4.8) to yield (2.5.4) is to insert a tuning parameter into the estimation to adjust the rate of observer error convergence. Note $\tilde{\nu}$ is in practice zero, and does not change the fact that z is perfect partial measurement.*

Since the system makes perfect partial measurement, x_t must be estimated at time t . An observer is derived through the optimization of the accumulation function. First, assume the form of the augmented state estimate $\hat{\xi}$ dynamic to be:

$$\dot{\hat{\xi}} = F(\hat{\xi}, u) + P\bar{Q}\hat{\xi} + K(z - \bar{H}\hat{\xi}), \quad (2.5.6)$$

where $F(\hat{\xi}, u)$ is defined as:

$$F(\hat{\xi}, u) = \begin{bmatrix} f(\hat{\xi}, u) \\ \mathbf{0}_{l \times 1} \\ \mathbf{0}_{k \times 1} \end{bmatrix}, \quad (2.5.7)$$

where

$$f(\hat{\xi}, u) = A(\hat{\alpha})\hat{x} + B(\hat{\beta})u. \quad (2.5.8)$$

P is a time-varying weighting function whose dynamic equation will be determined through the optimization of the accumulation function. K is an undetermined time-varying observer gain and may be a function of P . We will revisit the form of K after P is determined. The bias term $P\bar{Q}\hat{\xi}$ in the structure of the observer (2.5.6), is based on the results in [39], where there was also a bias term in the estimator. It will later be apparent that the bias term $P\bar{Q}\hat{\xi}$ is required to cancel out the cross term $2e'\bar{Q}\hat{\xi}$ in the cost function (2.5.17). In the following, the completion of squares method is used to optimize the accumulation function.

Define the estimation error to be:

$$e = \xi - \hat{\xi} = \begin{bmatrix} e_x \\ e_{\xi_r} \end{bmatrix}, \quad (2.5.9)$$

where $\xi'_r = \begin{bmatrix} \alpha' & \beta' \end{bmatrix}$. Since $F(\xi, u)$ can be transformed into a modifiable nonlinear function by changing into a different coordinate system if necessary, z is a function of ξ , then:

$$F(\xi, u) - F(\hat{\xi}, u) = \mathcal{A}(\hat{\xi}, u, z)e \quad (2.5.10)$$

$$z - \bar{H}\hat{\xi} = \bar{H}\xi + \tilde{\nu} - \bar{H}\hat{\xi} = \bar{H}e + \tilde{\nu}. \quad (2.5.11)$$

Using the definition of e (2.5.9), (2.1.8), (2.5.6), (2.5.10) and (2.5.11), the error dynamics can be

written as:

$$\begin{aligned}
\dot{e} &= \dot{\xi} - \dot{\hat{\xi}} \\
&= F(\xi, u) + \Gamma\omega - F(\hat{\xi}, u) - P\bar{Q}\hat{\xi} - K(z - \bar{H}\hat{\xi}) \\
&= (\mathcal{A}(\hat{\xi}, u, z) - K\bar{H})e - P\bar{Q}\hat{\xi} + \Gamma\omega - K\tilde{\nu}.
\end{aligned} \tag{2.5.12}$$

$\mathcal{A}(\hat{\xi}, u, z)$ and P has the following form:

$$\mathcal{A}(\hat{\xi}, u, z) = \begin{bmatrix} A(\hat{\alpha}) & g(z, u) \\ \mathbf{0}_{l+k \times n} & \mathbf{0}_{l+k \times l+k} \end{bmatrix}, \quad P = \begin{bmatrix} P_x & P_c \\ P'_c & P_{\xi_r} \end{bmatrix}, \tag{2.5.13}$$

where $g(z, u)$ is a function of the known measurement z and input u at current time t , and $g(z, u)$ is dependent on given A_i (2.1.5) and B_i (2.1.6). Then, using $\tilde{\nu} = \mathbf{0}$ and $K = P\bar{H}'V^{-1}$, the error dynamics for state and parameter can be written as:

$$\dot{e}_x = (A(\hat{\alpha}) - P_x H'V^{-1}H)e_x - P_x Q\hat{x} + g(z, u)e_{\xi_r} + G\omega \tag{2.5.14}$$

$$\dot{e}_{\xi_r} = -P'_c(Q\hat{x} - H'V^{-1}He_x). \tag{2.5.15}$$

Remark 2. *The steady state property of the parameter estimation error can be deduced by examining the dynamic equation (2.5.15) of e_{ξ_r} . By observation, if $P_c = \mathbf{0}$ or if $Q\hat{x} - H'V^{-1}He_x$ is in the null space of P_c , then $\dot{e}_{\xi_r} = \mathbf{0}$ and e_{ξ_r} reaches steady state. Since \hat{x} and e_x are both time-varying matrices and subject to their respective dynamic equations (2.5.6) and (2.5.14), if $\hat{x} \neq \mathbf{0}$ or $e_x \neq \mathbf{0}$, there is no guarantee $Q\hat{x} - H'V^{-1}He_x$ would be in the null space of P_c , which is also a time-varying matrix and is subject to a dynamic equation (2.5.23) that will be derived later in this section. It is possible $P_c \rightarrow \mathbf{0}$, this case is discussed in lemma 4.0.3, which is derived in a later section.*

Consider the case $P_c \neq \mathbf{0}$ and $Q\hat{x} - H'V^{-1}He_x$ is in the null space of P_c . If $\hat{x} = e_x = \mathbf{0}$, then $Q\hat{x} - H'V^{-1}He_x = \mathbf{0}$, and e_{ξ_r} reaches steady state value. Since ξ_r is constant by the definition (2.1.3 and 2.1.4), then a steady state e_{ξ_r} implies $\hat{\xi}_r$ is constant. Furthermore, if $Q = H'V^{-1}H$, then $Q\hat{x} - H'V^{-1}He_x = H'V^{-1}H(\hat{x} - (x - \hat{x})) = -H'V^{-1}Hx$, and if $Hx = \mathbf{0}$, then $\dot{e}_{\xi_r} = \mathbf{0}$. Hence in

the case where $Q = H'V^{-1}H$ and $Hx = \mathbf{0}$, then parameter estimation error e_{ξ_r} can reach nonzero steady state value. It is acceptable to have a steady state $e_{\xi_r} \neq \mathbf{0}$, as e_{ξ_r} does not imply an unstable x . $H'V^{-1}H\hat{x} = H'V^{-1}He_x = \mathbf{0}$ implies $H'V^{-1}Hx = Qx = \mathbf{0}$ in steady state, where $x'Qx$ is the integral part of the cost function (2.2.5) and $x'Qx \rightarrow \mathbf{0}$ is the main goal of the control design. Minimization of the steady state parameter error is a secondary control design goal, as a smaller e_{ξ_r} leads to a better control design for the plant.

Next, the completion of squares method is used to optimize the cost function with respect to $\omega_0^t(\cdot)$ by adding the zero term $- \|e\|_S^2|_0^t + \int_0^t \frac{d\|e\|_S^2}{d\tau} d\tau$ to the J_f . Using $\xi = e + \hat{\xi}$, we rewrite the cost function with optimized return function in terms of e and $\hat{\xi}$:

$$\begin{aligned}
& J_c^*(t, T) + J_f(0, t) \\
&= \frac{1}{2} \left(\|x_t\|_{\Pi_t(\alpha, \beta)}^2 - \|e_0\|_{P_0^{-1}}^2 - \|e\|_S^2|_0^t + \int_0^t \|\xi\|_Q^2 + \|u\|_R^2 - \|\omega\|_{W^{-1}}^2 - \|\tilde{v}\|_{V^{-1}}^2 + \frac{d\|e\|_S^2}{d\tau} d\tau \right) \\
&= \frac{1}{2} \left(\|x_t\|_{\Pi_t(\alpha, \beta)}^2 + \|e_0\|_{S_0 - P_0^{-1}}^2 - \|e_t\|_{S_t}^2 + \int_0^t \|e\|_Q^2 + \|\hat{\xi}\|_Q^2 + 2e'\bar{Q}\hat{\xi} + \|u\|_R^2 - \|\omega\|_{W^{-1}}^2 \right. \\
&\quad \left. - \|\tilde{v}\|_{V^{-1}}^2 + 2e'S\dot{e} + \|e\|_S^2 d\tau \right)
\end{aligned} \tag{2.5.16}$$

By selecting $S_0 = P_0^{-1}$, then $S_0 - P_0^{-1} = \mathbf{0}$, which eliminates the initial error term $\|e_0\|_{S_0 - P_0^{-1}}^2$ from the cost function. Now substitute the error dynamics (2.5.12) back into the cost function, and add the zero term $\|e\|_{S\Gamma W\Gamma'S}^2 - \|e\|_{S\Gamma W\Gamma'S}^2 + \|e\|_{S K V K'S}^2 - \|e\|_{S K V K'S}^2$ to the cost function. Further

simplification and apply the completion of squares yields:

$$\begin{aligned}
& J_c^*(t, T) + J_f(0, t) \\
&= \frac{1}{2} \left(\|x_t\|_{\Pi_t(\alpha, \beta)}^2 - \|e_t\|_{S_t}^2 + \int_0^t \|e\|_Q^2 + \|\hat{\xi}\|_Q^2 + 2e' \bar{Q} \hat{\xi} + \|u\|_R^2 - \|\omega\|_{W^{-1}}^2 - \|\tilde{v}\|_{V^{-1}}^2 \right. \\
&+ 2e' S(\mathcal{A}(\hat{\xi}, u, z) - K\bar{H})e - P\bar{Q}\hat{\xi} + \Gamma\omega - K\tilde{v}) + \|e\|_{\dot{S}}^2 + \|e\|_{S\Gamma W\Gamma' S} \\
&- \|e\|_{S\Gamma W\Gamma' S} + \|e\|_{SKVK'S}^2 - \|e\|_{SKVK'S}^2 d\tau) \\
&= \frac{1}{2} (\|x_t\|_{\Pi_t(\alpha, \beta)}^2 - \|e_t\|_{S_t}^2 + \int_0^t \|e\|_{\bar{Q} + S(\mathcal{A}(\hat{\xi}, u, z) - K\bar{H}) + (\mathcal{A}(\hat{\xi}, u, z) - K\bar{H})' S + S\Gamma W\Gamma' S + \dot{S}}^2 \\
&+ \|\hat{\xi}\|_{\bar{Q}}^2 + 2e'(\bar{Q} - SP\bar{Q})\hat{\xi} - \|\omega - W\Gamma' S e\|_{W^{-1}}^2 + \|u\|_R^2 \\
&- \|\tilde{v}\|_{V^{-1}}^2 - 2e' S K \tilde{v} + \|e\|_{SKVK'S}^2 - \|e\|_{SKVK'S}^2 d\tau) \\
&= \frac{1}{2} (\|x_t\|_{\Pi_t(\alpha, \beta)}^2 - \|e_t\|_{S_t}^2 \\
&+ \int_0^t \|e\|_{\bar{Q} + S(\mathcal{A}(\hat{\xi}, u, z) - K\bar{H}) + (\mathcal{A}(\hat{\xi}, u, z) - K\bar{H})' S + S\Gamma W\Gamma' S + SKVK'S + \dot{S}}^2 \\
&+ \|\hat{\xi}\|_{\bar{Q}}^2 + 2e'(\bar{Q} - SP\bar{Q})\hat{\xi} - \|\omega - W\Gamma' S e\|_{W^{-1}}^2 + \|u\|_R^2 \\
&- \|\tilde{v} + VK'S e\|_{V^{-1}}^2 d\tau)
\end{aligned} \tag{2.5.17}$$

By setting \dot{S} , P , ω , and \tilde{v} to the following values:

$$\mathbf{0} = \bar{Q} - SP\bar{Q} \rightarrow P = S^{-1} \tag{2.5.18}$$

$$-\dot{S} = \bar{Q} + S(\mathcal{A}(\hat{\xi}, u, z) - K\bar{H}) + (\mathcal{A}(\hat{\xi}, u, z) - K\bar{H})' S + S\Gamma W\Gamma' S + SKVK'S \tag{2.5.19}$$

$$\dot{P} = P\bar{Q}P + (\mathcal{A}(\hat{\xi}, u, z) - K\bar{H})' P + P(\mathcal{A}(\hat{\xi}, u, z) - K\bar{H}) + \Gamma W\Gamma' + KVK' \tag{2.5.20}$$

$$\omega_0^{t*} = W\Gamma' S e \tag{2.5.21}$$

$$\tilde{v}_0^{t*} = -VK'S e, \tag{2.5.22}$$

the error norm term and the cross term are eliminated, and the ω and \tilde{v} term in (2.5.17) are also maximized. If $P = S^{-1}$, then the cross term $e'(\bar{Q} - SP\bar{Q})\hat{\xi}$ would be zero and be eliminated from (2.5.17). Using \dot{S} in (2.5.19), we can eliminate the error norm term. The ω^* derived in (2.5.21) is the optimal strategy for $\omega_0^t(\cdot)$ and can maximizes (2.5.17).

We can choose $K = P\bar{H}'V^{-1}$, where $V \in \mathbb{R}^{r \times r}$ is a weighting parameter that can be used to tune observer convergence rate. By choosing $\bar{Q} = \bar{H}'\bar{H}$, the Riccati differential equation for P can be rewritten as:

$$\begin{aligned}\dot{P} &= \mathcal{A}(\hat{\xi}, u, z)'P + P\mathcal{A}(\hat{\xi}, u, z) + \Gamma W \Gamma' - P(\bar{H}'V^{-1}\bar{H} - \bar{Q})P \\ &= \mathcal{A}(\hat{\xi}, u, z)'P + P\mathcal{A}(\hat{\xi}, u, z) + \Gamma W \Gamma' - P\bar{H}'(V^{-1} - I_r)\bar{H}P\end{aligned}\tag{2.5.23}$$

If the pair $(\mathcal{A}(\hat{\xi}, u, z), \bar{H})$ is observable, a V can be chosen such that a solution to (2.5.23) exists. By decreasing the value of V , $I_r - V^{-1}$ decreases, which increases the steady-state value of S . In stochastic filters such as the Kalman filter, V corresponds to the measurement noise variance, while P corresponds to the estimation error variance. In the Kalman filter, a decrease in measurement noise variance results in a smaller error variance P . Since $P = S^{-1}$, a smaller P leads to a bigger S . Therefore, in the Kalman filter and the current nonlinear observer, the results are consistent: a decrease in V leads to an increase in the steady state value of S .

The observer can now be rewritten as:

$$\dot{\hat{\xi}} = F(\hat{\xi}, u) + S^{-1}\bar{Q}\hat{\xi} + S^{-1}\bar{H}'V^{-1}(z - \bar{H}\hat{\xi}), \quad \hat{\xi}(0) = \hat{\xi}_0\tag{2.5.24}$$

?? Using (2.5.18), (2.5.19) and (2.5.21), the optimal cost function (2.5.4) can now be written as:

$$J^* = \frac{1}{2} \max_{\xi} \left(\|x_t\|_{\Pi_t(\alpha, \beta)}^2 - \|e_t\|_{S_t}^2 + \int_0^t \|\hat{\xi}\|_{\bar{Q}}^2 + \|u\|_R^2 d\tau \right)\tag{2.5.25}$$

Now the only remaining player to be determined is ξ , which is used to derive the connection condition.

Remark 3. *Earlier in this section, a pseudo measurement noise \tilde{v} was added to the accumulation function. Without the addition of \tilde{v} to the measurement function and the cost function, the differential algebraic Riccati equation for P is:*

$$\dot{P} = P\bar{Q}P + (\mathcal{A}(\hat{\xi}, u, z) - K\bar{H})'P + P(\mathcal{A}(\hat{\xi}, u, z) - K\bar{H}) + \Gamma W \Gamma',$$

where K can be chosen as $P\bar{H}'V^{-1}$. The corresponding error dynamics does not change. With perfect partial measurement, some elements of P associated with the perfectly measured x_t element will tend to zero rapidly, while the part of P associated with the unknown parameters may lag behind and tend to a constant. Since $P^{-1} = S$, numerical propagation issues such as the inversion of P to obtain S may arise. Hence, $\tilde{\nu}$ and V are added to the measurement noise and the cost function to keep the steady state $P > c\mathbf{I} > \mathbf{0}$, where c is a positive scalar.

2.6 The Connection Condition

The maximization of (2.5.25) with respect to ξ_t is carried out in this section. Recall ξ_t contains both the initial state x_t as well as the unknown parameters. The integral term in (2.5.25) does not contain ξ_t and will not be part of the maximization. Therefore, only the boundary terms at time t in (2.5.25) are part of the maximization of ξ that yield the connection condition. Define the value function at current time t :

$$\mathbf{V}_t = \frac{1}{2} \left(\|x_t\|_{\Pi_t(\alpha, \beta)}^2 - \|e_t\|_{S_t}^2 \right). \quad (2.6.1)$$

Let $\xi_r = \begin{bmatrix} \alpha' & \beta' \end{bmatrix}'$. Define $S_t = S(t)$ at the current time t as:

$$S_t = \begin{bmatrix} S_x(t) & S_c(t) \\ S'_c(t) & S_{\xi_r}(t) \end{bmatrix}. \quad (2.6.2)$$

$S_x(t) \in \mathbb{R}^{n \times n}$ is the weighting for the error of x at time t . $S_c(t) \in \mathbb{R}^{n \times l+k}$ is the weighting between the error of x and the error of ξ_r at time t . $S_{\xi_r}(t) \in \mathbb{R}^{l+k \times l+k}$ is the weighting for the error of ξ_r at time t . For the value function \mathbf{V}_t to be maximizing, the first derivative of \mathbf{V}_t with respect to ξ is zero, while the second derivative of \mathbf{V}_t with respect to ξ is negative. The maximization of \mathbf{V}_t with

respect to ξ yields the first order optimality condition:

$$\begin{aligned} \left. \frac{\partial \mathbf{V}_t}{\partial \xi} \right|_{\xi=\xi^*(t)} &= \left(\left[\begin{array}{c} \Pi_t(\alpha, \beta)x_t \\ \frac{1}{2}x_t' \frac{\partial \Pi_t(\alpha, \beta)}{\partial \xi_r} x_t \end{array} \right] - S_t e_t \right) \Bigg|_{\xi=\xi^*(t)} = \mathbf{0} \\ &\rightarrow \left[\begin{array}{c} \Pi_t(\alpha, \beta)x_t \\ \frac{1}{2}x_t' \frac{\partial \Pi_t(\alpha, \beta)}{\partial \xi_r} x_t \end{array} \right] \Bigg|_{\xi=\xi^*(t)} = \left[\begin{array}{c} S_x(t)(x_t - \hat{x}_t) + S_c(t)(\xi_r(t) - \hat{\xi}_r(t)) \\ S'_c(t)(x_t - \hat{x}_t) + S_{\xi_r}(t)(\xi_r(t) - \hat{\xi}_r(t)) \end{array} \right]. \end{aligned} \quad (2.6.3)$$

Note $\frac{\partial \Pi_t(\alpha, \beta)}{\partial \xi_r}$ is a three dimensional tensor of size $n \times n \times l + k$. Hence, $x_t' \frac{\partial \Pi_t(\alpha, \beta)}{\partial \xi_r} x_t$ is a $l + k \times 1$ vector. The second derivative of \mathbf{V}_t with respect to ξ yields the second order sufficient condition for optimality:

$$\begin{aligned} \left. \frac{\partial^2 \mathbf{V}_t}{\partial \xi \partial \xi'} \right|_{\xi=\xi^*(t)} &= \left[\begin{array}{cc} \frac{\partial^2 \mathbf{V}_t}{\partial x \partial x'} & \frac{\partial^2 \mathbf{V}_t}{\partial x \partial \xi'_r} \\ \left(\frac{\partial^2 \mathbf{V}_t}{\partial x \partial \xi'_r} \right)' & \frac{\partial^2 \mathbf{V}_t}{\partial \xi_r \partial \xi'_r} \end{array} \right] \Bigg|_{\xi=\xi^*(t)} \\ &= \left[\begin{array}{cc} \Pi_t(\alpha, \beta) & \frac{\partial \Pi_t(\alpha, \beta)}{\partial \xi_r} x_t \\ \left(\frac{\partial \Pi_t(\alpha, \beta)}{\partial \xi_r} x_t \right)' & \frac{1}{2}x_t' \frac{\partial^2 \Pi_t(\alpha, \beta)}{\partial \xi_r \partial \xi'_r} x_t \end{array} \right] - S_t \Bigg|_{\xi=\xi^*(t)} \\ &= \left[\begin{array}{cc} \Pi_t(\alpha, \beta) - S_x(t) & \frac{\partial \Pi_t(\alpha, \beta)}{\partial \xi_r} x_t - S_c(t) \\ \left(\frac{\partial \Pi_t(\alpha, \beta)}{\partial \xi_r} x_t \right)' - S'_c(t) & \frac{1}{2}x_t' \frac{\partial^2 \Pi_t(\alpha, \beta)}{\partial \xi_r \partial \xi'_r} x_t - S_{\xi_r}(t) \end{array} \right] \Bigg|_{\xi=\xi^*(t)} < \mathbf{0} \end{aligned} \quad (2.6.4)$$

For (2.6.4) to be satisfied, the upper left term $\frac{\partial^2 \mathbf{V}_t}{\partial x \partial x'}$ must be negative definite. After evaluation, the upper left term is:

$$\frac{\partial^2 \mathbf{V}_t}{\partial x \partial x'} = \Pi_t(\alpha, \beta) - S_x < \mathbf{0}. \quad (2.6.5)$$

This is also the spectral radius condition that exists in many previous literatures, such as [50], [29], [5] and [32].

The partial derivative of $\Pi_t(\alpha, \beta)$ with respect to ξ_r in the first order optimality condition is an

$n \times n \times l + k$ tensor. Therefore $\frac{1}{2}x_t' \frac{\partial \Pi_t(\alpha, \beta)}{\partial \xi_r} x_t$ is a $l + k \times 1$ vector:

$$\frac{1}{2}x_t' \frac{\partial \Pi_t(\alpha, \beta)}{\partial \xi_r} x_t = \frac{1}{2} \left[\begin{array}{c} x_t' \frac{\partial \Pi_t(\alpha, \beta)}{\partial \alpha_1} x_t \\ \vdots \\ x_t' \frac{\partial \Pi_t(\alpha, \beta)}{\partial \alpha_l} x_t \\ x_t' \frac{\partial \Pi_t(\alpha, \beta)}{\partial \beta_1} x_t \\ \vdots \\ x_t' \frac{\partial \Pi_t(\alpha, \beta)}{\partial \beta_k} x_t \end{array} \right]_{\xi_r = \xi_r^*(t)} \quad (2.6.6)$$

The second partial of $\Pi_t(\alpha, \beta)$ with respect to ξ_r in the second order optimality condition is an $n \times n \times l + k \times l + k$ tensor. Therefore, the resulting derivative is an $l + k \times l + k$ matrix:

$$x_t' \frac{\partial^2 \Pi_t(\alpha, \beta)}{\partial \xi_r \partial \xi_r'} x_t = \begin{bmatrix} x_t' \frac{\partial^2 \Pi_t(\alpha, \beta)}{\partial \alpha_1^2} x_t & \cdots & x_t' \frac{\partial^2 \Pi_t(\alpha, \beta)}{\partial \alpha_1 \alpha_l} x_t & x_t' \frac{\partial^2 \Pi_t(\alpha, \beta)}{\partial \alpha_1 \beta_1} x_t & \cdots & x_t' \frac{\partial^2 \Pi_t(\alpha, \beta)}{\partial \alpha_1 \beta_k} x_t \\ \vdots & & & \cdots & & \vdots \\ x_t' \frac{\partial^2 \Pi_t(\alpha, \beta)}{\partial \alpha_l \alpha_1} x_t & \cdots & x_t' \frac{\partial^2 \Pi_t(\alpha, \beta)}{\partial \alpha_l^2} x_t & x_t' \frac{\partial^2 \Pi_t(\alpha, \beta)}{\partial \alpha_l \beta_1} x_t & \cdots & x_t' \frac{\partial^2 \Pi_t(\alpha, \beta)}{\partial \alpha_l \beta_k} x_t \\ x_t' \frac{\partial^2 \Pi_t(\alpha, \beta)}{\partial \beta_1 \alpha_1} x_t & \cdots & x_t' \frac{\partial^2 \Pi_t(\alpha, \beta)}{\partial \beta_1 \alpha_l} x_t & x_t' \frac{\partial^2 \Pi_t(\alpha, \beta)}{\partial \beta_1 \beta_1} x_t & \cdots & x_t' \frac{\partial^2 \Pi_t(\alpha, \beta)}{\partial \beta_1 \beta_k} x_t \\ \vdots & & & \cdots & & \vdots \\ x_t' \frac{\partial^2 \Pi_t(\alpha, \beta)}{\partial \beta_k \alpha_1} x_t & \cdots & x_t' \frac{\partial^2 \Pi_t(\alpha, \beta)}{\partial \beta_k \alpha_l} x_t & x_t' \frac{\partial^2 \Pi_t(\alpha, \beta)}{\partial \beta_k \beta_1} x_t & \cdots & x_t' \frac{\partial^2 \Pi_t(\alpha, \beta)}{\partial \beta_k \beta_k} x_t \end{bmatrix},$$

where each element of the matrix, such as $x_t' \frac{\partial^2 \Pi_t(\alpha, \beta)}{\partial \beta_k^2} x_t$, is a scalar number.

Remark 4. An optimal strategy (2.4.5) for ω_t^T was derived in the optimization of the return function. Similarly, an optimal strategy (2.5.22) for ω_0^t was derived in the optimization of the accumulation function. The optimal strategies ω_t^{T*} (2.4.5) and ω_0^{t*} (2.5.22) are equal at current time t due to the first order necessary condition (2.6.3). Define ω_0^{t*} evaluated at current time t as $\omega_0^{t*}(t)$, and define ω_t^{T*} evaluated at current time t as $\omega_t^{T*}(t)$. Then, by rewriting $\omega_0^{t*}(t)$ using the first order

necessary condition (2.6.3) at current time t yields:

$$\begin{aligned}
\omega_0^{t*}(t) &= W \begin{bmatrix} G' & \mathbf{0} \end{bmatrix} Se \Big|_{\xi=\xi^*} \\
&= WG' \left(S_x(t)(x_t - \hat{x}_t) + S_c(t)(\xi_r(t) - \hat{\xi}_r(t)) \right) \Big|_{\xi=\xi^*} \\
&= WG' \Pi_t(\alpha^*, \beta^*) x_t^* \\
&= \omega_t^{T*}(t).
\end{aligned} \tag{2.6.7}$$

This implies at the current time t , the worst case past process disturbance $\omega_0^{t*}(t)$ to the observer is the same as the worst case process disturbance $\omega_t^{T*}(t)$ for the controller.

Chapter 3

Existence of Saddle-Point

The optimization of the cost function (2.2.5) in the previous sections assumes the existence of saddle point in J . Now, the worst case solution derived in the previous section can be used to verify it is indeed a saddle point of the cost function J , which means it satisfies the saddle-point condition: $J(u^*, \xi, \omega) \leq J(u^*, \xi^*, \omega^*) \leq J(u, \xi^*, \omega^*)$.

Theorem 3.0.1. *If a saddle point of the cost function (2.2.5) exists, then the optimized cost function $J(u^*, \xi^*, \omega^*)$ derived using the worst case strategies u^* (2.4.4), ξ^* (2.6.3, 2.6.4), and ω^* (2.4.5) is a saddle point of the cost function J (2.2.5).*

Proof. As it was done before, we add two zero terms $\frac{1}{2}\{-x'\Pi x|_t^T + \int_t^T \frac{d}{d\tau} x'\Pi x d\tau\}$ and $\frac{1}{2}\{\int_0^t \frac{d}{d\tau} e'S e d\tau - e'S e|_0^t\}$ to the finite-time cost function (2.2.5). After performing similar algebraic manipulations as in sections V and VI and setting the current time $t = 0$, $S_0 = P_0^{-1}$, and $Q_T = \Pi_T(\alpha, \beta)$, the cost

function (2.2.5) can be written as:

$$\begin{aligned}
J &= \frac{1}{2} \{ \|x_0\|_{\Pi_0(\alpha, \beta)}^2 - \|e_0\|_{P_0^{-1}}^2 \\
&+ \int_0^T \|u + R^{-1}B(\beta)' \Pi x\|_R^2 - \|\omega - WG' \Pi x\|_{W^{-1}}^2 \\
&+ \|x\|_{(Q+A(\alpha)'\Pi+\Pi A(\alpha)+\Pi(GWG'-B(\beta)R^{-1}B(\beta)')\Pi+\dot{\Pi})}^2 d\tau \}.
\end{aligned} \tag{3.0.1}$$

If all players play their optimal strategies, then the optimal cost function is:

$$J(u^*, \xi_0^*, \omega^*) = \frac{1}{2} \{ \|x_0\|_{\Pi_0(\alpha, \beta)}^2 - \|e_0\|_{P_0^{-1}}^2 \} \Big|_{\xi_0 = \xi_0^*}. \tag{3.0.2}$$

Now consider $J(u^*, \xi, \omega)$, where the control is the worst case control u^* , $\Pi(\alpha^*, \beta^*)$ is propagated using worst case system parameters, and its derivative is defined as:

$$\begin{aligned}
-\dot{\Pi}(\alpha^*, \beta^*) &= Q + A(\alpha^*)' \Pi(\alpha^*, \beta^*) + \Pi(\alpha^*, \beta^*) A(\alpha^*) \\
&+ \Pi(\alpha^*, \beta^*) (GWG' - B(\beta^*) R^{-1} B(\beta^*)') \Pi(\alpha^*, \beta^*) \\
\Pi_T(\alpha^*, \beta^*) &= Q_T.
\end{aligned} \tag{3.0.3}$$

Then, the cost function using optimal input and suboptimal disturbances is:

$$\begin{aligned}
J(u^*, \xi, \omega) &= \frac{1}{2} \{ \|x_0\|_{\Pi_0(\alpha^*, \beta^*)}^2 - \|e_0\|_{P_0^{-1}}^2 \\
&- \int_0^T \|\omega - WG' \Pi(\alpha^*, \beta^*) x\|_{W^{-1}}^2 d\tau \}.
\end{aligned} \tag{3.0.4}$$

The integral in (3.0.4) is negative definite. Furthermore, e_0 , which is not maximized with respect to α and β , is a function of suboptimal α and β . Thus, $J(u^*, \xi, \omega) \leq J(u^*, \xi^*, \omega^*)$. Next, consider the cost function:

$$\begin{aligned}
J(u, \xi^*, \omega^*) &= \frac{1}{2} \{ \|x_0^*\|_{\Pi_0(\alpha, \beta)}^2 - \|e_0^*\|_{P_0^{-1}}^2 \\
&+ \int_0^T \|u + R^{-1}B(\beta^*)' \Pi(\alpha^*, \beta^*) x\|_R^2 d\tau \}.
\end{aligned} \tag{3.0.5}$$

The integral in (3.0.5) is positive and $-\|e_0^*\|_{P_0^{-1}}^2$ is the worst-case strategy played by ξ , so $J(u^*, \xi^*, \omega^*) \leq$

$J(u, \xi^*, \omega^*)$ and saddle-point exists. Hence, the order of the min and max operators can be exchanged without changing the optimality of cost function. \square

The following lemma is presented to assist in the derivation of Lemma 4.0.1.

Lemma 3.0.2. *The optimal value (3.0.2) of the cost function (2.2.5) is equal to the optimized cost function (2.5.25) at the current time t for all t as stated below:*

$$\begin{aligned} J(u^*, \xi^*, \omega^*) &= \frac{1}{2} \left\{ \|x_0\|_{\Pi_0(\alpha, \beta)}^2 - \|e_0\|_{P_0^{-1}}^2 \right\} \Big|_{\xi_0 = \xi_0^*} \\ &= \frac{1}{2} \left(\|x_t\|_{\Pi_t(\alpha, \beta)}^2 - \|e_t\|_{S_t}^2 + \int_0^t \|\hat{\xi}\|_Q^2 + \|u\|_R^2 d\tau \right) \Big|_{\xi_t = \xi_t^*}. \end{aligned}$$

Proof. The cost function (2.2.5) can be separated into the accumulation function (2.3.1) and the return function (2.3.2) at the current time t . The cost function, accumulation function and return function are repeated here for reference.

$$\begin{aligned} J &= \frac{1}{2} \left\{ \|x_T\|_{Q_T}^2 - \|e_0\|_{P_0^{-1}}^2 + \int_0^T \|x\|_Q^2 + \|u\|_R^2 - \|\omega\|_{W^{-1}}^2 d\tau \right\} \\ &= J_f(0, t) + J_c(t, T) \\ J_f(0, t) &= \frac{1}{2} \left\{ -\|e_0\|_{P_0^{-1}}^2 + \int_0^t \|x\|_Q^2 + \|u\|_R^2 - \|\omega\|_{W^{-1}}^2 d\tau \right\} \\ J_c(t, T) &= \frac{1}{2} \left\{ \|x_T\|_{Q_T}^2 + \int_t^T \|x\|_Q^2 + \|u\|_R^2 - \|\omega\|_{W^{-1}}^2 d\tau \right\}. \end{aligned}$$

The optimization of the cost function (2.2.5) was shown in the previous section to be:

$$J^* = \frac{1}{2} \left\{ \|x_0\|_{\Pi_0(\alpha, \beta)}^2 - \|e_0\|_{P_0^{-1}}^2 \right\} \Big|_{\xi_0 = \xi_0^*}.$$

The optimization of $J_f(0, t) + J_c(t, T)$ was also shown in the previous section to be:

$$\min_{u \in U} \max_{\xi, \omega \in \Omega} (J_f(0, t) + J_c(t, T)) = \frac{1}{2} \left(\|x_t\|_{\Pi_t(\alpha, \beta)}^2 - \|e_t\|_{S_t}^2 + \int_0^t \|\hat{\xi}\|_Q^2 + \|u\|_R^2 d\tau \right) \Big|_{\xi_t = \xi_t^*}.$$

Since $J = J_f(0, t) + J_c(t, T)$, then the optimal values must be equal, therefore:

$$J^* = \frac{1}{2} \{ \|x_0\|_{\Pi_0(\alpha, \beta)}^2 - \|e_0\|_{P_0^{-1}}^2 \} \Big|_{\xi_0 = \xi_0^*} = \frac{1}{2} \left(\|x_t\|_{\Pi_t(\alpha, \beta)}^2 - \|e_t\|_{S_t}^2 + \int_0^t \|\hat{\xi}\|_Q^2 + \|u\|_R^2 d\tau \right) \Big|_{\xi_t = \xi_t^*} .$$

□

Chapter 4

Infinite-Time Problem: Stability of Close-Loop System

In this section, we consider the stability of the close-loop system for the infinite-time problem. The dynamics of the worst-case state x^* can be written as:

$$\begin{aligned}\dot{x}^* &= f(\xi^*, u^*) + G\omega^* = A(\alpha^*)x^* + B(\beta^*)u^* + G\omega^* \\ &= \underbrace{(A(\alpha^*) - (B(\beta^*)R^{-1}B(\beta^*)' - GWG')\Pi(\alpha^*, \beta^*))}_{\tilde{A}(\alpha^*, \beta^*)} x^* \\ &= \tilde{A}(\alpha^*, \beta^*)x^*,\end{aligned}\tag{4.0.1}$$

where $\tilde{A}(\alpha^*, \beta^*)$ is the worst-case close-loop system matrix at time t . Note the parameter estimates $\hat{\xi}_r$, subject to the dynamic equation (2.5.24), are time-varying functions. Therefore, the worst-case parameters α^* and β^* , which satisfies the optimality conditions (2.6.3) and (2.6.4) at current time t , are also time-varying functions, i.e., $\alpha^* = \alpha^*(t)$ and $\beta^* = \beta^*(t)$. Hence, $\tilde{A}(\alpha^*, \beta^*) = \tilde{A}(\alpha^*(t), \beta^*(t))$. Due to the time-varying nature of $\tilde{A}(\alpha^*(t), \beta^*(t))$, the stability of the close loop system cannot be deduced from its eigenvalues. Further analysis must be performed to determine the stability of the

worst case controller.

To prove stability of the close-loop system for the infinite-time problem, we present five necessary assumptions for the existence of minimax solution to the uncertain system. Theorem 4.0.4 proves the disturbance attenuation property of the modified gain observer and the stability of the worst case controller using a Lyapunov function. Three lemmas are presented in order to assist in the derivation of theorem 4.0.4.

Remark 5. *One can also prove the stability of the close loop system by verifying the value function (2.6.1) satisfies the Hamilton-Jacobi-Issac's equation as was done in [26].*

Lemma 4.0.1 proves the worst case error is stable and converges to zero. Lemma 4.0.2 proves the worst case input generated using $\Pi(\alpha^*, \beta^*)$ stabilizes the worst case close loop system $\tilde{A}(\alpha^*, \beta^*)$. Lemma 4.0.3 proves that the steady state value of S_c is zero. Using lemmas 4.0.1- 4.0.3 in theorem 4.0.4, it is proved that the state estimation error $e_x \rightarrow 0$, parameter estimation error e_{ξ_r} is bounded, and the resulting close loop state x is stable and tends to zero.

In the infinite-time system, the terminal time $T \rightarrow \infty$, and we arbitrarily set $Q_T = \mathbf{0}$ for simplicity. Q_T may be any finite positive semi-definite matrix. Note that the different user defined values of Q_T does not change the steady-state solution of the control algebraic Riccati equation [51]. We make the following five assumptions:

Assumption 1. *For all α and β , $(A(\alpha), B(\beta))$ is a stabilizable pair, and $(A(\alpha), H)$ is a detectable pair.*

Remark 6. *Assumption 1 is required for the design of any feasible controller and observer.*

Assumption 2. *For all α , $(A(\alpha), G)$ is a controllable pair, and $(A(\alpha), C)$ is a observable pair, where $Q = C'C$.*

Assumption 3. *There exists a minimal bounded positive definite solution $\Pi_t(\alpha, \beta) > \mathbf{0}$ of the differential Riccati equation (2.4.6) with terminal boundary condition $\Pi_\infty(\alpha, \beta) = Q_T = \mathbf{0}$ for all α and β .*

Remark 7. Given Assumption 2, if the solution $\Pi(\alpha, \beta)$ to the Riccati equation (2.4.6) in Assumption 3 exists, then $\Pi(\alpha, \beta) > \mathbf{0}$ [2] [52]. In the standard H_∞ problem as presented by Doyle, Glover, Khargonekar, and Francis [5], Doyle et al. assume a weaker assumption of $(A(\alpha), G)$ is a stabilizable pair, and $(A(\alpha), C)$ is a detectable pair. With a weaker assumption, if the resulting solution to the Riccati equation exists, the solution is guaranteed to be nonnegative, i.e., $\Pi_t(\alpha, \beta) \geq \mathbf{0}$.

Assumption 4. There exists a minimal positive-definite bounded solution $S > \mathbf{0}$ of the differential Riccati equation (2.5.19) with terminal boundary condition $S(0) = Q_0 > \mathbf{0}$.

Remark 8. Since \mathbf{V}_t (2.6.1) is a function of $\Pi_t(\alpha, \beta)$ and S , Assumption 3 and Assumption 4 are required for the existence of the value function \mathbf{V}_t .

Assumption 5. The value function \mathbf{V}_t (2.6.1) is finite for all possible α and β .

Remark 9. Assumption 5 is required for the existence of a maximizing solution that satisfies the connection condition. If the value function is infinite, then no maximum exists, and hence no saddle point solution exists.

Given the above assumptions, in order to facilitate the stability analysis of the H_∞ controller with a modified-gain observer, we introduce the following lemmas.

Lemma 4.0.1. Given Assumptions (1-5) are satisfied and suppose the minimax solution exists for all time, then as $t \rightarrow \infty$ the worst case error $e^* \rightarrow \mathbf{0}$ and $\|\hat{x}\|_Q \rightarrow 0$.

Proof. The optimal cost function J^* (3.0.2) is dependent on the initial worst case ξ_0^* , $\hat{\xi}_0$ and the initial weighting S_0 . The initial estimate $\hat{\xi}_0$ and initial boundary condition S_0 can be chosen such that the optimal cost is bounded, i.e., $J^* < \infty$. This implies that ξ^* is finite and can be obtained from $\hat{\xi}_0$ and S_0 . At current time t , the optimal cost can be written as (2.5.25). Since there is only

one optimal cost as shown in lemma 3.0.2, setting (3.0.2) equal to (2.5.25) and taking $t \rightarrow \infty$ yields:

$$\begin{aligned} & \frac{1}{2} \max_{\xi_\infty} \left(\|x_\infty\|_{\Pi_\infty(\alpha, \beta)}^2 - \|e_\infty\|_{S_\infty}^2 \right) + \int_0^{t \rightarrow \infty} \|\hat{x}\|_Q^2 + \|u\|_R^2 d\tau \\ & = \frac{1}{2} \left\{ \|x_0\|_{\Pi_0(\alpha, \beta)}^2 - \|e_0\|_{P_0^{-1}}^2 \right\} \Big|_{\xi_0 = \xi_0^*} < \infty. \end{aligned} \quad (4.0.2)$$

Since Assumption 3 is satisfied for all time, the boundary condition of $\Pi_\infty(\alpha, \beta) = \mathbf{0}$ must also satisfy the connection condition at the terminal time. The value function at terminal time can be written as:

$$\begin{aligned} \mathbf{V}_\infty^* & = \max_{\xi} \|x_\infty\|_{\Pi_\infty(\alpha, \beta)}^2 - \|\xi_\infty - \hat{\xi}_\infty\|_{S_\infty}^2 \\ & = \max_{\xi} -\|\xi_\infty - \hat{\xi}_\infty\|_{S_\infty}^2 = \max_{\xi} -\|e_\infty^*\|_{S_\infty}^2. \end{aligned}$$

Since $S_\infty > \mathbf{0}$, the maximization of the value function at terminal time yields the worst case error $e_\infty^* = \mathbf{0}$ and $\xi_\infty^* = \hat{\xi}_\infty$. Since the optimal cost function J^* (3.0.2) is bounded, the integral term $\int_0^\infty \|\hat{x}\|_Q^2 + \|u\|_R^2 d\tau$, which is positive semi-definite, must also be bounded. Since R is invertible, u must tend to zero as $t \rightarrow \infty$. Since Q is a positive semi-definite matrix, $\|\hat{x}\|_Q^2 \rightarrow 0$ as $t \rightarrow \infty$. Since $e^* \rightarrow \mathbf{0}$ and $\|\hat{x}\|_Q^2 \rightarrow 0$ as $t \rightarrow \infty$, $\|x^*\|_Q^2 \rightarrow 0$ as $t \rightarrow \infty$. \square

Lemma 4.0.2. *Given Assumption 3 is satisfied and suppose the worst-case ξ_r^* is time-invariant for $t < \tau < \infty$, then the worst-case close loop system is stable.*

Proof. The worst-case state x^* is subject to:

$$\dot{x}^* = A(\alpha^*)x^* + B(\beta^*)u^* + G\omega^* = \tilde{A}(\xi_r^*)x^*, \quad (4.0.3)$$

where the worst-case close loop dynamic is $\tilde{A}(\xi_r^*) = A(\alpha^*) - (B(\beta^*)R^{-1}B(\beta^*)' - GWG')\Pi(\xi_r^*)$. Add the zero term $\pm \Pi B(\beta)R^{-1}B(\beta)'\Pi \pm \Pi GWG'\Pi$ to (2.4.6) so that it can be rewritten in terms of the close loop dynamic $\tilde{A}(\xi_r^*)$ to yield:

$$\mathbf{0} = \dot{\Pi} + Q + \tilde{A}(\xi_r^*)'\Pi + \Pi\tilde{A}(\xi_r^*) + \Pi(B(\beta^*)R^{-1}B(\beta^*)' - GWG')\Pi. \quad (4.0.4)$$

Since (2.4.6) exists and is bounded per Assumption 3 for all t , then $\tilde{A}(\xi_r^*)$ is Hurwitz at every time instance t . This has been proved in section 5 of [29] using Lemma 4.1 and Lemma 4.2 from [53]. Classical stability results in [54] states that if $\tilde{A}(\xi_r^*, t)$ tends to a constant Hurwitz matrix \bar{A} as $t \rightarrow \infty$, then the system is exponentially stable. By the assumption that ξ_r^* is time-invariant for the time period $t < \tau < \infty$, then $\tilde{A}(\xi_r^*) = \bar{A}$ for $t < \tau < \infty$. Since $\tilde{A}(\xi_r^*)$ is Hurwitz at all times, \bar{A} must also be Hurwitz, and $x^* \rightarrow \mathbf{0}$ as $t \rightarrow \infty$. \square

Lemma 4.0.3. *Let the steady state solution to the observer Riccati equation (2.5.19) be defined as S_{ss} , where S_{ss} is defined as:*

$$S_{ss} = \begin{bmatrix} S_{ss,x} & S_{ss,c} \\ S'_{ss,c} & S_{ss,\xi_r} \end{bmatrix} \quad (4.0.5)$$

Suppose $z = \mathbf{0}$ and $u = \mathbf{0}$, then $S_{ss,c} = \mathbf{0}$

Proof. Suppose both the measurement z and input u are zero, then $\mathcal{A}(\hat{\xi}, u, z)$ has the form:

$$\mathcal{A}(\hat{\xi}, \mathbf{0}, \mathbf{0}) = \begin{bmatrix} A(\hat{\alpha}) & \mathbf{0} \\ \mathbf{0} & \mathbf{0} \end{bmatrix}. \quad (4.0.6)$$

Note $S_{ss}^{-1} = P_{ss}$, where P_{ss} is the steady state value of P . Then, the steady state Riccati equation

for the observer (2.5.19) can be written as:

$$\begin{aligned}
\mathbf{0} &= \begin{bmatrix} Q & \mathbf{0} \\ \mathbf{0} & \mathbf{0} \end{bmatrix} + S_{ss} \mathcal{A}(\hat{\xi}, \mathbf{0}, \mathbf{0}) - S_{ss} P \bar{H}' V^{-1} \bar{H} + A'(\hat{\xi}, \mathbf{0}, \mathbf{0}) S_{ss} - \bar{H}' V^{-1} \bar{H} P S_{ss} \\
&+ S_{ss} \begin{bmatrix} G W G' & \mathbf{0} \\ \mathbf{0} & \mathbf{0} \end{bmatrix} S_{ss} + S_{ss} P \bar{H}' V^{-1} \bar{H} P S_{ss} \\
&= \begin{bmatrix} Q & \mathbf{0} \\ \mathbf{0} & \mathbf{0} \end{bmatrix} + S_{ss} \mathcal{A}(\hat{\xi}, \mathbf{0}, \mathbf{0}) + A'(\hat{\xi}, \mathbf{0}, \mathbf{0}) S_{ss} - \begin{bmatrix} H' V^{-1} H & \mathbf{0} \\ \mathbf{0} & \mathbf{0} \end{bmatrix} + S_{ss} \begin{bmatrix} G W G' & \mathbf{0} \\ \mathbf{0} & \mathbf{0} \end{bmatrix} S_{ss} \\
&= \begin{bmatrix} Q & \mathbf{0} \\ \mathbf{0} & \mathbf{0} \end{bmatrix} + \begin{bmatrix} S_{ss,x} A(\hat{\alpha}) & \mathbf{0} \\ S'_{ss,c} A(\hat{\alpha}) & \mathbf{0} \end{bmatrix} + \begin{bmatrix} A'(\hat{\alpha}) S_{ss,x} & A'(\hat{\alpha}) S_{ss,c} \\ \mathbf{0} & \mathbf{0} \end{bmatrix} - \begin{bmatrix} H' V^{-1} H & \mathbf{0} \\ \mathbf{0} & \mathbf{0} \end{bmatrix} \\
&+ \begin{bmatrix} S_{ss,x} G W G' S_{ss,x} & S_{ss,x} G W G' S_{ss,c} \\ S'_{ss,c} G W G' S_{ss,x} & S'_{ss,c} G W G' S_{ss,c} \end{bmatrix} \\
&= \begin{bmatrix} Q + S_{ss,x} A(\hat{\alpha}) + A'(\hat{\alpha}) S_{ss,x} - H' V^{-1} H + S_{ss,x} G W G' S_{ss,x} & A'(\hat{\alpha}) S_{ss,c} + S_{ss,x} G W G' S_{ss,c} \\ S'_{ss,c} A(\hat{\alpha}) + S'_{ss,c} G W G' S_{ss,x} & S'_{ss,c} G W G' S_{ss,c} \end{bmatrix}.
\end{aligned} \tag{4.0.7}$$

Upon examination, equation (4.0.7) yields the following result:

$$-\dot{S}_{ss,x} = \mathbf{0} = Q + S_{ss,x} A(\hat{\alpha}) + A'(\hat{\alpha}) S_{ss,x} - H' V^{-1} H + S_{ss,x} G W G' S_{ss,x} \tag{4.0.8}$$

$$-\dot{S}_{ss,c} = \mathbf{0} = A'(\hat{\alpha}) S_{ss,c} + S_{ss,x} G W G' S_{ss,c} \tag{4.0.9}$$

$$-\dot{S}_{ss,\xi_r} = \mathbf{0} = S'_{ss,c} G W G' S_{ss,c}. \tag{4.0.10}$$

Since $-\dot{S}_{ss,\xi_r} = \mathbf{0}$ in steady state and W is full rank, $G' S_{ss,c} = \mathbf{0}$. Since G is given and cannot be zero, either $S_{ss,c} = \mathbf{0}$ or $S_{ss,c} \neq \mathbf{0}$ is in the null space of G . Consider the case $S_{ss,c} = \mathbf{0}$, then $S'_{ss,c} G W G' S_{ss,c} = \mathbf{0}$, which satisfies both (4.0.9) and (4.0.10). Consider the second case where $S_{ss,c} \neq \mathbf{0}$ but $S_{ss,c}$ is in the null space of G . As such, (4.0.10) is satisfied, but (4.0.9) might not be. Therefore, to ensure both (4.0.9) and (4.0.10) are satisfied, $S_{ss,c}$ must be zero. Since $S_{ss,x} > \mathbf{0}$, $S_{ss,\xi_r} > \mathbf{0}$, and $S_{ss,c} = \mathbf{0}$, then $S_{ss} > \mathbf{0}$. \square

The following theorem proves disturbance attenuation as well as the stability of the close loop system using a Lyapunov function.

Theorem 4.0.4. *Given Assumptions (1-5), suppose a minimax solution to the infinite-time problem for the uncertain system exists for all time, then the close loop system is stable, and the estimation error is bounded as $t \rightarrow \infty$. Furthermore, $\hat{x} \rightarrow \mathbf{0}$ and $e_x \rightarrow \mathbf{0}$ as $t \rightarrow \infty$.*

Remark 10. *The proof for theorem 4.0.4) is summarized. A Lyapunov function \mathbf{W} is defined in (4.0.11). Its derivative (4.0.12) is simplified to five quadratic terms as shown in (4.0.16). Using Assumptions (1-5) and lemma 4.0.1, as $t \rightarrow \infty$, then $e^* \rightarrow \mathbf{0}$, $\omega^* \rightarrow \mathbf{0}$ and $\|\hat{x}\|_Q^2 \rightarrow 0$. Assumption 1 is used to deduce $\|He_x\|_{V^{-1}}^2 \rightarrow 0$ and $e_x \rightarrow \mathbf{0}$. Assumption 2, lemma 4.0.2, and $e_x \rightarrow \mathbf{0}$ implies the stability of the close loop system and $\|He_x\|_{V^{-1}}^2 \rightarrow 0$. Lastly, lemma 4.0.3 and $e_x \rightarrow \mathbf{0}$ implies $\|\mathbf{W}\Gamma'Se\|_{W^{-1}}^2 \rightarrow 0$ and e_{ξ_r} is a bounded vector. Since all terms in (4.0.12) tends to zero as $t \rightarrow \infty$, then \mathbf{W} is bounded.*

Proof. Let \mathbf{W} be a Lyapunov function for the error defined as:

$$\mathbf{W} = \frac{1}{2}e'Se \geq 0, \quad S > \mathbf{0}. \quad (4.0.11)$$

The time derivative of \mathbf{W} is shown below:

$$\dot{\mathbf{W}} = e'S\dot{e} + \frac{1}{2}e'\dot{S}e. \quad (4.0.12)$$

Substituting \dot{e} (2.5.12) and \dot{S} (2.5.19) back into $\dot{\mathbf{W}}$ (4.0.12) yields:

$$\begin{aligned}
\dot{\mathbf{W}} &= e'S \left((\mathcal{A}(\hat{\xi}, u, z) - K\bar{H})e - P\bar{Q}\hat{\xi} + \Gamma\omega - K\tilde{\nu} \right) \\
&\quad - \frac{1}{2} \|e\|_{\bar{Q}+S(\mathcal{A}(\hat{\xi}, u, z) - K\bar{H})+(\mathcal{A}(\hat{\xi}, u, z) - K\bar{H})'S+S\Gamma W\Gamma'+SKVK'S}^2 \\
&= \frac{1}{2} \|e\|_{S(\mathcal{A}(\hat{\xi}, u, z) - K\bar{H})+(\mathcal{A}(\hat{\xi}, u, z) - K\bar{H})'S - (\bar{Q}+S(\mathcal{A}(\hat{\xi}, u, z) - K\bar{H})+(\mathcal{A}(\hat{\xi}, u, z) - K\bar{H})'S+S\Gamma W\Gamma'+SKVK'S)}^2 \\
&\quad - e'\bar{Q}\hat{\xi} + e'S\Gamma\omega - e'SK\tilde{\nu} \\
&= \frac{1}{2} \|e\|_{-(\bar{Q}+S\Gamma W\Gamma'+SKVK'S)}^2 - e'\bar{Q}\hat{\xi} + e'S\Gamma\omega - e'SK\tilde{\nu}
\end{aligned} \tag{4.0.13}$$

Next, the zero term $\pm \frac{1}{2}\omega'W^{-1}\omega \pm \frac{1}{2}\tilde{\nu}'V^{-1}\tilde{\nu} \pm \frac{1}{2}\hat{\xi}'\bar{Q}\hat{\xi}$ is added to $\dot{\mathbf{W}}$. Then, the completion of squares method can be used to check if $\dot{\mathbf{W}}$ is negative definite as shown below:

$$\begin{aligned}
\dot{\mathbf{W}} &= \frac{1}{2} \|e\|_{-(\bar{Q}+S\Gamma W\Gamma'+SKVK'S)}^2 - e'\bar{Q}\hat{\xi} + e'S\Gamma\omega - e'SK\tilde{\nu} \\
&\quad + \frac{1}{2}\omega'W^{-1}\omega - \frac{1}{2}\omega'W^{-1}\omega + \frac{1}{2}\tilde{\nu}'V^{-1}\tilde{\nu} - \frac{1}{2}\tilde{\nu}'V^{-1}\tilde{\nu} + \frac{1}{2}\hat{\xi}'\bar{Q}\hat{\xi} - \frac{1}{2}\hat{\xi}'\bar{Q}\hat{\xi} \\
&= \frac{1}{2}\omega'W^{-1}\omega - \frac{1}{2}\|\omega - W\Gamma'Se\|_{W^{-1}}^2 + \frac{1}{2}\tilde{\nu}'V^{-1}\tilde{\nu} - \frac{1}{2}\|\tilde{\nu} - VK'Se\|_{V^{-1}}^2 \\
&\quad + \frac{1}{2}\hat{\xi}'\bar{Q}\hat{\xi} - \frac{1}{2}\|e + \hat{\xi}\|_{\bar{Q}}^2
\end{aligned} \tag{4.0.14}$$

To examine the stability of the error e , assume the disturbance players play their worst case strategy of $\omega = \omega^* = WG\Pi^*(\alpha, \beta)x^* = W\Gamma'Se^*$, where $e^* = \xi^* - \hat{\xi}$. Note $\tilde{\nu}$ is a pseudo measurement noise that is nominally zero as the system have perfect partial measurement. By choosing $K = P\bar{H}'V^{-1}$ and using $S = P^{-1}$, $VK'Se = VV^{-1}\bar{H}PSe = \bar{H}e$. Therefore, the time derivative of the Lyapunov function becomes:

$$\dot{\mathbf{W}} = \frac{1}{2} \|W\Gamma'Se^*\|_{W^{-1}}^2 - \frac{1}{2} \|W\Gamma'S(e^* - e)\|_{W^{-1}}^2 - \frac{1}{2} \|\bar{H}e\|_{V^{-1}}^2 + \frac{1}{2} \|\hat{\xi}\|_{\bar{Q}} - \frac{1}{2} \|e + \hat{\xi}\|_{\bar{Q}}^2 \tag{4.0.15}$$

Using the definition of \bar{Q} (2.5.5), two quadratic terms can be simplified: $\hat{\xi}'\bar{Q}\hat{\xi} = \|\hat{x}\|_{\bar{Q}}^2$ and $\|e + \hat{\xi}\|_{\bar{Q}}^2 =$

$\|x\|_Q^2$, where $Q = C'C$. The time derivative of the Lyapunov function can be reduced to:

$$\begin{aligned} \dot{\mathbf{W}} &= \frac{1}{2}\|W\Gamma'Se^*\|_{W^{-1}}^2 - \frac{1}{2}\|W\Gamma'S(e^* - e)\|_{W^{-1}}^2 \\ &\quad - \frac{1}{2}\|He_x\|_{V^{-1}}^2 + \frac{1}{2}\|\hat{x}\|_Q - \frac{1}{2}\|x\|_Q^2. \end{aligned} \quad (4.0.16)$$

Given Assumptions (1-5), as $t \rightarrow \infty$, Lemma 4.0.1 yields the following results:

$$\begin{aligned} e^* &\rightarrow \mathbf{0}, & \|\hat{x}\|_Q^2 &\rightarrow 0 \\ \xi_r^* &\rightarrow \hat{\xi}_r, & \Pi(\alpha^*, \beta^*) &\rightarrow \Pi(\hat{\alpha}, \hat{\beta}). \end{aligned} \quad (4.0.17)$$

Furthermore, since $e^* \rightarrow \mathbf{0}$ as $t \rightarrow \infty$ and $\omega^* = W\Gamma'Se^*$,

$$\omega^* \rightarrow \mathbf{0}, \text{ as } t \rightarrow \infty. \quad (4.0.18)$$

Since the positive terms $\|W\Gamma'Se^*\|_{W^{-1}}^2 = \|\omega^*\|_{W^{-1}}^2 \rightarrow 0$ and $\|\hat{x}\|_Q^2 \rightarrow 0$ in (4.0.16) as shown in (4.0.17) and (4.0.18), the negative terms $-\|He_x\|_{V^{-1}}^2 - \|x\|_Q^2 - \|W\Gamma'Se\|_{W^{-1}}^2$ dominate $\dot{\mathbf{W}}$ and leads to a decrease in \mathbf{W} and e . As $t \rightarrow \infty$, $\dot{\mathbf{W}}$ cannot tend to ∞ , because the negative terms dominate, whereas the positive terms goes to zero. On the other hand, $\dot{\mathbf{W}}$ cannot tend to $-\infty$ as $t \rightarrow \infty$, because it violates the property that $\mathbf{W} \geq 0$ (4.0.11) for all time. In the worst case, since $\mathbf{W} \geq 0$, $\dot{\mathbf{W}} \rightarrow 0$ implies the negative terms must also tend to zero. The dynamics of the negative terms are assessed separately below to confirm that each negative term does indeed tend to zero. If any of these negative terms does not tend to zero as $t \rightarrow \infty$, then \mathbf{W} would continue to decrease, which violates the definition of \mathbf{W} (4.0.11) and the property that $\mathbf{W} \geq 0$.

Let us consider the negative term $-\|He_x\|_{V^{-1}}^2$. Given Assumption 1, suppose $-\|He_x\|_{V^{-1}}^2 < 0$ for $0 \leq \tau < \infty$ and

$$\|W\Gamma'Se^*\|_{W^{-1}}^2 \rightarrow 0, \quad \|\hat{x}\|_Q^2 \rightarrow 0, \quad -\|x\|_Q^2 \rightarrow 0, \quad -\|W\Gamma'Se\|_{W^{-1}}^2 \rightarrow 0. \quad (4.0.19)$$

Then, $-\|He_x\|_{V^{-1}}^2$ would eventually dominate $\dot{\mathbf{W}}$, reducing \mathbf{W} and thereby decreasing $\|e\|$. As

$\|e\| \rightarrow 0$, $\|e_x\| \rightarrow 0$, which contradicts the assumption that $-\|He_x\|_{V^{-1}}^2 < 0$ for $0 \leq \tau < \infty$. Hence, as $t \rightarrow \infty$, $-\|He_x\|_{V^{-1}}^2$ must tend to zero.

Furthermore, Assumption 1 states that $(A(\alpha), H)$ is a detectable pair for all possible α . Since $\hat{\alpha}$ is a subset of the possible α , then Assumption 1 implies $(A(\hat{\alpha}), H)$ is a detectable pair. Recall the system matrix of \dot{e}_x (2.5.14) is $A(\hat{\alpha}) - P_x H' V^{-1} H$, where $P_x > \mathbf{0}$. Since $(A(\hat{\alpha}), H)$ is a detectable pair, $(A(\hat{\alpha}) - P_x H' V^{-1} H, H)$ is also a detectable pair [53] [55]. By the definition of detectability, $\|He_x\|_{V^{-1}}^2 \rightarrow 0$ implies $e_x \rightarrow \mathbf{0}$. Hence, as $t \rightarrow \infty$,

$$-\|He_x\|_{V^{-1}}^2 \rightarrow 0, \quad e_x \rightarrow \mathbf{0}. \quad (4.0.20)$$

Let us consider the negative term $-\|x\|_Q^2$. Given Assumption 2, suppose the close loop system is initially unstable. Then, $-\|x\|_Q^2 < 0$ eventually dominates the positive terms $\|W\Gamma' S e^*\|_{W^{-1}}^2$ and $\|\hat{x}\|_Q^2$ in $\dot{\mathbf{W}}$ (4.0.16), leading to $\dot{\mathbf{W}} < 0$ and $\mathbf{W} \rightarrow 0$. Given $S > \mathbf{0}$ defined in (4.0.11), as $\mathbf{W} \rightarrow 0$, $e \rightarrow \mathbf{0}$, which implies both the state estimation error $e_x \rightarrow \mathbf{0}$ and the parameter estimation error $e_{\xi_r} \rightarrow \mathbf{0}$. As $e_{\xi_r} \rightarrow \mathbf{0}$ and $e^* \rightarrow \mathbf{0}$ (4.0.17), $\xi_r^* \rightarrow \xi_r$, where ξ_r is the constant true system parameter. Thus, $\Pi_t(\alpha^*, \beta^*) \rightarrow \Pi_t(\alpha, \beta)$, where $\Pi_t(\alpha, \beta)$ is the stable control gain generated using the true system parameters as shown in lemma 4.0.2. As $\Pi_t(\alpha^*, \beta^*) \rightarrow \Pi_t(\alpha, \beta)$, leading to a stable close loop system, $x \rightarrow \mathbf{0}$, which implies $-\|x\|_Q^2 \rightarrow 0$. Since $e^* \rightarrow \mathbf{0}$ (4.0.17) and $e_x \rightarrow \mathbf{0}$ (4.0.20), $x^* \rightarrow \hat{x} \rightarrow x \rightarrow \mathbf{0}$. Moreover, since u^* is a linear function of x^* , $u^* \rightarrow \mathbf{0}$. Hence, as $t \rightarrow \infty$,

$$-\|x\|_Q^2 \rightarrow 0, \quad x \rightarrow \mathbf{0}, \quad x^* \rightarrow \mathbf{0}, \quad u^* \rightarrow \mathbf{0}, \quad (4.0.21)$$

and the close loop system is stable.

We consider the last negative term $\|W\Gamma' S e\|_{W^{-1}}^2$. Using the definitions of Γ (2.1.8), S (2.6.2), and e (2.5.9), $W\Gamma' S e$ can be rewritten in terms of e_x and e_{ξ_r} as:

$$W\Gamma' S e = W G' S_x e_x + W G' S_c e_{\xi_r}. \quad (4.0.22)$$

Suppose $-\|W\Gamma'Se\|_{W^{-1}}^2 < 0$ for $0 \leq \tau < \infty$, whereas all other terms in (4.0.16) tends to zero, then $-\|W\Gamma'Se\|_{W^{-1}}^2$ would eventually dominate $\dot{\mathbf{W}}$ (4.0.16), leading to a smaller \mathbf{W} and thereby a smaller e . Since $e_x \rightarrow \mathbf{0}$ (4.0.20), the term $WG'S_x e_x \rightarrow \mathbf{0}$. In addition, since $x \rightarrow \mathbf{0}$ and $u^* \rightarrow \mathbf{0}$ (4.0.21), lemma 4.0.3 implies $S_c \rightarrow \mathbf{0}$. So, $WG'S_c e_{\xi_r} \rightarrow \mathbf{0}$. Hence, as $t \rightarrow \infty$,

$$W\Gamma'Se \rightarrow \mathbf{0}. \quad (4.0.23)$$

It must be noted that $\dot{\mathbf{W}} \rightarrow 0$ only implies \mathbf{W} is a bounded value and e_{ξ_r} is a bounded vector. This is because even for nonzero e_{ξ_r} , the term $WG'S_c e_{\xi_r} \rightarrow \mathbf{0}$ due to $S_c \rightarrow \mathbf{0}$. Similar to results in remark 2, if $C\hat{x} \rightarrow \mathbf{0}$ and $He_x \rightarrow \mathbf{0}$ or if $Q\hat{x} - H'V^{-1}He_x \rightarrow \mathbf{0}$, then $\dot{e}_{\xi_r} \rightarrow \mathbf{0}$, and e_{ξ_r} approaches a constant bounded vector.

□

Lemma 4.0.5. *Consider a class of linear time-invariant system with unknown parameters in both the system and the control matrix, where the pair $(\sum_{i=1}^l A_i \alpha_i, \sum_{i=1}^k B_i \beta_i)$ is stabilizable. Given Assumptions (1-5), suppose a minimax solution to the infinite-time problem for the uncertain system exists for all time, if $\|\xi\| \rightarrow \infty$, then the value function $\mathbf{V}_t \rightarrow -\infty$.*

Proof. The value function \mathbf{V}_t at current time can be written as:

$$2\mathbf{V}_t = \max_{\xi} \left[x' \Pi_t(\alpha, \beta) x - (\xi - \hat{\xi})' S (\xi - \hat{\xi}) \right] \quad (4.0.24)$$

where $\hat{\xi}$ is not a function of ξ . S is independent of ξ and is always positive definite by construction. Since there are two variables, x and ξ_r , then there are three cases to consider. The first case is when $\|x\| \rightarrow \infty$, while $\|\xi_r\| < \infty$. The second case is when $\|x\| < \infty$, while $\|\xi_r\| \rightarrow \infty$, and the last case is when $\|\xi\| \rightarrow \infty$. In the first case, suppose $\|x\| \rightarrow \infty$ while $\|\xi_r\|$ remain finite. Since the minimax solution exists, then it must satisfy the first order necessary condition and second order sufficient

condition. The first order necessary condition (2.6.3) requires:

$$\Pi_t(\alpha, \beta)x = S_x(x - \hat{x}) + S_c(\xi_r - \hat{\xi}_r)$$

By moving $S_x x$ to the left hand side of the equation, and taking the norm of the first order necessary connection condition 2.6.3 yields:

$$\|(\Pi_t(\alpha, \beta) - S_x)x\| = \|-S_x \hat{x} + S_c \xi_r - S_c \hat{\xi}_r\| \quad (4.0.25)$$

Since $\Pi_t(\alpha, \beta) - S_x < \mathbf{0}$ is required by the second order sufficient condition, it is clear that in the case $\|x\| \rightarrow \infty$ and $\|\xi_r\| < \infty$ violates the first order necessary condition. Since $\Pi_t(\alpha, \beta) - S_x < \mathbf{0}$ and $\|x\| \rightarrow \infty$, then the left hand side of (4.0.25) tends to ∞ , while the right hand side of (4.0.25) is finite as propagated by the differential Algebraic Riccati equation for S and the dynamic equation of $\hat{\xi}_r$. Therefore a worst case solution, where $\|x\|$ tend to infinity while the parameters remain finite cannot exist.

We consider the second case where $\|x\| < \infty$ and $\|\xi_r\| \rightarrow \infty$. $\Pi_t(\alpha, \beta)$ is bounded as required by Assumption 3 and it is upperbounded by S_x as required by the second order sufficient condition. Furthermore, since $\beta \rightarrow \infty$ and the pair $(\sum_{i=1}^l A_i \alpha_i, \sum_{i=1}^k B_i \beta_i)$ is stabilizable, then the worst case $B(\beta)$ have infinite control authority. Hence $\Pi_t(\alpha, \beta) \rightarrow \mathbf{0}$ as $\xi_r \rightarrow \infty$. Then the value function is dominated by the negative quadratic error term $-(\xi - \hat{\xi})' S (\xi - \hat{\xi}) \rightarrow -\infty$. Hence the value function tends to $-\infty$ as $\|\xi_r\| \rightarrow \infty$ while $\|x\|$ remain finite.

We consider the last case where both $\|x\|$ and $\|\xi_r\|$ tends to infinity. Using the same analysis as the previous case, as $\|\beta\| \rightarrow \infty$, the worst case system has infinite control authority, leading to $\Pi_t(\alpha, \beta) \rightarrow \mathbf{0}$ and yielding $-(\xi - \hat{\xi})' S (\xi - \hat{\xi}) \rightarrow -\infty$ to dominate the value function. Hence the value function tends to $-\infty$ as $\|\xi\| \rightarrow \infty$. Hence, for all three cases, as $\|\xi\| \rightarrow \infty$, the value function tends to $-\infty$. □

Chapter 5

A Case Study: A Modifiable Nonlinear SISO Example

Consider the following single-input single-output (SISO) dynamic system with unknown parameters ρ :

$$\begin{aligned} \dot{x} &= A(\rho)x + B(\rho)u + G\omega \\ z &= Hx, \quad H \in \mathbf{R}^{1 \times n} \\ \dot{\rho} &= 0, \end{aligned} \tag{5.0.1}$$

where $A(\rho) \in \mathbf{R}^{n \times n}$, $B(\rho) \in \mathbf{R}^{n \times 1}$, and $G \in \mathbf{R}^{n \times 1}$. The state vector x has n elements. The input u and the process disturbance ω are both scalar. z measures a single element of the state x . Furthermore, assume the unknown parameters multiply elements of x that are not part of the state measurement. For example, consider the following two state system:

$$\begin{bmatrix} \dot{x}_1 \\ \dot{x}_2 \end{bmatrix} = \begin{bmatrix} \rho_1 & \rho_2 \\ 0 & 1 \end{bmatrix} \begin{bmatrix} x_1 \\ x_2 \end{bmatrix}, \tag{5.0.2}$$

where ρ_1 and ρ_2 are the unknown parameters. To apply the modified gain H_∞ filter directly, one needs to form the corresponding universal linearization matrix $\mathcal{A}(\hat{\xi}, u, z)$ (2.5.13), which can be written as:

$$\mathcal{A}(\hat{\xi}, 0, z) = \begin{bmatrix} \hat{\rho}_1 & \hat{\rho}_2 & x_1 & x_2 \\ 0 & 1 & 0 & 0 \\ 0 & 0 & 0 & 0 \\ 0 & 0 & 0 & 0 \end{bmatrix}, \quad (5.0.3)$$

where x_1 and x_2 must both be measured, such as $z = \mathbf{I}_2 x$. If the system is single output, and only measures either x_1 or x_2 , then a direct application of the nonlinear modified gain observer is impossible, as it requires a perfect measurement of both x_1 and x_2 . Hence, for single output system with multiple unknown parameters that times multiple elements of the state, the original SISO system must be transformed into the observable canonical form, so that the nonlinear modified gain observer only uses the single output in $\mathcal{A}(\hat{\xi}, u, z)$.

For SISO system, such as (5.0.1), can be transformed into the observable canonical form using the corresponding observability matrix and the coefficients of the characteristic polynomial of the system matrix. Let \mathbf{O} be defined as the observability matrix and c_i be defined as the coefficients of the characteristic polynomial of the system matrix:

$$\det(s\mathbf{I} - A(\xi_r)) = s^n + c_1 s^{n-1} + \cdots + c_{n-1} s + c_n. \quad (5.0.4)$$

Note that depending on the location of the unknown parameters in the system matrix, certain c_i is a function of the unknown parameters ρ , i.e. $c_i = c_i(\rho)$. For the purpose of this analysis, let us assume all c_i are functions of ρ , therefore in the transformed state, there are n unknowns in the system matrix. Since the system is assumed to be observable, then the observability matrix is invertible, and the transformation from the original state to the transformed observable canonical

state can be written as:

$$T_o = \begin{bmatrix} c_{n-1} & c_{n-2} & c_{n-3} & \cdots & c_1 & 1 \\ c_{n-2} & c_{n-3} & \cdots & \cdots & 1 & 0 \\ c_{n-3} & \cdots & \cdots & \cdots & 0 & 0 \\ \vdots & \vdots & \vdots & \vdots & \vdots & \vdots \\ c_1 & 1 & \cdots & \cdots & 0 & 0 \\ 1 & 0 & \cdots & \cdots & 0 & 0 \end{bmatrix} \begin{bmatrix} H \\ HA(\rho) \\ HA(\rho)^2 \\ \vdots \\ \underbrace{HA(\rho)^{(n-1)}}_O \end{bmatrix}. \quad (5.0.5)$$

Since T_o is a function of c_i , then T_o is also a function of the unknown parameters. The transformed state is defined as $x_o = T_o x$. The transformed state space representation can be written as:

$$\begin{aligned} \dot{x}_o &= \underbrace{(T_o A(\rho) T_o^{-1})}_{A_o(\rho)} x_o + \underbrace{T_o B(\rho)}_{B_o(\rho)} u + \underbrace{T_o G}_{G_o(\rho)} \omega = A_o(\rho) x_o + B_o(\rho) u + G_o(\rho) \omega \\ z &= \underbrace{H T_o^{-1}}_{H_o} x_o = H_o x_o. \end{aligned} \quad (5.0.6)$$

Let $\alpha = [\alpha_n \ \alpha_{n-1} \ \cdots \ \alpha_1]'$ and $\alpha_{n-1:1} = [\alpha_{n-1} \ \cdots \ \alpha_1]'$, then $\alpha = [\alpha_n \ \alpha'_{n-1:1}]'$, where α_i are the elements in $A_o(\rho)$ that are functions of the unknown parameter ρ , i.e. $\alpha_i = \alpha_i(\rho)$. Let $\beta \in \mathbf{R}^k = [\beta_1 \ \cdots \ \beta_k]'$, where β_i are the elements in $B_o(\rho)$ that are functions of the unknown parameter ρ , i.e. $\beta_i = \beta_i(\rho)$. Note \mathbf{I}_{n-1} is an identity matrix of size $n-1$. Then the transformed system matrix $A_o(\alpha)$, the control matrix $B_o(\beta)$, and the measurement matrix has the following form:

$$\begin{aligned} A_o(\alpha) &= \begin{bmatrix} \mathbf{0}_{1 \times n-1} & -\alpha_n \\ \mathbf{I}_{n-1} & -\alpha_{n-1:1} \end{bmatrix}, & B_o(\beta) &= B_0 + \sum_{i=1}^k \beta_i B_i \\ H_o &= \begin{bmatrix} \mathbf{0}_{1 \times n-1} & 1 \end{bmatrix}. \end{aligned} \quad (5.0.7)$$

Define the augmented state $\xi = [x'_o \ \alpha' \ \beta']'$ and $\bar{H} = [H_o \ \mathbf{0}_{1 \times n+k}]$. In the transformed SISO system, z is the last element of the x_o . The dynamics of the augmented state ξ written as a function

of ξ , z and u is shown below:

$$\dot{\xi} = \underbrace{\begin{bmatrix} f(\xi, z) + \sum_{i=1}^k \beta_i B_i u \\ \mathbf{0}_{n+k \times 1} \end{bmatrix}}_{F(\xi, z, u)} + \underbrace{\begin{bmatrix} B_0 \\ \mathbf{0}_{n+k \times 1} \end{bmatrix}}_{\bar{B}_0} u + \underbrace{\begin{bmatrix} G_o \\ \mathbf{0}_{n+k \times 1} \end{bmatrix}}_{\Gamma} \omega \quad (5.0.8)$$

$$= F(\xi, z, u) + \bar{B}_0 u + \Gamma \omega$$

$$f(\xi, z) = \begin{bmatrix} -\alpha_n z & x_{o,1} - \alpha_{n-1} z & \cdots & x_{o,n-1} - \alpha_1 z \end{bmatrix}'. \quad (5.0.9)$$

The error of the augmented state is defined to be:

$$e = \xi - \hat{\xi}. \quad (5.0.10)$$

Define the estimate of the augmented state to be a function of $\hat{\xi}$ and u :

$$\dot{\hat{\xi}} = \underbrace{\begin{bmatrix} f(\hat{\xi}) + \sum_{i=1}^k \hat{\beta}_i B_i u \\ \mathbf{0}_{n+k \times 1} \end{bmatrix}}_{F(\hat{\xi}, u)} + \bar{B}_0 u + P Q \hat{\xi} + K(z - \bar{H} \hat{\xi}) \quad (5.0.11)$$

$$= F(\hat{\xi}, u) + \bar{B}_0 u + P Q \hat{\xi} + K(z - \bar{H} \hat{\xi})$$

$$f(\hat{\xi}) = \begin{bmatrix} -\hat{\alpha}_n \hat{x}_{o,n} & \hat{x}_{o,1} - \hat{\alpha}_{n-1} \hat{x}_{o,n} & \cdots & \hat{x}_{o,n-1} - \hat{\alpha}_1 \hat{x}_{o,n} \end{bmatrix}'. \quad (5.0.12)$$

Combining 5.0.10, 5.0.8 and 5.0.11, results in the dynamics of the error:

$$\dot{e} = \dot{\xi} - \dot{\hat{\xi}} = F(\xi, z, u) - F(\hat{\xi}, u) + \Gamma \omega - P Q \hat{\xi} - K \bar{H} e. \quad (5.0.13)$$

Let us first note:

$$\begin{aligned}
f(\xi, z) - f(\hat{\xi}) &= \begin{bmatrix} -\alpha_n z - (-\hat{\alpha}_n \hat{x}_{o,n}) \\ x_{o,1} - \alpha_{n-1} z - (\hat{x}_{o,1} - \hat{\alpha}_{n-1} \hat{x}_{o,n}) \\ \vdots \\ x_{o,n-1} - \alpha_1 z - (\hat{x}_{o,n-1} - \hat{\alpha}_1 \hat{x}_{o,n}) \end{bmatrix} + \underbrace{\begin{bmatrix} -\hat{\alpha}_n z + \hat{\alpha}_n z \\ -\hat{\alpha}_{n-1} z + \hat{\alpha}_{n-1} z \\ \vdots \\ -\hat{\alpha}_1 z + \hat{\alpha}_1 z \end{bmatrix}}_{\mathbf{0}_{n \times 1}} \\
&= \begin{bmatrix} -(\alpha_n - \hat{\alpha}_n)z - \hat{\alpha}_n(z - \hat{x}_{o,n}) \\ (x_{o,1} - \hat{x}_{o,1}) - (\alpha_{n-1} - \hat{\alpha}_{n-1})z - \hat{\alpha}_{n-1}(z - \hat{x}_{o,n}) \\ \vdots \\ (x_{o,n-1} - \hat{x}_{o,n-1}) - (\alpha_1 - \hat{\alpha}_1)z - \hat{\alpha}_1(z - \hat{x}_{o,n}) \end{bmatrix} \tag{5.0.14} \\
&= \underbrace{\begin{bmatrix} 0 & \cdots & 0 & -\hat{\alpha}_n & -z & 0 & \cdots & 0 \\ 1 & \cdots & 0 & -\hat{\alpha}_{n-1} & 0 & -z & \ddots & \vdots \\ & \ddots & \vdots & \vdots & \vdots & 0 & \ddots & 0 \\ 0 & \cdots & 1 & -\hat{\alpha}_1 & 0 & \cdots & 0 & -z \end{bmatrix}}_{\mathcal{F}(\hat{\alpha}, z)} \begin{bmatrix} x_{o,1} - \hat{x}_{o,1} \\ \vdots \\ x_{o,n} - \hat{x}_{o,n} \\ \alpha_n - \hat{\alpha}_n \\ \vdots \\ \alpha_1 - \hat{\alpha}_1 \end{bmatrix}.
\end{aligned}$$

Using the definition of $F(\xi, z, u)$ and $F(\hat{\xi}, u)$ in (5.0.8) and (5.0.11) respectively, as well as (5.0.14), we can write:

$$F(\xi, z, u) - F(\hat{\xi}, u) = \mathcal{A}(\hat{\xi}, z, u)(\xi - \hat{\xi}) = \mathcal{A}(\hat{\xi}, z, u)e \tag{5.0.15}$$

where $\mathcal{A}(\hat{\xi}, z, u)$ is defined as:

$$\mathcal{A}(\hat{\xi}, z, u) = \begin{bmatrix} \mathcal{F}(\hat{\alpha}, z) & B_1 u & \cdots & B_k u \\ \mathbf{0}_{n+k \times 2n} & \mathbf{0}_{n+k \times 1} & \cdots & \mathbf{0}_{n+k \times 1} \end{bmatrix} \tag{5.0.16}$$

Using (5.0.15), the error dynamic of e can now be written as:

$$\dot{e} = \left(\mathcal{A}(\hat{\xi}, z, u) - K\bar{H} \right) e + \Gamma\omega - PQ\hat{\xi}. \quad (5.0.17)$$

In the following example, we examine the performance of the worst case controller applied to a SISO dynamical system with unknown parameters in the system matrix only. No unknown parameters were introduced in the control matrix, because such examples can be found in previous literatures such as [39] and one can utilize the known input u to estimation the unknown control parameters. By comparison, the estimation of the unknown parameters in the system matrix is more complicated, as the unknown system parameters $A(\rho)$ multiply the unknown state x in the state dynamics, such as $A(\rho)x$ in (5.0.1). Hence, it is more difficult to determine the respective uncertainties in the system matrix $A(\rho)$ and the state x than the uncertainties in the control matrix $B(\rho)$. As such, it is more difficult to design a controller to stabilize unstable systems with uncertain parameters in the system matrix.

Example 5.0.1. *In this example, we apply an adaptive worst case controller to a SISO dynamic system, where the unknown parameters are only located in the system matrix. The control matrix as well as the process coefficient are known:*

$$\begin{aligned} \dot{x} &= A(a)x + Bu + G\omega \\ z &= Hx, \end{aligned} \quad (5.0.18)$$

where the system coefficients are:

$$\begin{aligned}
 A &= \begin{bmatrix} 0 & 1 & 0 & 0 \\ 0 & 0 & 1 & 0 \\ 0 & 0 & 0 & 1 \\ a_1 & a_2 & a_3 & a_4 \end{bmatrix}, \quad B = \begin{bmatrix} 0 \\ 0 \\ 0 \\ 1 \end{bmatrix} \\
 G &= \begin{bmatrix} 0 & 0 & 0 & 1 \end{bmatrix}', \quad H = \begin{bmatrix} 1 & 0 & 0 & 0 \end{bmatrix} \\
 a &= \begin{bmatrix} a_1 & a_2 & a_3 & a_4 \end{bmatrix}.
 \end{aligned} \tag{5.0.19}$$

Let a_1 , a_2 , a_3 , and a_4 be the unknown parameters in the system matrix. Since unknown parameters are multiplied by all elements of the state in the dynamics of x_4 , all elements of the state must be then be available to directly use the modified gain observer. Unfortunately, this is not the case here. Although this SISO system is observable and controllable, only the first element x_1 is measured perfectly.

5.0.1 Application of the Modified Gain Observer

To apply the modified gain observer (MGO), the SISO system (5.0.18) needs to be transformed into an observerable canonical form as shown below:

$$\begin{aligned}
 \dot{x}_o &= A_o x_o + B_o u + G_o \omega \\
 z &= H_o x_o,
 \end{aligned} \tag{5.0.20}$$

where the transformed system coefficients are:

$$\begin{aligned}
 A_o &= \begin{bmatrix} 0 & 0 & 0 & a_1 \\ 1 & 0 & 0 & a_2 \\ 0 & 1 & 0 & a_3 \\ 0 & 0 & 1 & a_4 \end{bmatrix}, \quad B_o = \begin{bmatrix} 1 \\ 0 \\ 0 \\ 0 \end{bmatrix} \\
 G'_o &= \begin{bmatrix} 1 & 0 & 0 & 0 \end{bmatrix}, \quad H_o = \begin{bmatrix} 0 & 0 & 0 & 1 \end{bmatrix}.
 \end{aligned} \tag{5.0.21}$$

The transformation matrix T_o used to transform (5.0.18) to (5.0.20) is:

$$T_o(a) = \begin{bmatrix} -a_2 & -a_3 & -a_4 & 1 \\ -a_3 & -a_4 & 1 & 0 \\ -a_4 & 1 & 0 & 0 \\ 1 & 0 & 0 & 0 \end{bmatrix}. \quad (5.0.22)$$

Let us augment the unknown parameters a to x_o , then the augmented nonlinear state ξ can be written as:

$$\begin{aligned} \xi' &= \begin{bmatrix} x_{o,1} & x_{o,2} & x_{o,3} & x_{o,4} & a_1 & a_2 & a_3 & a_4 \end{bmatrix} \\ &= \begin{bmatrix} \xi_1 & \xi_2 & \xi_3 & \xi_4 & \xi_5 & \xi_6 & \xi_7 & \xi_8 \end{bmatrix}. \end{aligned} \quad (5.0.23)$$

Define $\xi_r = \begin{bmatrix} \xi_5 & \xi_6 & \xi_7 & \xi_8 \end{bmatrix}'$, then the nonlinear dynamic of the augmented state is:

$$\begin{aligned} \dot{\xi} &= \begin{bmatrix} \xi_5 \xi_1 \\ \xi_1 + \xi_6 \xi_4 \\ \xi_2 + \xi_7 \xi_4 \\ \xi_3 + \xi_8 \xi_4 \\ \mathbf{0}_{4,1} \end{bmatrix} + \begin{bmatrix} 1 \\ 0 \\ 0 \\ 0 \\ \mathbf{0}_{4,1} \end{bmatrix} u + \begin{bmatrix} 1 \\ 0 \\ 0 \\ 0 \\ \mathbf{0}_{4,1} \end{bmatrix} \omega \\ &= f(\xi) + \bar{B}_0 u + \Gamma \omega \\ z &= \begin{bmatrix} 0 & 0 & 0 & 1 & 0 & 0 & 0 & 0 \end{bmatrix} \xi = \bar{H} \xi = \xi_4. \end{aligned} \quad (5.0.24)$$

The nonlinear estimator can be written as:

$$\begin{aligned} \dot{\hat{\xi}} &= \begin{bmatrix} \hat{\xi}_5 \hat{\xi}_1 \\ \hat{\xi}_1 + \hat{\xi}_6 \hat{\xi}_4 \\ \hat{\xi}_2 + \hat{\xi}_7 \hat{\xi}_4 \\ \hat{\xi}_3 + \hat{\xi}_8 \hat{\xi}_4 \\ \mathbf{0}_{4,1} \end{bmatrix} + \begin{bmatrix} 1 \\ 0 \\ 0 \\ 0 \\ \mathbf{0}_{4,1} \end{bmatrix} u + K(z - \bar{H}\hat{\xi}) + P\bar{Q}\hat{\xi} \\ &= f(\hat{\xi}) + \bar{B}_0 u + K\bar{H}e + P\bar{Q}\hat{\xi}. \end{aligned} \quad (5.0.25)$$

Using the estimator dynamics, the resulting linear error dynamics become:

$$\dot{e} = \left(\mathcal{A}(\hat{\xi}, z) - K\bar{H} \right) e + \Gamma\omega - P\bar{Q}\hat{\xi}, \quad (5.0.26)$$

where

$$\mathcal{A}(\hat{\xi}, z) = \begin{bmatrix} A_o(\hat{a}) & z\mathbf{I}_4 \\ \mathbf{0}_4 & \mathbf{0}_4 \end{bmatrix}. \quad (5.0.27)$$

Since we assume perfect measurement of ξ_4 , $z = \xi_4$ in $\mathcal{A}(\hat{\xi}, z)$.

5.0.2 Application of Worst Case Control

The controller is generated using the four-state observable canonical dynamical system (5.0.20). The corresponding steady-state control ARE and control input of this infinite-time problem is:

$$\mathbf{0} = Q + A_o(a^*)'\Pi + \Pi A_o(a^*) + \Pi(G_o W G_o' - \bar{B}_0 R^{-1} \bar{B}_0')\Pi \quad (5.0.28)$$

$$u^* = -R^{-1} \bar{B}_0' \Pi(a^*) x^*. \quad (5.0.29)$$

The first derivative of Π with respect to the unknown parameters, which are four Lyapunov equations, are defined as:

$$\begin{aligned} \mathbf{0} = & A'_i \Pi + \Pi A_i + [A_o(a)' + \Pi(G_o W G'_o - \bar{B}_0 R^{-1} \bar{B}'_0)] \frac{\partial \Pi}{\partial a_i} \\ & + \frac{\partial \Pi}{\partial a_i} [A_o(a) + (G_o W G'_o - \bar{B}_0 R^{-1} \bar{B}'_0) \Pi] \Big|_{a=a^*}, \end{aligned} \quad (5.0.30)$$

where

$$A_1 = \begin{bmatrix} 0 & 0 & 0 & 1 \\ 0 & 0 & 0 & 0 \\ 0 & 0 & 0 & 0 \\ 0 & 0 & 0 & 0 \end{bmatrix}, \quad A_2 = \begin{bmatrix} 0 & 0 & 0 & 0 \\ 0 & 0 & 0 & 1 \\ 0 & 0 & 0 & 0 \\ 0 & 0 & 0 & 0 \end{bmatrix} \quad (5.0.31)$$

$$A_3 = \begin{bmatrix} 0 & 0 & 0 & 0 \\ 0 & 0 & 0 & 0 \\ 0 & 0 & 0 & 1 \\ 0 & 0 & 0 & 0 \end{bmatrix}, \quad A_4 = \begin{bmatrix} 0 & 0 & 0 & 0 \\ 0 & 0 & 0 & 0 \\ 0 & 0 & 0 & 0 \\ 0 & 0 & 0 & 1 \end{bmatrix}. \quad (5.0.32)$$

The worst-case parameters, the first-order condition (2.6.3), the control algebraic Riccati equation (5.0.28), and the partial derivatives of Π with respect to the unknown parameters (5.0.30) all must be solved simultaneously together using a numerical solver. The sufficient condition must also be satisfied to ensure the newly found critical point is indeed a minimum value of the connection condition. It is possible the close form solution of the worst-case solution might exist for a specific simple case. However, the close form solution of the worst case parameters is generally difficult to obtain and must be solved using numerical methods.

5.0.3 Simulation Setup

The control input u^* is generated at 100 Hz and is held constant for 0.01 second. The close-loop dynamical system is propagated using the ODE45 function in Matlab. The following weightings are

used for this simulation:

$$\begin{aligned} Q &= 0.1\bar{H}'\bar{H}, & W &= 5 \times 10^{-2} \\ R &= 0.011, & V &= 1 \times 10^{-5}. \end{aligned} \tag{5.0.33}$$

The true parameter values for this simulation is:

$$a = \begin{bmatrix} 1.4 & 1.4 & 1.4 & 1.4 \end{bmatrix}'. \tag{5.0.34}$$

The initial parameter estimate for this simulation is:

$$\hat{a}(0) = \begin{bmatrix} 1 & 1 & 1 & 1 \end{bmatrix}'. \tag{5.0.35}$$

The largest eigenvalue of the true system matrix $\lambda_1(A_o(a))$ is 2.3544, whereas the largest eigenvalue of the initial estimated system matrix $\lambda_1(A_o(\hat{a}(0)))$ is 1.9276. The true system is more unstable than the initial estimated system, hence the controllers generated using the initial parameter estimates might not be able to stabilize the true plant.

The initial state starts at $x(0) = \begin{bmatrix} 1 & 0 & 0 & 0 \end{bmatrix}'$. In the observable canonical form, the initial state $x_o(0)$ is defined as:

$$x_o(0) = T_o(a)x(0) = \begin{bmatrix} -1.4 & -1.4 & -1.4 & 1 \end{bmatrix}'. \tag{5.0.36}$$

We set the initial state estimate $\hat{x}_o(0) = x_o(0)$. This example demonstrates a step response of the state to the worst case input u^* . Furthermore, this example illustrates a step response of the system parameter estimate to the modified gain observer. Although the state estimation error is initially zero, the initial system parameter error is nonzero, which drives the state estimate away from the true state in the transient period. Even though this example does not exemplify a step response of the state estimation error e_x , e_x is still being introduced to the system through parameter estimation error e_{ξ_r} . The convergence property of the modified gain observer is demonstrated in this example. One can choose $\hat{x}_o(0)$ to be a different value, such as $T_o(\hat{a}(0))x(0)$, to examine the step response of

the state estimation error. However, a nonzero initial state estimation error might lead to a faster convergence of the parameter estimation error.

The initial error weighting for $x(0)$ is set to:

$$P_x(0) = \begin{bmatrix} 1 & 0 & 0 & 0 \\ 0 & 1.01 & 0 & 0 \\ 0 & 0 & 1.02 & 0 \\ 0 & 0 & 0 & 1.16 \end{bmatrix} \quad (5.0.37)$$

The initial state error weighting for $x_o(0)$ is chosen to be:

$$P_{o,x}(0) = T_o(\hat{a}(0))P_x(0)T_o(\hat{a}(0))', \quad (5.0.38)$$

where $T_o(\hat{a}(0))$ is the initial observable canonical form transformation matrix as a function of the initial parameter estimate $\hat{a}(0)$. One may choose a different value for $P_{o,x}(0)$, which could increase or decrease the convergence rate of the state estimation. The initial parameter error weighting $P_a(0)$ is chosen to be:

$$P_a(0) = \begin{bmatrix} 0.1 & 0 & 0 & 0 \\ 0 & 0.1 & 0 & 0 \\ 0 & 0 & 0.105 & 0 \\ 0 & 0 & 0 & 0.1 \end{bmatrix} \quad (5.0.39)$$

The initial error weighting $P(0)$ is defined as:

$$P(0) = \begin{bmatrix} P_{o,x}(0) & \mathbf{0}_4 \\ \mathbf{0}_4 & P_a(0) \end{bmatrix}. \quad (5.0.40)$$

In this simulation, the performance of the disturbance attenuation controller coupled with MGO as derived in this chapter is compared to the linear quadratic regulator (LQR) coupled with modified

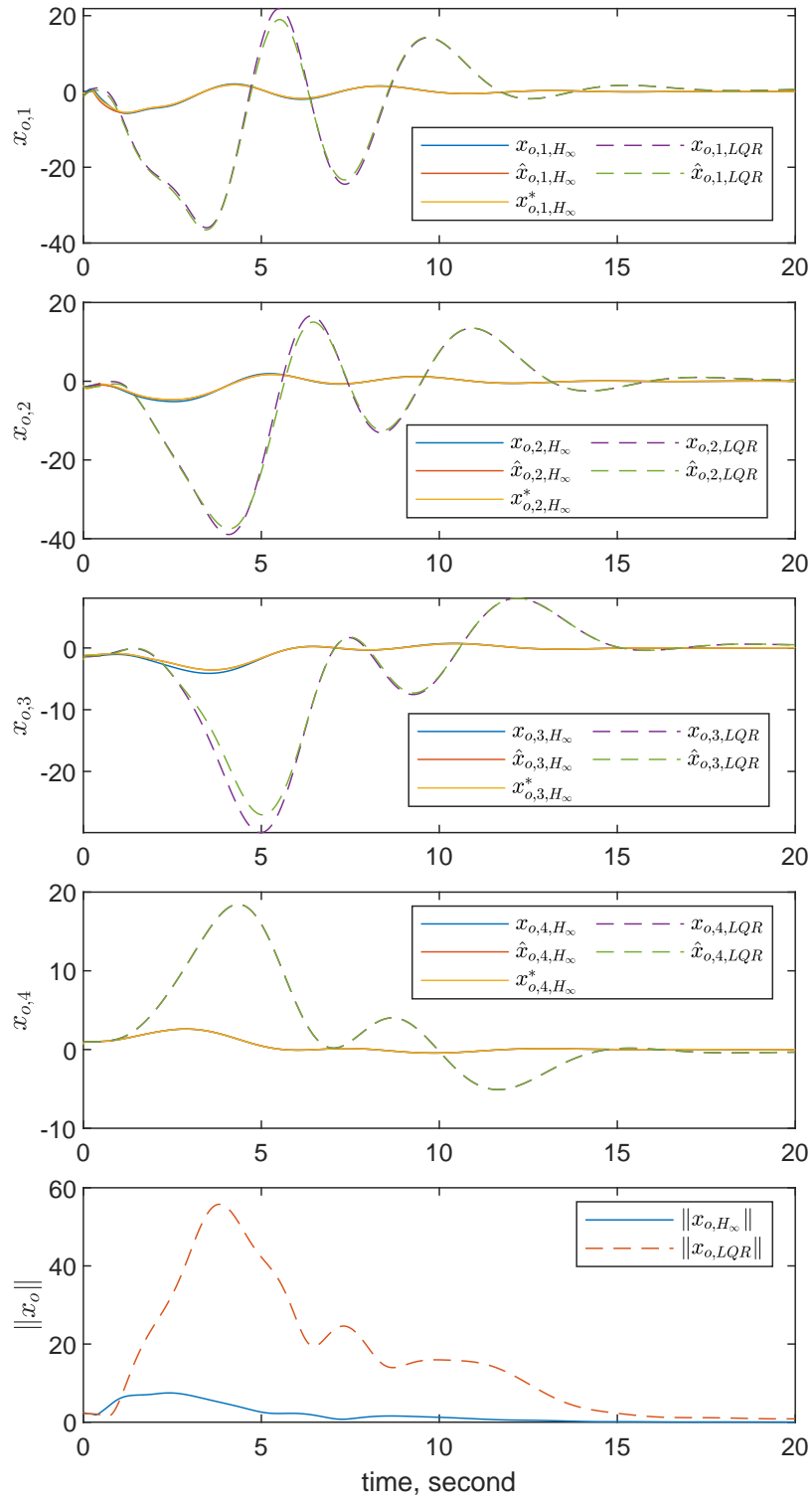


Figure 5.1: x_o , \hat{x}_o and x_o^* plots using disturbance attenuating controller (solid lines). x_o and \hat{x}_o plots using LQR controller (dash lines). The disturbance attenuation controller yields better performance than the LQR controller.

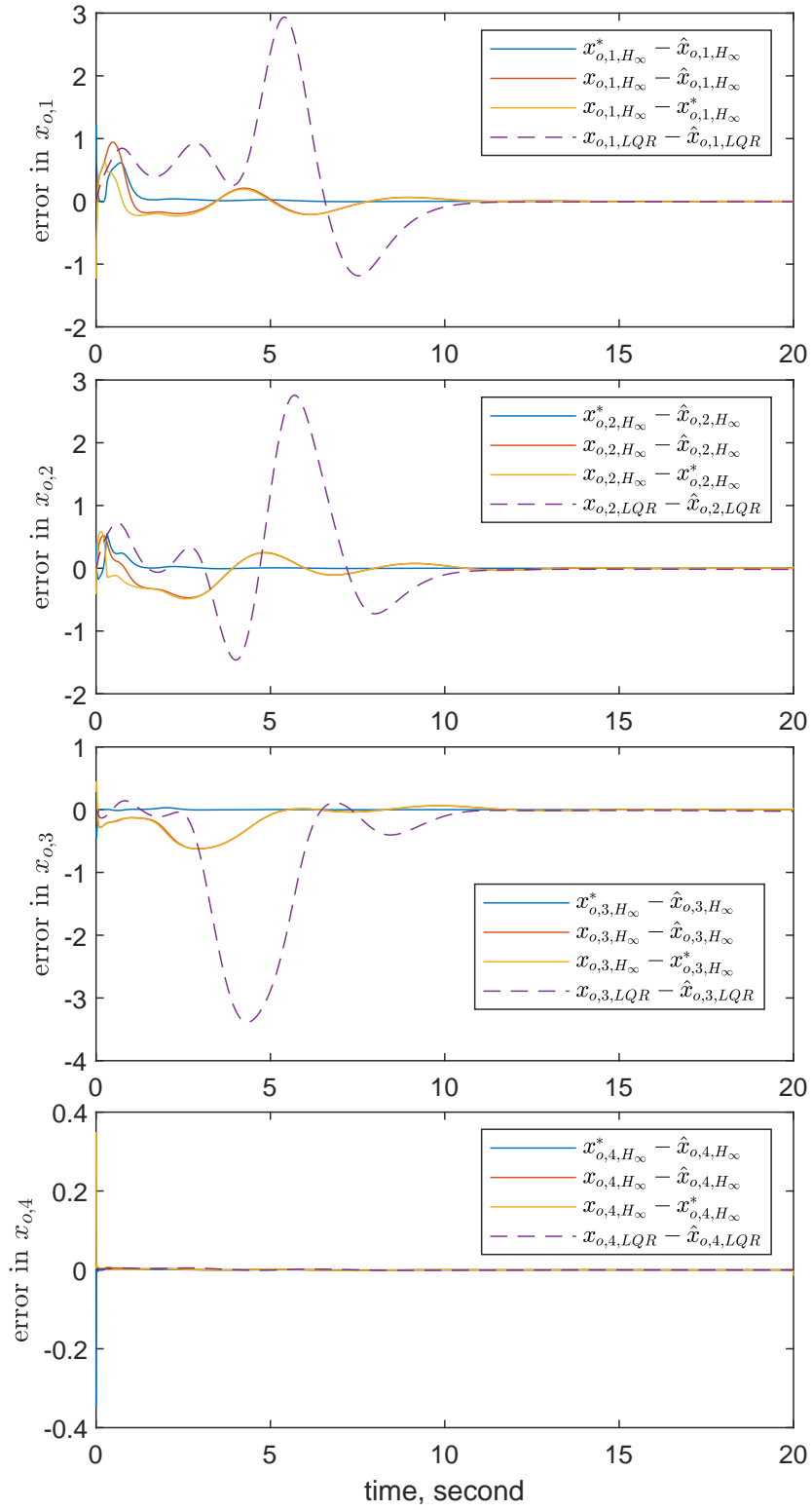


Figure 5.2: Various types of state estimation errors for both control algorithms.

gain extended Kalman observer (MGEKO)[47]. MGEKO is chosen as a comparison scheme because it was shown to have better performance than the extended Kalman filter [47]. In the following, these two sets of algorithms will be referred to as worst case controller (or H_∞ in the figures) and the LQR/MGEKO (or LQR in the figures). The simulation ran for 20 seconds. Both algorithms use the same set of weightings and initial conditions whenever possible. ω^* , generated at 100 Hz and held constant for 0.01 second, is applied to both controllers to ensure a fair evaluation of the controller performance.

5.0.4 Result

In the following figures, the disturbance attenuation control simulation results are displayed using solid lines, whereas the LQR/MGEKO simulation results are displayed using dashed lines. Figure 5.1 presents the state history and observer estimates for both algorithms. The disturbance attenuation controller yields three plots: true state x_{o,H_∞} , state estimate \hat{x}_{o,H_∞} and worst case state x_{o,H_∞}^* . The LQR algorithm yields two plots: the true state $x_{o,LQR}$ and the estimated state $\hat{x}_{o,LQR}$. Clearly, both observers are able to track their respective true states. Both sets of control algorithms were eventually able to stabilize the system due to the parameter adaptation performed by their respective observers. However, the disturbance attenuation controller exhibits a better performance overall than the LQR algorithm as shown in Figure 5.1, where $\|x_{H_\infty}\|$ with peak value of 7.5 is much lower than $\|x_{LQR}\|$ with peak value of 56. $\|x_{o,H_\infty}\|$ is predominantly smaller than $\|x_{o,LQR}\|$, except briefly during the first second of the simulation where performance is traded for better parameter estimate. Although both controllers started off with the same initial state, the LQR algorithm yields much larger instability in all states than the disturbance attenuation controller.

Figure 5.2 plots various types of state estimation error for both controllers all tends to zero rapidly after initial transient period. The estimated state error $x_{o,H_\infty} - \hat{x}_{o,H_\infty}$ is smaller and converges to zero faster than $x_{o,LQR} - \hat{x}_{o,LQR}$ overall. It could be that the LQR algorithm generated much larger instability than the disturbance attenuation controller, i.e $x_{o,LQR}$ is larger than x_{o,H_∞} overall, hence the estimated state error may also be larger. Since the system makes perfect measurement of $x_{o,4}$ and V^{-1} is very large, any type of initial error estimate of $x_{o,4}$, such as $x_{o,4,H_\infty}^* - \hat{x}_{o,4,H_\infty}$, or

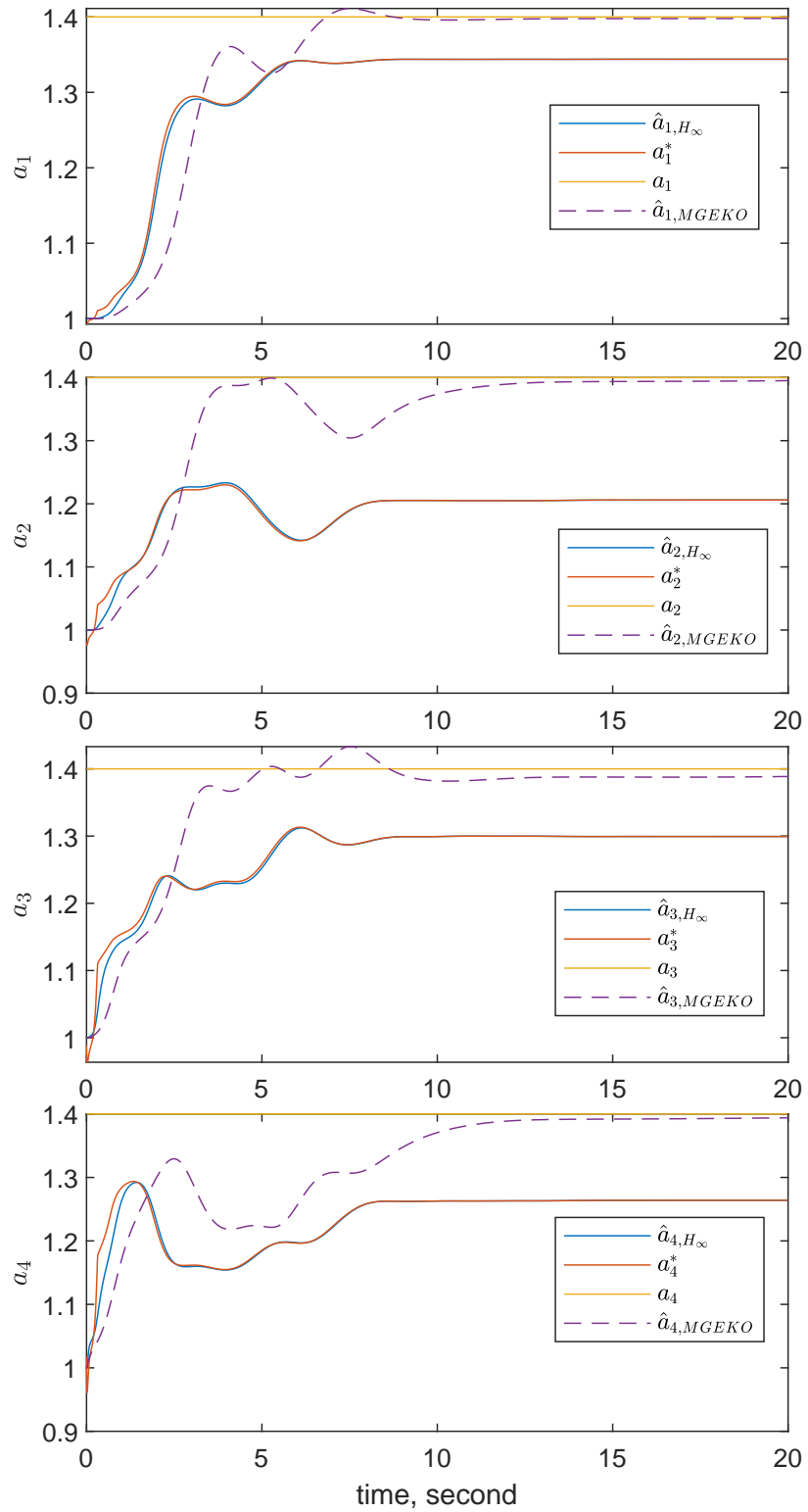


Figure 5.3: Parameter estimates from nonlinear modified gain observer and MGEKO.

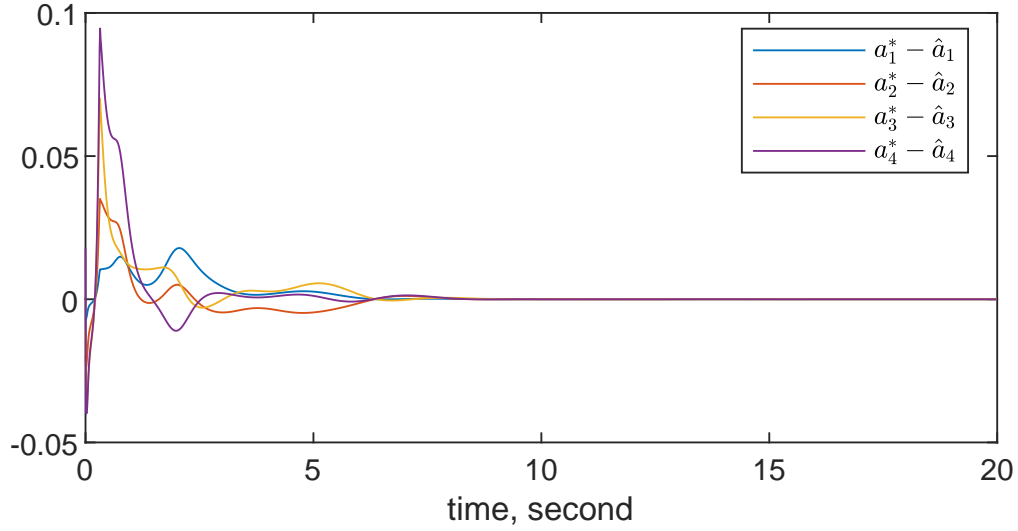


Figure 5.4: Worst case parameter estimation error.

$x_{o,4,H_\infty} - \hat{x}_{o,4,H_\infty}$, will converge to zero within a few time steps.

Lemma 4.0.1 proved $e^* \rightarrow \mathbf{0}$ as $t \rightarrow \infty$, where the worst case estimation error in this example is defined as:

$$e^* = \begin{bmatrix} x_{o,H_\infty}^* - \hat{x}_{o,H_\infty} \\ a_{H_\infty}^* - \hat{a}_{H_\infty} \end{bmatrix}. \quad (5.0.41)$$

This property is demonstrated in figure 5.2 and figure 5.4. Figure 5.2 plots the worst case state estimate error $x_{o,H_\infty}^* - \hat{x}_{o,H_\infty}$ (blue solid line). Figure 5.4 plots the worst case parameter estimation error $a_{H_\infty}^* - \hat{a}_{H_\infty}$ (blue solid line). All elements of e^* tend to zero rapidly after the initial transient period.

Theorem 4.0.4 proved the stability of $e_x = x_{o,H_\infty} - \hat{x}_{o,H_\infty}$, i.e., as $t \rightarrow \infty$, $e_x \rightarrow \mathbf{0}$. Figure 5.2 plots the state estimation error $x_{o,H_\infty} - \hat{x}_{o,H_\infty}$ for MGO (solid red line) and demonstrates the convergence property of e_x . All elements of e_x converges to zero by $t = 15$ second.

Figure 5.3 shows the parameter estimation results from both observers. Remark 2 states that given any two combinations of $\hat{x}_o = \mathbf{0}$, $e_x = \mathbf{0}$ or $x_o = \mathbf{0}$, then the system parameter observability disap-

pears, and the parameter estimation error remains constant. Furthermore, $\mathbf{A}(\hat{\xi}, z)$, which multiplies the parameter error, is a function of z . Then, as $z \rightarrow \mathbf{0}$, the observability of a also decreases. Hence, the faster x_o tends to zero, the faster the system loses parameter observability. Initially, the worst case MGO performed better than MGEKO, i.e., \hat{a}_{H_∞} converges faster towards the true parameter than the MGEKO estimate, hence leading to a stabilizing controller faster, decreasing the magnitude of x_o . However, after the first two seconds, due to smaller state x_o , convergence rate of the worst case estimator slows down and reaches steady state at around $t = 9$ seconds. The worst case parameters converged towards the true state faster in the first two seconds, yielding a stabilizing controller even faster than the estimated parameters from the modified gain observer. Hence, in comparison to LQR/MGEKO, the worst case input leads to faster convergence of state, causing a to be unobservable faster, and preventing \hat{a}_{H_∞} from converging to the true a . Initially, MGEKO converged to the true parameters slower than MGO, hence the LQR was unable to control the system in the first four seconds of the simulation, leading to a larger state. In turn, the observability in a increased. Therefore, MGEKO converged closer to the true a than the worst case MGO. Although the $\hat{a}_{H_\infty}^*$ did not reach true parameter a in steady state, the worst case controller had already stabilized the system and $x \rightarrow 0$, which is the main design goal. To decrease steady state parameter estimation error, the user can decide on the trade-off between the observability of a and the convergence of x by adding a dither signal to u^* to perturb the state and thereby increasing the observability of a . This leads to a better estimate of a .

Figure 5.5 shows four possible inputs, where two of the four inputs (u^* and u_{LQR}) are used in this simulation. u^* (blue solid line) is the worst case controller, and u_{LQR} (purple dash line) is the LQR/MGEKO controller. During the first 0.8 seconds, the disturbance attenuation controller generated a larger input than the LQR input and stabilized the true plant faster than LQR. By stabilizing the system faster than LQR, the total disturbance attenuation input cost for this 20 second simulation is smaller than the LQR input cost, i.e., $\int_0^{20} \|u^*\|_R^2 dt < \int_0^{20} \|u_{LQR}\|_R^2 dt$. Furthermore, u^* has a smaller peak magnitude than u_{LQR} .

The three solid lines of the input plot (figure 5.5) represent the worst case control gain K_{H_∞} multiplied by $x_{H_\infty}^*$, \hat{x}_{H_∞} , and x_{H_∞} , respectively. The blue line is the worst case control input u^* used

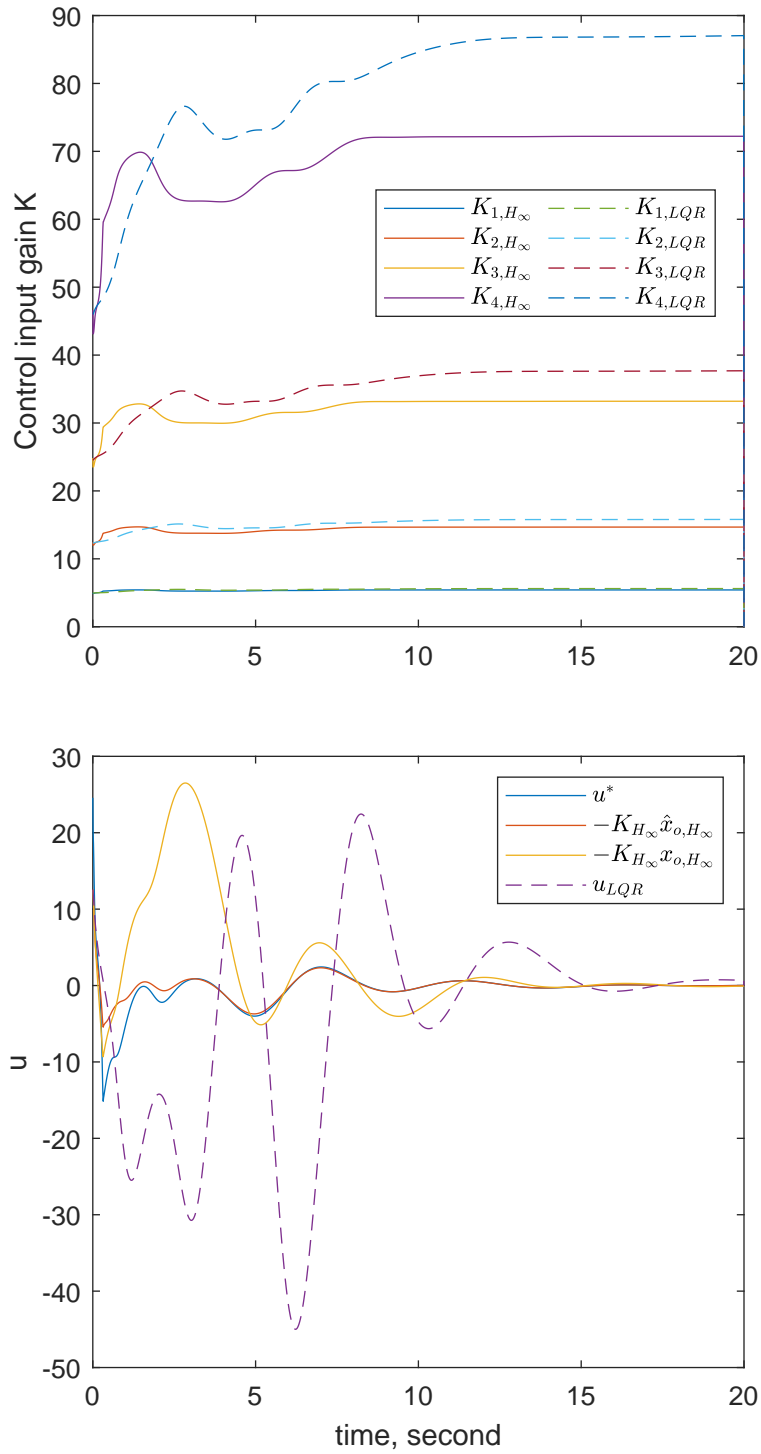


Figure 5.5: Control gain and input for worst case control and LQR.

in this simulation. At first glance, it might seem that the differences between x_{o,H_∞} , \hat{x}_{o,H_∞} , and x_{o,H_∞}^* (figure 5.1) are negligible, as they might generate similar inputs and offer similar controller performance. However, this is not the case as shown in figure 5.5. $x_{H_\infty}^*$, \hat{x}_{H_∞} , and x_{H_∞} yields different inputs (solid lines) as shown in figure 5.5. As shown in figure 5.5, the input $-K_{H_\infty}\hat{x}_{o,H_\infty}$ has a smaller peak input than u^* , whereas $-K_{H_\infty}x_{o,H_\infty}$ generates a much larger peak input that is comparable to u_{LQR} .

Lemma 4.0.3 shows that given $x_o \rightarrow \mathbf{0}$ and $u^* \rightarrow \mathbf{0}$, the steady state value of $S_c \rightarrow \mathbf{0}$. To demonstrate, the simulation is run for 100 seconds and at the end, $x_o(100)$ and $u^*(100)$ are effectively zero:

$$x_o(100) = \begin{bmatrix} -7.456 \times 10^{-15} \\ 3.185 \times 10^{-14} \\ -8.3514 \times 10^{-15} \\ -1.5061 \times 10^{-15} \end{bmatrix} \quad (5.0.42)$$

$$u^*(100) = -2.0546 \times 10^{-14}. \quad (5.0.43)$$

The corresponding S_{100} is defined as:

$$S_{100} = \begin{bmatrix} S_x(100) & S_c(100) \\ S'_c(100) & S_{\xi_r}(100) \end{bmatrix},$$

and the respective $S_x(100)$, $S_c(100)$ and $S_{\xi_r}(100)$ are:

$$S_x(100) = \begin{bmatrix} 134.77 & -454.07 & 877.56 & -758.9 \\ -454.07 & 2182.2 & -5154.5 & 5299.4 \\ 877.56 & -5154.5 & 14624 & -19253 \\ -758.9 & 5299.4 & -19253 & 43676 \end{bmatrix}$$

$$S_c(100) = 10^{-12} \begin{bmatrix} 0.01 & -0.004 & -0.01 & 5 \\ -0.09 & 1 & 1 & -22 \\ -0.7 & -1 & -0.4 & 44 \\ 0.7 & 0.6 & -0.5 & -36 \end{bmatrix}$$

$$S_{\xi_r}(100) = \begin{bmatrix} 337.18 & -14.692 & -103.03 & -13.96 \\ -14.692 & 97.731 & -3.3814 & -101.83 \\ -103.03 & -3.3814 & 105.12 & -2.4346 \\ -13.96 & -101.83 & -2.4346 & 183.08 \end{bmatrix}.$$

Both $S_x(100)$ and $S_{\xi_r}(100)$ are positive definite matrices, so S_{100} is a positive definite matrix.

Chapter 6

Application to Autonomous Hypersonic Flight Cruise Control

The autonomous cruise control of hypersonic flight is known to be notoriously challenging. At hypersonic speeds, which are above Mach 5, several challenges present itself, First, the aerodynamic data of hypersonic flight vehicles (HFV) are typically difficult to obtain. Nominal aerodynamic data are often derived from wind tunnel data using scaled down aircraft models, which can deviate significantly from the actual real-time aerodynamic. Secondly, the aerodynamic nonlinearities increase the complexities involved in the autonomous hypersonic flight control. Moreover, the boundary layers around the vehicle become extremely turbulent. Additionally, the shock waves that are generated by the body causes a huge temperature increase across the boundary layers, heating up the vehicle surface, which can possibly cause ablation of the airfoil surfaces and change the vehicle aerodynamics [56]. For example, on October 2, 1967, in the flight test for X-15, the vehicle reached Mach 6.7, but the high temperature around the vehicle had melted the pylon that attached the engine to the fuselage [57] [58]. Over the years, technological advances in various sciences enabled the engineers to develop better heat resistant airframes, enabling the plane to fly at higher Mach numbers and for longer duration. However, heat ablation of the airframe as well as panel deformation leading

to unknown time-varying changes in the vehicle aerodynamics remain serious obstacles in hypersonic flight [58]. HFV can be separated into two categories; the glider, such as the DARPA Falcon HTV-2, and the air breathing vehicle, such as the Boeing X-51 Waverider. The DARPA Falcon program flew two glider hypersonic technology vehicles (HTV) in 2010 and 2011. The first HTV glider travelled 139 seconds at Mach number ranging from 17 to 22, but terminated nine minutes into the mission as the vehicle started to roll uncontrollably. Similarly, the second HTV glider also terminated nine minutes out of the thirty minute test due to loss of contact [59], demonstrating the difficulties involved in controlling HFV.

6.1 Background

In [60], a linear quadratic regulator (LQR) designed from a linear perturbation model, which is derived from the nonlinear truth model at a certain trim condition. The LQR is applied to the truth model to track angle of attack (AoA), velocity and altitude. Without parameter uncertainty, the LQR can be used to control hypersonic aircrafts [60]. Unfortunately, the true inertial and aerodynamic coefficients are rarely known a priori, hence in practice, LQR alone is insufficient to stabilize HFV. Therefore, researchers looked to other types of control designs, such as robust control [61] [62], adaptive control [63] [64] [65] [66], nonlinear control methods [67][45] [68], and machine learning [18] [19], for close loop system stability and better tracking performance. The primary goal of hypersonic flight control is stability of the close-loop system, hence robust control is often the preferred choice of controller design for hypersonic flight control, as aircraft stability can be guaranteed for uncertain parameters within a given known bound [69]. On the other hand, for a less conservative controller and without requiring known parameter bounds, adaptive robust control with parameter estimation is considered.

In [64], an adaptive controller is used to stabilize a HFV cruising at Mach 8 and subject to five parameter uncertainties; mass, center of gravity, actuator saturation, pitch moment, lift and time-delay. In [65], the longitudinal dynamics of HFV is linearized through dynamics inversion. An adaptive controller, derived from the Lyapunov method with full state information coupled with a sliding observer, is applied to a HFV with partial state measurement. This observer based adaptive

controller yields satisfactory tracking performance in the presence of actuator faults. In [66] a low-complexity controller is applied to an air breathing HFV, subject to 20% variation in aerodynamic coefficients with asymmetric AoA constraints, where larger range of positive AoA is allowed than the negative values of AoA. The control law contains a non-adaptive altitude tracking control loop and an adaptive velocity tracking control loop. The tracking performance of the low-complexity controller is shown to be satisfactory for 20% change in aerodynamic coefficients. To improve robustness to aerodynamic coefficients, the sliding mode controller is a popular choice in HFV control due to its robustness properties; however, the resulting controller can chatter due to uncertainties and disturbances. Therefore, adaptive sliding mode controllers are proposed that eliminate this chattering behavior, such as [70] [71].

The following literatures examine an air breathing HFV cruiser at a height of 110,000 feet with a speed of Mach 15 subject to varying degrees of parameter uncertainties. In [72] and [70], smaller aerodynamic uncertainties were considered than those in [45] and [68]. In [72], a nonlinear dynamic inversion (NDI) is applied to an air breathing HFV with full state feedback and subject to 28 parameter uncertainties, which consist of both inertial and aerodynamic uncertainties. The 28 parameter uncertainties are assumed to be normally distributed. Monte Carlo simulation shows the NDI outperforms a linear quadratic control design. In [70], the air breathing vehicle with velocity and altitude measurements experiences small variations in seven uncertainties consisting of both inertial and aerodynamic uncertainties. The seven uncertainties are combined to yield two parameters, which vary by 10.4% and 25.4%. By estimating these two parameters, an adaptive sliding mode controller is used to stabilize the aircraft and track the reference signal and is shown to have superior performance over a sliding mode controller, which yields a chattering input. In [45], the HFV experiences a much larger aerodynamic uncertainty of a 50% loss in thrust, 50% loss in lift, and 25% increase in drag. Despite experiencing a large drop in altitude during the transient period, the Sum-of-Squares (SOS) method coupled with a NDI controller stabilizes the aircraft while tracking the reference height and velocity. A NDI only controller is shown to be an unstable controller for HFV with large parameter uncertainties [45]. Continuing their work, [68] expanded the number of uncertainties to six aerodynamic coefficients and demonstrates the SOS/NDI method can stabilize

the aircraft with up to a 60% parameter variation through Monte Carlo simulations. Below, we discuss how our controller achieves superior performance.

6.2 Autonomous Hypersonic Flight Cruise Control

In this case study, we consider the same flight condition and aerodynamic uncertainties as those in [45]. The worst case control scheme coupled with MGO is applied to an air breathing HFV cruising at Mach 15, with perfect full state measurement. The aircraft is subject to 50% loss in thrust and in lift, and a 25% increase in drag. The worst case scheme is able to stabilize the HFV and appears to have superior performance than those in [45]. The nominal longitudinal dynamics model is linearized to yield a nominal linearized model at a certain trim condition. However, due to the large aerodynamic uncertainties, the derived nominal equilibrium point and the nominal linearized model deviates significantly from the true equilibrium point and the true linearized model of the true nonlinear longitudinal dynamics. Hence, certain parameters in the nominal linearized model need to be estimated to accommodate for the error contributed by the large aerodynamic uncertainties. This problem can be viewed as a linear system with unknown parameters in both the system matrix and the input matrix. An observer is used to estimate the unknown parameters in the system and input matrices to yield an estimated linearized model for the controller. Without additional parameter adaptations, controllers based on the nominal linearized model might not be able to stabilize the true plant or yield satisfactory tracking performance. Therefore the worst case controller is coupled with the nonlinear MGO, derived based on an estimated linear model and is applied to the true longitudinal dynamics with large aerodynamic uncertainties. The simulation demonstrates the stability of the close loop system and the tracking performance of the worst case control scheme.

The small perturbations theory was applied to the nonlinear longitudinal dynamics to derive a linearized perturbation model, because the proposed the disturbance attenuation controller assumes a linear system dynamics for the state. Typically, small perturbation theory is used for small perturbation system and not used in systems with large uncertainties, as the error in the equilibrium point becomes too big such that the linear perturbation approximation does not hold. In this case,

a set of parameters were chosen to be estimated to account for some of error contributed by the equilibrium point such that the adaptive worst case controller still leads to a stable closed loop system as shown in the result. Although the perturbations are large and the large equilibrium change influences the linearization terms, which masks the actual values of the unknown parameters being estimated, the adaptive worst case controller still was able to stabilize the uncertain system. Consequently, the proposed worst case scheme is quite robust, even though the linearization is violated.

During the transient period, in comparison to the SOS/NDI method, which have longer transient period and a large drop in altitude, the worst case scheme reacts to the aerodynamic uncertainties faster with a small drop in velocity of about 40 ft/s in response to 50% in thrust and in lift as well as 25% in drag. The worst case scheme also converges to steady state faster with a smooth input, that does not chatter after the transient period. The SOS/NDI methods yields a highly varying or chattery input for its 1500 seconds of simulation, which is suboptimal, as this leads to an increase of the input cost. Practically, long periods of varying or chattery inputs in hypersonic vehicles can leads to faster actuator deterioration. Hence the worst case control scheme yields overall superior performance over the SOS/NDI method.

6.2.1 Aerodynamics of Hypersonic Flight

The hypersonic flight model used in this simulation as well as the truth model in [45] is a conical aircraft developed by the National Aero-Space Plane Program (NASP) at NASA [73]. A set of simulated aerodynamic tables for a conical hypersonic aircraft were created in [73], then simulated aerodynamic data in [73] were fitted at a height of 110,000 ft and a velocity of 15,060 ft/s to a set of functions presented here. Table 6.1 presents the relevant constant parameters and variables for this simulation.

The nonlinear longitudinal dynamics equations for the five rigid-body states of the aircraft, which

Constant Parameter and Variable Definition			
Constant Parameter	Description	Variable	Description
a	speed of sound, ft/sec	α	angle of attack (AoA), rad
\bar{c}	mean aerodynamic chord length, 80 ft	C_d	drag coefficient
I_{yy}	moment of inertia, 7×10^6 slug-ft ²	C_l	lift coefficient
m	mass, 9,375 slugs	$C_{M(\alpha)}$	pitching moment coefficient due to α
R_E	radius of Earth, 20,903,500 ft	$C_{M(\delta_e)}$	pitching moment coefficient due to δ_e
S	reference area, 3,603 ft ²	$C_{M(q)}$	pitching moment coefficient due to q
μ	gravitational constant, 1.39×10^{16} ft ³ /sec ²	C_T	thrust coefficient
α_0	angle of attack at trim condition, 3.1225×10^{-2} rad	δ_e	elevation deflection, rad, $-20^\circ \leq \delta_e \leq 20^\circ$
M_0	Mach number at trim condition, 15	θ	throttle setting, $0 \leq \theta \leq 1$
h_0	height at trim condition, 110,000 ft	v	velocity, ft/sec
v_0	air speed at trim condition, 15,060 ft/sec	γ	flight-path angle, rad
θ_0	throttle setting at trim condition, 0.1762	h	altitude, ft
δ_{e0}	deflection angle at trim condition, -0.00694 rad	q	pitch rate, rad/sec
		T	Thrust
		L	Lift
		D	Drag

Table 6.1: Constant and variable definition for hypersonic flight simulation.

includes velocity v , flight path angle γ , height h , AoA α , and pitch rate q , are given as follows:

$$\dot{X} = f(X, U) = \begin{bmatrix} \dot{v} \\ \dot{\gamma} \\ \dot{h} \\ \dot{\alpha} \\ \dot{q} \end{bmatrix} = \begin{bmatrix} \frac{T \cos(\alpha) - D}{m} - \frac{\mu \sin(\gamma)}{(h + R_E)^2} \\ \frac{L + T \sin(\alpha)}{mv} - \frac{(\mu - v^2(h + R_E)) \cos(\gamma)}{v(h + R_E)^2} \\ v \sin(\gamma) \\ q - \dot{\gamma} \\ \frac{\bar{q} S \bar{c} (C_{M(\alpha)} + C_{M(\delta_{el})} + C_{M(q)})}{I_{yy}} \end{bmatrix}, \quad (6.2.1)$$

where the five rigid-body state X and the control input U are defined as follows:

$$X = \begin{bmatrix} v & \gamma & h & \alpha & q \end{bmatrix}' \quad (6.2.2)$$

$$U = \begin{bmatrix} \theta & \delta_e \end{bmatrix}'. \quad (6.2.3)$$

There are three forces, thrust T , drag D , and lift L , that are affected by aerodynamic uncertainties

in this truth model. The three affected forces are defined as follows:

$$T = \kappa_1 \bar{q} S C_T, \quad D = \kappa_2 \bar{q} S C_D, \quad L = \kappa_3 \bar{q} S C_L, \quad \bar{q} = \frac{\rho v^2}{2}, \quad (6.2.4)$$

where κ_1 , κ_2 and κ_3 are the unknown aerodynamic coefficients that affect thrust, drag and lift, respectively. The aerodynamic coefficients functions derived in [74] at the trim condition v_e and h_e based on the simulated data in [73] are defined below:

$$\begin{aligned} C_L &= (0.493 + 1.91/M)\alpha \\ C_D &= 0.0082(171\alpha^2 + 1.15\alpha + 1)(0.0012M^2 - 0.054M + 1) \\ C_T &= 0.0105(1 - 164(\alpha - \alpha_e)^2)(1 + 17/M)1.15\theta \\ C_{M(\alpha)} &= 1 \times 10^{-4} (0.06 - \exp(-M/3)) (-6565\alpha^2 + 6875\alpha + 1) \\ C_{M(q)} &= \frac{\bar{c}q}{2v} (1.37 - 0.025M)(-6.83\alpha^2 + 0.303\alpha - 0.23) \\ C_{M(\delta_{el})} &= 0.0292(\delta_{el} - \alpha). \end{aligned} \quad (6.2.5)$$

Air density ρ and Mach number M are defined as:

$$\begin{aligned} \rho &= 0.00238 \exp\left(-\frac{h}{24000}\right) \\ M &= \frac{v}{8.99 \times 10^{-9} h^2 - 9.16 \times 10^{-4} h + 996}. \end{aligned} \quad (6.2.6)$$

The nominal value of the unknown aerodynamic coefficients k^o is assumed to be:

$$\kappa^o = \begin{bmatrix} \kappa_1^o & \kappa_2^o & \kappa_3^o \end{bmatrix}' = \begin{bmatrix} 1 & 1 & 1 \end{bmatrix}'. \quad (6.2.7)$$

Since the control design engineer only have access to the nominal plant (6.2.1-6.2.6, 6.2.7), then κ^o is used in deriving the nominal linearized perturbation model. However, the actual value of κ implemented in the nonlinear truth model is:

$$\kappa = \begin{bmatrix} \kappa_1 & \kappa_2 & \kappa_3 \end{bmatrix}' = \begin{bmatrix} 0.5 & 1.25 & 0.5 \end{bmatrix}'. \quad (6.2.8)$$

This set of uncertainty (6.2.8) is the same aerodynamic uncertainty implemented in [45]. This set of κ reflects 50% drop in thrust, 25% increase in drag and 50% loss in lift. The truth model (6.2.1-6.2.6, 6.2.8) presented here is the same truth model implemented in [45], where the SOS/NDI method yields a transient response of 15,000 feet drop in altitude. In practice, the difference between the nominal and actual aircraft configurations, such as the increase in drag and the loss of thrust and lift, may be due to heat ablation of the airframe during the high speed aircraft re-entry phase. These ablation effects are not known a priori, hence there exists error between the nominal plant and true plant, specifically $\kappa^o \neq \kappa$. Since the nominal aircraft configuration (6.2.1-6.2.6, 6.2.7) is different than the actual aircraft configuration (6.2.1-6.2.6, 6.2.8), their respective equilibrium point, or trim condition, may be different as well.

The actuator dynamics for engine thrust θ and elevation deflections δ_{el} are assumed to have very high bandwidth and thus is not included in the system dynamic.

6.2.2 Simulation Setup

The main goal of the controller is to stabilize the aircraft, with a secondary goal of tracking the aircraft height at $h_e = 110,000$ ft and velocity at $v_e = 15,060$ ft/s. Hence, the reference rigid-body state X_{ref} and reference input U_{ref} is defined as:

$$X_{ref} = \begin{bmatrix} v_e & 0 & h_e & \alpha_e & 0 \end{bmatrix}' \quad (6.2.9)$$

$$U_{ref} = \begin{bmatrix} \theta_e & \delta_{el_e} \end{bmatrix}', \quad (6.2.10)$$

where the values of α_e , θ_e and δ_{el_e} are defined in the nomenclature. The aircraft is initialized at a height of 108,000 ft and a velocity of 14,960 ft/s, which corresponds to a positive altitude command of 2,000 ft and a positive velocity command of 100 ft/s. Similar step function commands in velocity and altitude are also tested separately in [45]. The initial flight path angle and initial pitch rate are both zero. The initial AoA is set at α_e . The control inputs, consists of the throttle setting θ and the elevation deflection angle δ_{el} , is generated at 100 Hz and is held constant for each 0.01 second

interval. Since the system cannot have infinite input, the following bounds are imposed on the input:

$$0 \leq \theta \leq 1, \quad -20^\circ \leq \delta_{el} \leq 20^\circ. \quad (6.2.11)$$

The close-loop dynamic system is propagated using ODE45 function in Matlab. Since the system has perfect full state measurement, the initial estimate of the state can be set using the initial measurement. Hence the initial state and initial state estimates are both written as:

$$X(0) = \hat{X}(0) = \begin{bmatrix} 14,960 & 0 & 108,000 & \alpha_e & 0 \end{bmatrix}'. \quad (6.2.12)$$

6.3 Linearization of the Nonlinear Longitudinal Dynamics

The main goal of this problem is to find a set of command inputs to stabilize the aircraft around the reference point (6.2.9) from a perturbed initial velocity and height. Since the worst case control scheme assumes a linear plant (2.1.1), small perturbation theory is applied to the nonlinear longitudinal dynamics (6.2.1) around a set of nominal trim condition (X_e^o, U_e^o) (6.3.1) to derive a linearized perturbation model for the worst case control scheme. The worst case control scheme then uses the linearized model to generate worst case command inputs. The nominal equilibrium rigid-body state X_e^o and the nominal equilibrium input U_e^o , which also happen to be the reference point (X_{ref}^o, U_{ref}^o) , are defined as follows:

$$\begin{aligned} X_e^o &= X_e(\kappa^o) = \begin{bmatrix} v_e & 0 & h_e & \alpha_e & 0 \end{bmatrix}' \\ U_e^o &= U_e(\kappa^o) = \begin{bmatrix} \theta_e & \delta_{el_e} \end{bmatrix}', \end{aligned} \quad (6.3.1)$$

where the equilibrium values α_e , h_e , v_e , θ_e and δ_{el_e} defined in the nomenclature are derived using nominal coefficient κ^o . Using the definition of X (6.2.2) and X_e^o (6.3.1), the perturbed state x_p and

the perturbed input u for the linearized perturbation model is defined as follows:

$$\begin{aligned} x_p &= X - X_e^o = \begin{bmatrix} \Delta v & \Delta \gamma & \Delta h & \Delta \alpha & \Delta q \end{bmatrix} \\ u &= U - U_e^o = \begin{bmatrix} \Delta \theta & \Delta \delta_{el} \end{bmatrix}. \end{aligned} \quad (6.3.2)$$

Note the unit of Δv is km/s, not ft/s. The unit of Δh is kilometers, not feet. The units of $\Delta \gamma$, $\Delta \alpha$ and Δ_{el} are degrees, while the unit for Δq is deg/s. The change of unit in the state is to ensure the magnitude of each element is of similar order. For example, the expected variation in α is a few degrees, which is very small in radians, while an expected change in altitude can be a few kilometers, which is thousands of feet. Although this unit conversion is not necessary, but by keeping the elements in similar magnitudes, the respective error weighting S of the observer is less ill-conditioned. Note for the linearized perturbation model and the rest of the simulation, the units for x_p would remain to be in kilometers, km/s, degrees and deg/s.

Linearizing the nonlinear dynamics (6.2.1) around the nominal trim condition (6.3.1) and rewrite (6.2.1) in terms of the linearized model yields:

$$\dot{X} = f(X_e^o, U_e^o) + A_p^o(X - X_e^o) + B_p^o(U - U_e^o) + \epsilon = f(X_e^o, U_e^o) + A_p^o x_p + B_p^o u + \epsilon, \quad (6.3.3)$$

where $f(X_e^o, U_e^o)$ is nominally $\mathbf{0}_{5 \times 1}$ for aircraft dynamic with no aerodynamic uncertainty. ϵ is assumed to be a small linearization error. Furthermore, the nominal linearized system matrix A_p^o and input matrix B_p^o are defined as follows:

$$\begin{aligned} A_p^o &= \left. \frac{\partial f(X, U)}{\partial X} \right|_{X=X_e^o, U=U_e^o} \\ B_p^o &= \left. \frac{\partial f(X, U)}{\partial U} \right|_{X=X_e^o, U=U_e^o}. \end{aligned} \quad (6.3.4)$$

Unfortunately, the actual longitudinal dynamics (6.2.1-6.2.6, 6.2.8) contains aerodynamic uncertainty κ (6.2.8). Hence the true equilibrium point $(X_e(\kappa), U_e(\kappa))$ is different than the nominal

equilibrium point (6.3.1). The true equilibrium point is written as:

$$\begin{aligned} X_e(\kappa) &= \begin{bmatrix} v_e & 0 & h_e & \alpha_e(\kappa) & 0 \end{bmatrix}' \\ U_e(\kappa) &= \begin{bmatrix} \theta_e(\kappa) & \delta_{el_e}(\kappa) \end{bmatrix}', \end{aligned} \quad (6.3.5)$$

where the actual equilibrium values of AoA, thrust setting and deflection angle differ from their respective nominal values as shown below:

$$\alpha_e(\kappa) = 3.513^\circ, \quad \theta_e(\kappa) = 0.7378, \quad \delta_{el_e}(\kappa) = -0.6448^\circ. \quad (6.3.6)$$

The difference between the actual equilibrium point (6.3.5) and nominal equilibrium point (6.3.1) introduces error in the linearized perturbation model (6.3.4) and $f(X_e^o, U_e^o)$, which is no longer $\mathbf{0}_{5 \times 1}$. This is because the linearization of the actual nonlinear dynamics (6.2.1) in terms of the true equilibrium point (6.3.5) is:

$$\dot{X} = f(X_e(\kappa), U_e(\kappa)) + A_p(X - X_e(\kappa)) + B_p(U - U_e(\kappa)) + \epsilon, \quad (6.3.7)$$

where $f(X_e(\kappa), U_e(\kappa))$ is $\mathbf{0}_{5 \times 1}$ for the actual aircraft dynamic (6.2.1-6.2.6, 6.2.8). Furthermore, the true linearized system matrix A_p and input matrix B_p are defined as follows:

$$\begin{aligned} A_p &= \left. \frac{\partial f(X, U)}{\partial X} \right|_{X=X_e(\kappa), U=U_e(\kappa)} \\ B_p &= \left. \frac{\partial f(X, U)}{\partial U} \right|_{X=X_e(\kappa), U=U_e(\kappa)}. \end{aligned} \quad (6.3.8)$$

Due to the large difference between κ^o and κ , controllers generated using the nominal linearized system (6.3.4) may not yield stabilizing input. Moreover, the nominal aircraft configuration has different equilibrium point than the true aircraft configuration, i.e., $X_e(\kappa^o) \neq X_e(\kappa)$ and $U_e(\kappa^o) \neq U_e(\kappa)$. This difference can introduce errors into the linearized perturbation model. Hence, certain elements of the nominal linearized perturbation model need to be estimated to account for the error in κ^o and the error in (X_e^o, U_e^o) , so a set of estimated linear system that can be derived to yield a stabilizing controller. The question is which element of the nominal linearize system should be

estimated? To address this question, we examine the difference between (6.3.4) and (6.3.8). First, note the difference between (6.3.5) and (6.3.1) lies only in the AoA and the two inputs. Hence, we can evaluate the first order derivatives at the states with common equilibrium point, i.e.:

$$\begin{aligned} A_p(\kappa, \alpha, \theta, \delta_{el}) &= \left. \frac{\partial f(X, U)}{\partial X} \right|_{v=v_e, \gamma=0, h=h_e, q=0} \\ B_p(\kappa, \alpha, \theta, \delta_{el}) &= \left. \frac{\partial f(X, U)}{\partial U} \right|_{v=v_e, \gamma=0, h=h_e, q=0}. \end{aligned} \quad (6.3.9)$$

Since the elements of (6.3.9) are functions of κ , α , and inputs, then one can examine each individual elements to see the effects of the error in the equilibrium point. For example, we define the following terms:

$$\eta_1 = -0.25366 \cos(0.01745\alpha)(1.72(0.01745\alpha - 0.0312)^2 - 0.0105) \quad (6.3.10)$$

$$\eta_2 = -0.04575(4.27 \times 10^{-4}\alpha^2 + 1.646 \times 10^{-4}\alpha + 0.0082), \quad (6.3.11)$$

then the top left element of $A_p(\kappa, \alpha, \theta, \delta_{el})$ can be written as:

$$A_p(\kappa, \alpha, \theta, \delta_{el})(1, 1) = \eta_1 \kappa_1 \theta + \eta_2 \kappa_2. \quad (6.3.12)$$

This implies the thrust uncertainty κ_1 and the drag uncertainty κ_2 affect $A_p(\kappa, \alpha, \theta, \delta_{el})(1, 1)$ linearly. By considering different possible ranges of κ , one can conclude the variation in η_1 and η_2 induced by the difference in the equilibrium point of α is relatively small in comparison to $\kappa_1 \theta$ and κ_2 , which contains larger variations. Define $\kappa_1 \theta$ and κ_2 as a function of the nominal κ^o and θ_e :

$$\kappa_1 \theta = \kappa_1^o \theta_e + \zeta_1 \quad (6.3.13)$$

$$\kappa_2 = \kappa_2^o + \zeta_2, \quad (6.3.14)$$

where ζ_1 and ζ_2 are elements of the unknown parameters to be estimated by the observer. Using

(6.3.12), (6.3.13) and (6.3.14), then $A_p(\kappa, \alpha, \theta, \delta_{el})(1, 1)$ can be approximate as:

$$\begin{aligned}
A_p(\kappa, \alpha, \theta, \delta_{el})(1, 1) &\approx \eta_1|_{\alpha_e}(\kappa_1^o\theta_e + \zeta_1) + \eta_2|_{\alpha_e}(\kappa_2^o + \zeta_2) \\
&= \underbrace{\eta_1|_{\alpha_e}\kappa_1^o\theta_e + \eta_2|_{\alpha_e}\kappa_2^o}_{A_0(1,1)} + \underbrace{\eta_1|_{\alpha_e}}_{A_1(1,1)}\zeta_1 + \underbrace{\eta_2|_{\alpha_e}}_{A_2(1,1)}\zeta_2 \\
&= A_0(1, 1) + A_1(1, 1)\zeta_1 + A_2(1, 1)\zeta_2,
\end{aligned} \tag{6.3.15}$$

where A_0 is the nominal system matrix, A_1 and A_2 are the known coefficients in (2.1.5) of the unknown parameters to be estimated by the observer. Note η_1 (6.3.10) and η_2 (6.3.11) are evaluated at α_e for the purpose of approximating $A_p(\kappa, \alpha, \theta, \delta_{el})(1, 1)$, because it is the nominal equilibrium point for α and is known to the control design engineer. Furthermore, as mentioned before, η_1 and η_2 have relatively small variations due to changes in the equilibrium point of α in comparison to $\kappa_1\theta$ and κ_2 .

Remark 11. *Small perturbation theory is normally used for systems with small uncertainties so that the error contributed by $f(X_e^o, U_e^o) - f(X_e(\kappa), U_e(\kappa))$ is sufficiently small so that the first order approximation still holds. However, for large perturbations, $f(X_e^o, U_e^o) - f(X_e(\kappa), U_e(\kappa))$ is no longer insignificant. The first order perturbation system based on nominal parameters and the perturbation system based on actual parameters are no longer similar to each other, i.e. (6.3.4) is no longer similar to (6.3.8). This difference masks the actual value of the unknown parameters, which are being estimated. Hence for the estimation of the unknown parameters does not converge to the actual parameter value. For example, since $\eta_1|_{\alpha_e} \neq \eta_1|_{\alpha_e(\kappa)}$ and $\eta_2|_{\alpha_e} \neq \eta_2|_{\alpha_e(\kappa)}$, then the estimate of ζ_1 and ζ_2 does not converge to the actual value of ζ_1 and ζ_2 . However, the estimation of ζ_1 and ζ_2 does reach steady state value. However, parameter estimates does converge rapidly to steady state for which the close loop system remains stable.*

We define the rest of the unknown parameters:

$$\kappa_3 = \kappa_3^o + \zeta_3 \tag{6.3.16}$$

$$\kappa_1 = \kappa_1^o + \zeta_4. \tag{6.3.17}$$

κ_i and Affected Partial Derivatives							
	∂v	$\partial \gamma$	∂h	$\partial \alpha$	∂q	$\partial \theta$	$\partial \delta_{el}$
\dot{v}	κ_1, κ_2		κ_1, κ_2	κ_1, κ_2		κ_1	
$\dot{\gamma}$	κ_1, κ_3		κ_1, κ_3	κ_1, κ_3		κ_1	
\dot{h}							
$\dot{\alpha}$	κ_1, κ_3		κ_1, κ_3	κ_1, κ_3		κ_1	
\dot{q}							

Table 6.2: The effect of κ on the perturbation model

Take the analysis that was done for $A_p(\kappa, \alpha, \theta, \delta_{el})(1, 1)$, and repeat the process for all elements of (6.3.9). One can see that $\kappa_1\theta$, the drag uncertainty κ_2 and lift uncertainty κ_3 enters elements of $A_p(\kappa, \alpha, \theta, \delta_{el})$ linearly, while κ_1 enters $B_p(\kappa, \alpha, \theta, \delta_{el})$ linearly. The effect of κ on the linear perturbation model can be seen in table 6.2. Hence we choose to estimate the following set of four unknown parameters ζ :

$$\zeta = \left[\kappa_1\theta_e(\kappa) - \kappa_1^o\theta_e \quad \kappa_2 - \kappa_2^o \quad \kappa_3 - \kappa_3^o \quad \kappa_1 - \kappa_1^o \right]'. \quad (6.3.18)$$

Upon examining Table 6.2 and (6.3.8), one might immediately suggest to estimate the difference between κ^o and κ (6.2.8), rather than the four parameters (6.3.18). However, the error from the equilibrium point can degrade the worst case controller performance. Hence, we choose to estimate the four parameters as shown in (6.3.18) to account for some of the errors contributed by both the κ and the equilibrium point. Obviously, one can also choose to estimate more parameters in the hopes of leading to a better controller performance, but the trade off would be an increase in computational time required to find the worst case control input.

Using (6.3.2) and (6.3.8), we define the following linear perturbation system with perfect measurement:

$$\begin{aligned} \dot{x}_p &= A_p x_p + B_p u + G_p \omega \\ z &= x_p, \end{aligned} \quad (6.3.19)$$

where ϵ is approximated by $G_p\omega$. In this case, we choose G_p as

$$G_p = \begin{bmatrix} 1 & 1 & 0 & -1 & 0 \\ 0 & 0 & 0 & 0 & 1 \end{bmatrix}'. \quad (6.3.20)$$

This choice of G_p is selected to ensure the existence of the solution to the control Riccati equation (2.4.6).

The error in the nominal equilibrium point (6.3.1) can lead to steady-state error in height and velocity. To ensure that the controller can track both height and velocity, x_p is augmented with integral action on velocity and height to yield the state x as defined below:

$$x = \begin{bmatrix} x'_p & \int_0^t \Delta v d\tau & \int_0^t \Delta h d\tau \end{bmatrix}'. \quad (6.3.21)$$

Recalling $A(\zeta)$ (2.1.5) and $B(\zeta)$ (2.1.6), we present the nominal system and control matrix for the nominal perturbation model. Evaluating A_p^o and B_p^o (6.3.4) leads to:

$$A_p^o = \begin{bmatrix} 1.7789 \times 10^{-5} & -1.6746 \times 10^{-4} & -2.8333 \times 10^{-7} & -2.5244 \times 10^{-4} & 0 \\ 4.862 \times 10^{-2} & 0 & -1.067 \times 10^{-2} & 4.3989 \times 10^{-2} & 0 \\ 0 & 8.0116 \times 10^{-2} & 0 & 0 & 0 \\ -4.862 \times 10^{-2} & 0 & 1.067 \times 10^{-2} & -4.3989 \times 10^{-2} & 1 \\ 9.9967 \times 10^{-1} & 0 & -1.5921 \times 10^{-2} & 5.9448 \times 10^{-1} & -6.8203 \times 10^{-2} \end{bmatrix} \quad (6.3.22)$$

$$B_p^o = \begin{bmatrix} 8.3201 \times 10^{-3} & 0 \\ 3.2438 \times 10^{-3} & 0 \\ 0 & 0 \\ -3.2438 \times 10^{-3} & 0 \\ 0 & 3.3168 \end{bmatrix}. \quad (6.3.23)$$

The nominal A_0 and B_0 generated using the nominal κ^o as a function of A_p^o and B_p^o are defined as

follows:

$$\begin{aligned}
 A_0 &= \begin{bmatrix} A_p^o & & & \mathbf{0}_{5 \times 2} \\ 1 & \mathbf{0}_{1 \times 2} & \mathbf{0}_{1 \times 2} & \mathbf{0}_{1 \times 2} \\ \mathbf{0}_{1 \times 2} & 1 & \mathbf{0}_{1 \times 2} & \mathbf{0}_{1 \times 2} \end{bmatrix} \\
 B_0 &= \begin{bmatrix} B_p^o \\ \mathbf{0}_{2 \times 2} \end{bmatrix}.
 \end{aligned} \tag{6.3.24}$$

The respective nominal A_i for ζ are defined as follows:

$$\begin{aligned}
 A_1 &= \begin{bmatrix} 2.6622 \times 10^{-3} & 0 & -1.122 \times 10^{-3} & -4.5357 \times 10^{-6} & \mathbf{0}_{1 \times 3} \\ 3.3124 \times 10^{-4} & 0 & -4.3745 \times 10^{-4} & 1.8125 \times 10^{-3} & \mathbf{0}_{1 \times 3} \\ 0 & 0 & 0 & 0 & \mathbf{0}_{1,3} \\ -3.3124 \times 10^{-4} & 0 & 4.3745 \times 10^{-4} & -1.8125 \times 10^{-3} & \mathbf{0}_{1 \times 3} \\ \mathbf{0}_{3,1} & \mathbf{0}_{3,1} & \mathbf{0}_{3,1} & \mathbf{0}_{3,1} & \mathbf{0}_{3 \times 3} \end{bmatrix} \\
 A_2 &= \begin{bmatrix} -4.5124 \times 10^{-4} & 0 & 1.974 \times 10^{-4} & -2.5164 \times 10^{-4} & \mathbf{0}_{1 \times 3} \\ \mathbf{0}_{6 \times 1} & \mathbf{0}_{6 \times 1} & \mathbf{0}_{6 \times 1} & \mathbf{0}_{6 \times 1} & \mathbf{0}_{6 \times 3} \end{bmatrix} \\
 A_3 &= \begin{bmatrix} 0 & 0 & 0 & 0 & \mathbf{0}_{1 \times 3} \\ 1.3526 \times 10^{-2} & 0 & -1.0624 \times 10^{-2} & 4.3669 \times 10^{-2} & \mathbf{0}_{1 \times 3} \\ 0 & 0 & 0 & 0 & \mathbf{0}_{1 \times 3} \\ -1.3526 \times 10^{-2} & 0 & 1.0624 \times 10^{-2} & -4.3669 \times 10^{-2} & \mathbf{0}_{1 \times 3} \\ \mathbf{0}_{3 \times 1} & \mathbf{0}_{3 \times 1} & \mathbf{0}_{3 \times 1} & \mathbf{0}_{3 \times 1} & \mathbf{0}_{3 \times 3} \end{bmatrix} \\
 A_4 &= \mathbf{0}_7.
 \end{aligned} \tag{6.3.25}$$

The derived respective nominal B_i are as follows:

$$\begin{aligned}
 B_1 &= B_2 = B_3 = \mathbf{0}_{7 \times 2} \\
 B_4 &= B_0.
 \end{aligned} \tag{6.3.26}$$

6.4 Defining the Augmented System and Weightings for Worst Case Controller

Using the derived nominal A_i and B_i , we proceed to form the augmented system. Recall that the augmented state ξ defined in (2.1.7) with the respective nonlinear dynamics of the augmented state (2.1.8) and the measurement (2.5.3) are defined as follows:

$$\dot{\xi} = \begin{bmatrix} A(\zeta)x + B(\zeta)u \\ \mathbf{0}_{4 \times 1} \end{bmatrix} + \begin{bmatrix} G \\ \mathbf{0}_{4 \times 1} \end{bmatrix} \omega = f(\xi, u) + \Gamma\omega, \quad \text{where } G = \begin{bmatrix} G_p \\ \mathbf{0}_{2 \times 2} \end{bmatrix}. \quad (6.4.1)$$

$$z = \begin{bmatrix} \mathbf{I}_7 & \mathbf{0}_{7 \times 4} \end{bmatrix} \begin{bmatrix} x \\ \zeta \end{bmatrix} = \bar{H}\xi, \quad (6.4.2)$$

where G_p is defined previously in (6.3.20). Note the last two states of x in (6.3.21) are integral actions on velocity and height, which are measured perfectly. Hence, both integrals can be assumed to have perfect measurements.

The augmented system matrix in (2.5.13) for the MGO is defined as follows:

$$\mathcal{A}(\hat{\xi}, z, u) = \begin{bmatrix} A(\hat{\zeta}) & A_1z + B_1u & \cdots & A_4z + B_4u \\ \mathbf{0}_{4 \times 7} & \mathbf{0}_{4 \times 1} & \cdots & \mathbf{0}_{4 \times 1} \end{bmatrix}. \quad (6.4.3)$$

The following worst case controller constant weightings (2.2.3), which are defined in the performance index (2.2.5), selected for this case study are:

$$\bar{Q} = \begin{bmatrix} Q & \mathbf{0}_{7 \times 4} \\ \mathbf{0}_{4 \times 7} & \mathbf{0}_4 \end{bmatrix} \quad (6.4.4)$$

$$Q = \text{diag}(50, 1 \times 10^{-4}, 1, 1 \times 10^{-3}, 0.1, 0.01, 1 \times 10^{-5}) \quad (6.4.5)$$

$$W = \text{diag}(0.01, 0.01) \quad (6.4.6)$$

$$V = \text{diag}(1 \times 10^{-8}, 1 \times 10^{-3}, 1 \times 10^{-8}, 1 \times 10^{-3}, 1 \times 10^{-3}, 1 \times 10^{-8}, 1 \times 10^{-8}) \quad (6.4.7)$$

$$R = \text{diag}(0.001, 0.001). \quad (6.4.8)$$

Note the Δv and Δh units are km/s and kilometer, while attitude states are in degrees or deg/s, then the variation in velocity and height is smaller in comparison to the attitude states. For example, the one km/s drop in Δv translates to 3,280 ft/s, this is a very big and unacceptable drop in Δv . Hence, the large weighting on Δv is placed in $Q(1, 1)$ in (6.4.5). A drop of one kilometer in height is a relatively acceptable magnitude in comparison to velocity, as the initial Δh starts off with a drop of 2,000 feet. Hence, the smaller weighting used in $Q(3, 3)$. The attitude states can vary a few degrees or deg/s, hence the much smaller weighting in $Q(2, 2)$, $Q(4, 4)$ and $Q(5, 5)$ for the attitude states. The integral state weightings are relatively small, as we want a gradual convergence of the tracking error. Too fast of a convergence in Δh and Δv can yield higher transient pitch rate and overly large transient AoA. For stability and to prevent engine stall, AoA should remain between $\pm 11^\circ$ [64].

Recall V is a constant weighting on the measurement in the accumulation function (2.5.4). V is used as a tuning parameter to adjust the rate of convergence for the augmented state estimates. Since Δv and Δh measurements can be very precise, we choose small weightings in the corresponding elements of V in (6.4.7). However, it must be noted from stochastic point of view, a variance of 1×10^{-8} km² corresponds to 0.328 feet in standard deviation. This might seem small, but we had assumed that we have perfect measurement of the state, so this is acceptable. Note the small weightings in V for Δv and Δh , indicating the level of confidence in the velocity and height measurement, would lead to very negligible differences between their true states, their state estimates and their worst case state estimates. The attitude states are in degrees, hence the relatively larger weighting in V on the order of 0.001 is set for the attitude states.

The initial augmented state and estimate of augmented state is set at:

$$\xi(0) = \begin{bmatrix} -0.03048 & 0 & -0.6096 & \mathbf{0}_{1 \times 2} & \zeta' \end{bmatrix}' \quad (6.4.9)$$

$$\hat{\xi}(0) = \begin{bmatrix} -0.03048 & 0 & -0.6096 & \mathbf{0}_{1 \times 2} & \mathbf{0}_{1 \times 4} \end{bmatrix}', \quad (6.4.10)$$

which corresponds to the initial Δv at -100 ft/s and the initial Δh of $-2,000$ feet. Again, note the velocity and height units are km/s and kilometers respectively. The initial estimate of ζ is

initialized at zero, as we expect the nominal system to be the correct model. The respective initial error weighting $P(0)$ is set as

$$P(0) = \text{diag}(0.03, 0.1, 0.03, 0.5, 0.1, 0.1, 0.1, 0.001, 0.001, 0.001, 0.001). \quad (6.4.11)$$

The error weighting in $P(0)$ for height is 0.03 km^2 might seem small at first glance. However, from stochastic point of view, the variance of 0.03 km^2 corresponds to a variance of 322917 ft^2 or a standard deviation of 568 feet. So the initial error weighting for velocity and height are fairly large. The respective angle error weightings are 0.1. The aerodynamic coefficients are thought to be fairly accurate, hence the error weightings on those elements are small at 0.001. If the initial estimated uncertainties differ significantly from the actual uncertainties, then the smaller the error weighting on the uncertain parameters, the slower the convergence rate of the uncertainty estimates. However, in this case, even though the error weightings are small, the convergence rate of the worst case parameters still yield a stable input.

6.5 Simulation Result

The simulation ran for 1,000 seconds to demonstrate the performance of the worst case controller in stabilizing a hypersonic aircraft with uncertain aerodynamic coefficients. Figure 6.1 presents the state history x in blue lines, state estimate \hat{x} in red lines and worst case state x^* in green lines. Since V (6.4.7) is small, the three lines are on very close to each other. As shown, the initial velocity is 100 ft/sec slower than the target velocity v_e , and the initial height is 2,000 ft lower than the target height h_e . Controller using only the nominal A_0 and B_0 as plant model might yield conservative inputs, have suboptimal performance, and might be unable to stabilize the aircraft, due to the error in the A_0 and B_0 . The worst case controller scheme was able to quickly generate a set of control inputs that not only stabilize the aircraft, but also track both height and velocity to zero due to the integral actions on these two states. If the integral actions were not included as part of the state, there would exist a steady state error in height and possibly velocity, but the aircraft would still be stable.

As shown in figure 6.1, the velocity dropped initially by approximately 40 ft/sec due to the effect of the uncertain parameters. The MGO was able to quickly adjust the parameter estimates to yield a stabilizing controller. Hence, the controller was able to quickly converge in height and velocity. The integral weighting on height is very small at 1×10^{-5} to prevent large transient AoA and engine stall as mentioned before, hence the convergence of height to zero is slow, but the aircraft still reaches target height by the end of the simulation.

The parameter error in dynamics of pitch rate is not estimated as no parameter uncertainties enter into the pitch rate dynamics, however a small error contributing from error in the nominal equilibrium point remains in the nominal pitch rate dynamics used by the observer. This leads to a bias of 0.0635° in the steady state pitch rate. However, 300 seconds into the simulation, the true pitch rate reaches $6.79 \times 10^{-5} \text{ }^\circ/\text{s}$ and remain in steady state despite the bias in pitch rate estimate. Practically, the pitch rate is in steady state.

The true AoA trim condition for the aircraft is 3.513° . The true trim condition of the thrust setting is 0.738, and the true trim condition of the deflection angle is -0.645° . Although error exists in the nominal equilibrium value α_e and U_e , the worst case controller stills converge towards the true equilibrium point of the aircraft and stabilize the system. The aircraft reaches sufficiently close to the true equilibrium point at around 700 seconds and remains in steady state for the rest of the simulation. By the end of the simulation, the steady state AoA is 3.518° which is very close to the true AoA trim condition.

Figure 6.2 shows the initial first 0.1 seconds of the simulation. The initial worst case state differs from the initial state and initial estimate. The differences are significant in velocity and height, where the difference in velocity is about 65 ft/s and the difference in height is about 950 feet. However, due to the small weighting V in the velocity and height position, the worst case velocity and height converges quickly to the estimates values. This is shown in figure 6.2. If one wishes to slow down the convergence rate of ξ^* to $\hat{\xi}$, one can increase V .

Figure 6.3 presents the estimation of the unknown parameters. The observer was able to react quickly to the error introduced by the different aircraft configurations ($\kappa \neq \kappa^\circ$) and yield a stabilizing worst

case controller. The parameter estimates are similar to the worst case parameters, as the error weighting elements in $P(0)$ corresponding to the unknown parameters are very small and is on the order of 0.001. One can increase the parameter error weightings in $P(0)$ to increase the difference between the worst case parameter and the estimates. As mentioned in remark 11, the error in the linearization due to the large parameter perturbation masks the true parameters being estimated, hence $\hat{\zeta}$ does not tend to the actual value of ζ . However, the parameter estimates does reach steady state value and worst case scheme yields a stable controller.

Figure 6.4 presents the input signal for the thrust setting θ and the deflector angle δ_{el} . The controller saturates the thrust setting at the beginning to increase velocity towards its target velocity. After approximately 47 seconds, the thrust setting converges towards the equilibrium point. Figure 6.5 presents a closer view of the transient behavior of the input.

A similar hypersonic aircraft truth model was also considered in [45], with 50% decreases in thrust coefficient, 50% decrease in lift coefficient and 25% increase in drag. In [45], the nonlinear dynamic system is split into two parts, a slow dynamics containing all states except pitch rate, and a fast dynamics that only contains pitch rate. A SOS based controller is used to derive the thrust setting θ and a command pitch rate. A NDI based controller then takes the commanded pitch rate to derive a deflection angle. The SOS/NDI algorithm was shown to stabilize the hypersonic aircraft around the reference signal while subject to the large aerodynamic uncertainties. As comparison, the SOS/NDI method is compared to the NDI/NDI method, where the NDI method was also used to control the slow dynamics. The NDI/NDI method was unable to stabilize the hypersonic aircraft subject to such large parameter uncertainties. Though the SOS/NDI algorithm was able to stabilize the aircraft with uncertainties, the transient response of the aircraft was sluggish.

When subject to a 100 ft/sec airspeed command, the aircraft dropped about 15,200 feet during the transient period before recovering back to the reference height. Furthermore, it takes about 700 seconds to recover the loss in height during the transient period. When subject to a 2,000 feet altitude command, altitude drop of roughly 14,500 feet was also observed. By comparison, when simultaneously subject to a 100 ft/sec airspeed command and a 2,000 feet altitude command, the

worst case controller was able to stabilize the aircraft at the reference velocity and height without such significant loss in altitude during the transient period. The respective deflection angle in [45] also fluctuates around the equilibrium point and does not remain in steady state for the 1,500 seconds of their simulation. This implies wasted actuator energy over a long period of time and suggests an increase in input cost. Practically, frequent actuation of the deflector is stressful on the actuator itself. In contrast, the worst case deflection angle reaches steady state value quickly after stabilizing the aircraft around v_e and h_e . Hence, in terms of performance and input efficiency, the worst case control scheme has outperformed the SOS/NDI algorithm as presented in [45].

6.5.1 Future Work

In this case study, the system has perfect full state measurement. In practice, the altitude and velocity can be measured with reasonable accuracy using data from global positioning system (GPS). The flight path angle can also be calculated from the change in altitude and velocity. However, AoA measurements can be noisy [70]. For HFV with perfect partial measurements, the original controllable and observable linearized system must first be transformed into an observable canonical form. The disturbance attenuation controller coupled with the nonlinear MGO can then be applied to the transformed system.

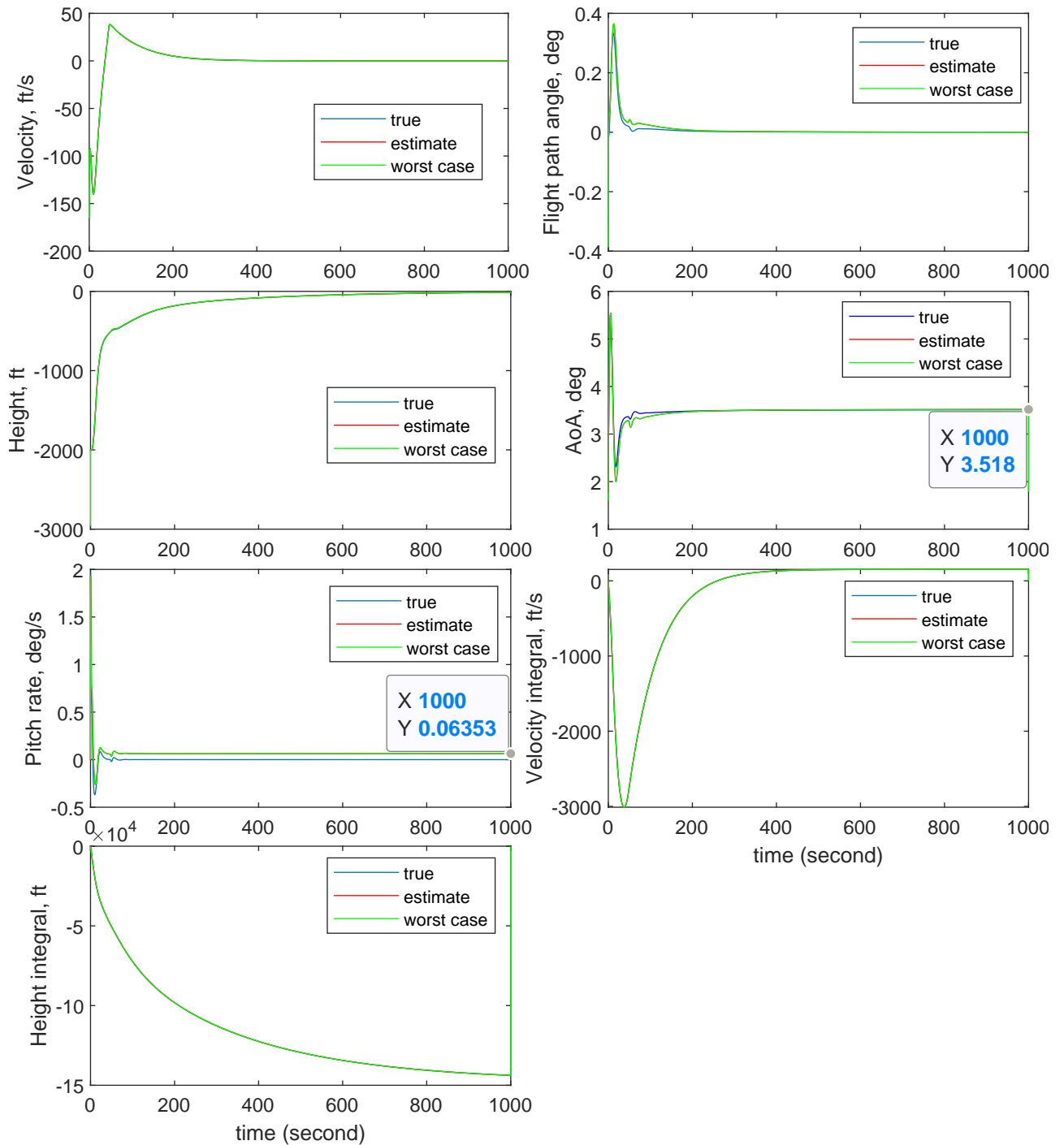


Figure 6.1: True state x , state estimate \hat{x} and worst-case state x^* are displayed in blue, red and green, respectively. Since V (6.4.7) is small, the three lines are very close to each other. The error in the nominal equilibrium point leads to the small steady state bias between the pitch rate estimate and the true pitch rate.

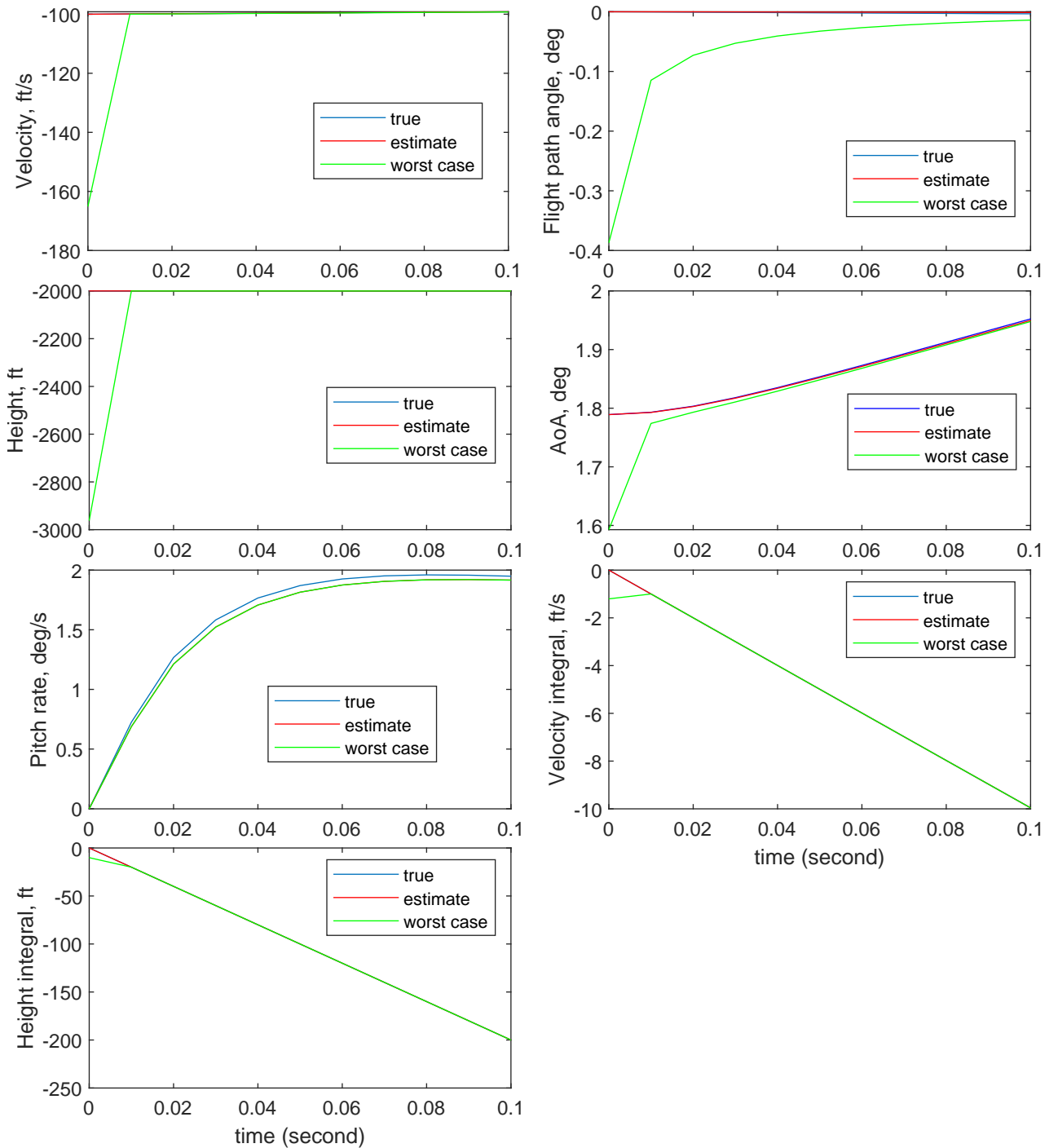


Figure 6.2: This is a close up look of the state history for the first 0.1 seconds. The initial worst case state is different than the initial state estimate as well as initial state. Since the system is assumed to have perfect measurement and V is very small, then the state estimate is very close to the true state. The initial differences between the worst case velocity and the initial velocity is about 65 ft/s. The initial differences between the worst case height and the initial height is about 950 feet.

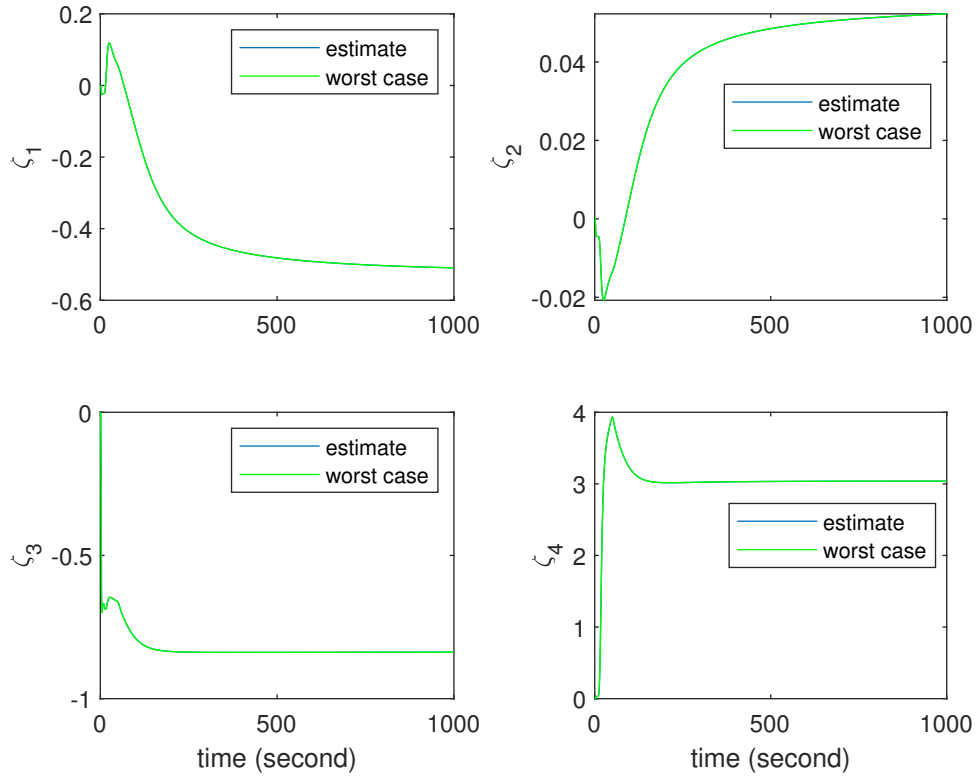


Figure 6.3: $\hat{\zeta}$ and ζ^* are displayed in blue and green lines, respectively. Since initial error weighting in ζ is very small, $\hat{\zeta}$ and ζ^* is very close to each other, hence the blue and green lines are on top of each other. The large equilibrium change influences the linearization terms A_i and B_i , and mask the actual values of the unknown parameters, which are being estimated. Hence $\hat{\zeta}$ does not tend to actual ζ . However, the observer does yield a stable worst case controller, even though the linearization is violated.

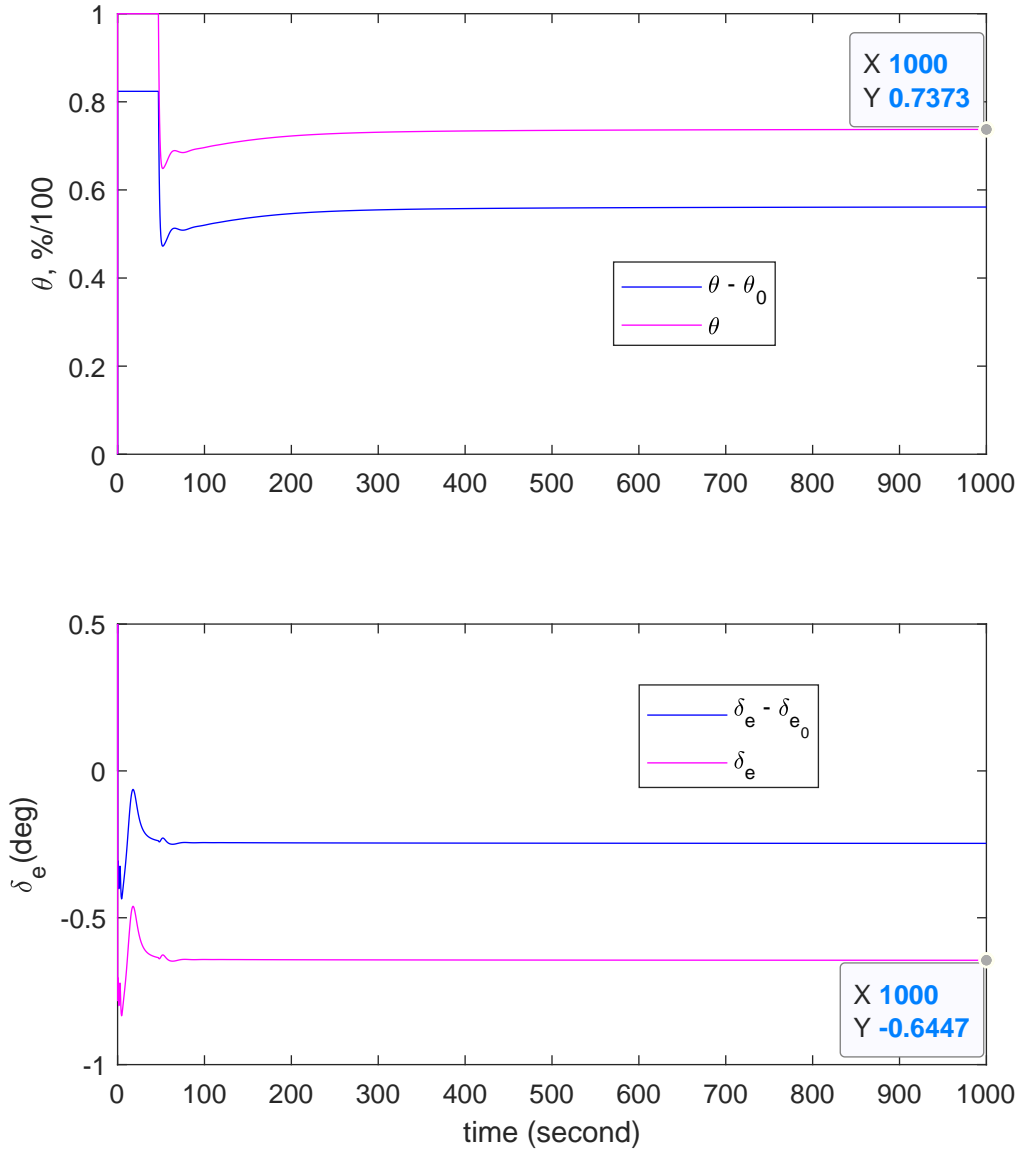


Figure 6.4: The input history of 1000 seconds are displayed here. The thrust setting θ was saturated initially to increase velocity towards v_e . After velocity reaches past v_e , the thrust setting converges towards the true equilibrium setting of the aircraft. The deflection angle also saturated initially, but quickly converges towards the equilibrium deflection angle after the aircraft reaches sufficiently close to the target velocity v_e .

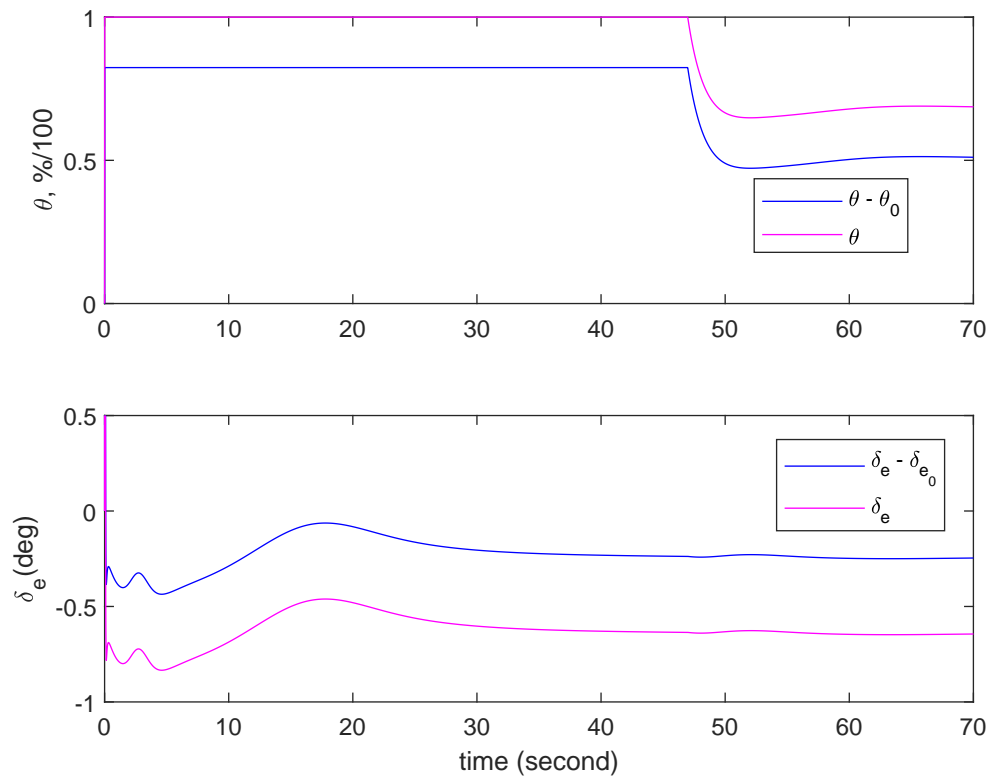


Figure 6.5: The input history of 70 seconds are displayed here.

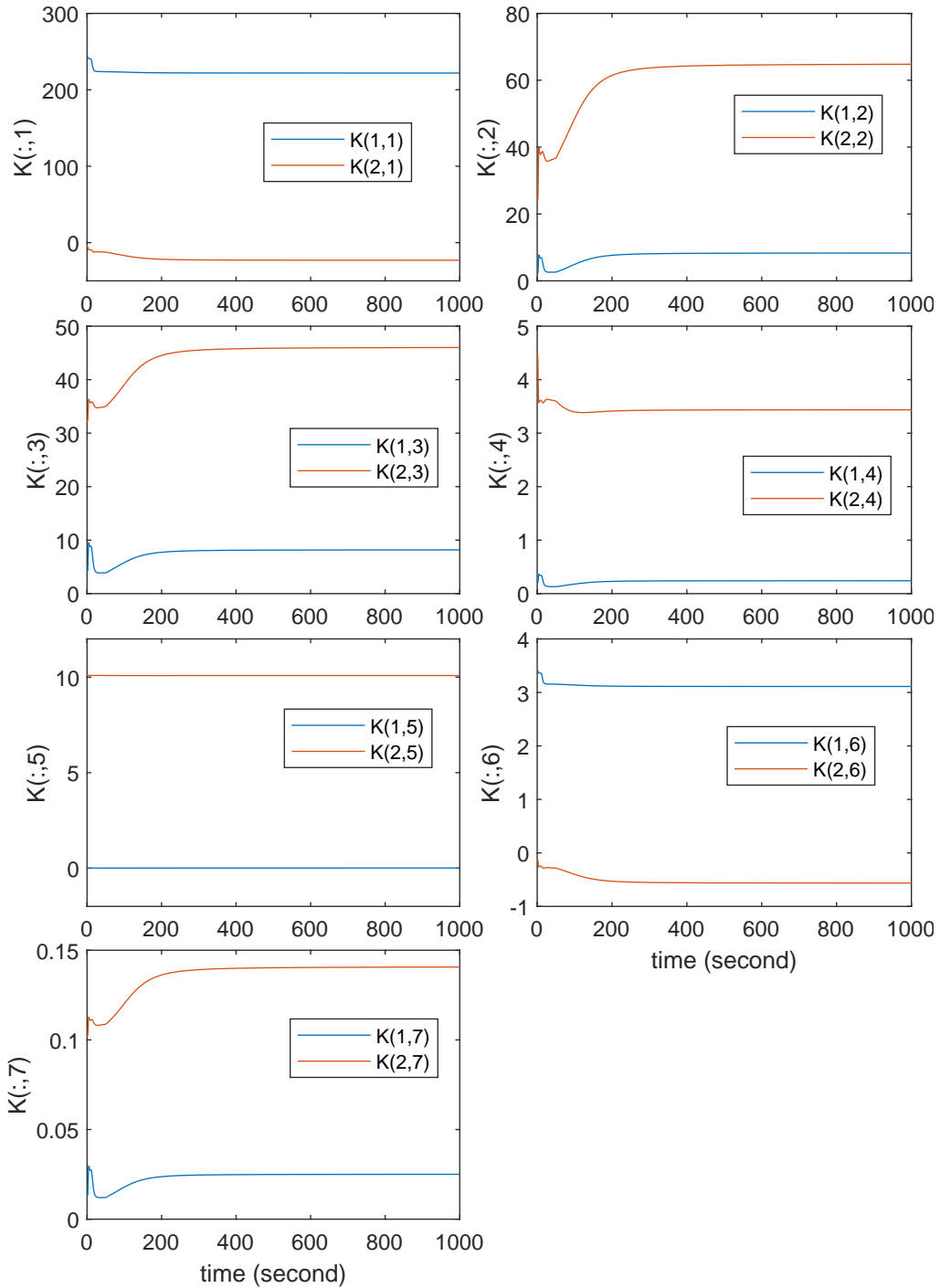


Figure 6.6: Worst case control input gain history for 1000 seconds. The blue lines represent the top row of the input gain, which is associated with the thrust. The red lines represent the bottom row of the input gain, which is associated with the deflection angle.

Chapter 7

Conclusion and Future Work

In the current work, we examined a linear system subject to process disturbance and unknown plant variations in both system and control matrices. The plant makes perfect partial measurement and is subject to a differential games cost function based on disturbance attenuation function, which pits the input against process disturbances and plant uncertainties. The optimization yields a worst-case controller coupled with a nonlinear modified gain observer to stabilize the plant. The observer yields an estimate of the state and the system parameters as well as the respective weightings associated with the error of those estimates. Base on both the estimates and the weighting on the estimation error, a set of worst-case parameters is derived with respect to the cost function. Using the worst-case parameters, the worst-case control gain is generated for the system. The current work also presented the saddle point condition as well as the stability conditions for the disturbance attenuation controller. It was shown given a certain conditions, such as observability and controllability as well as existence of solutions to the Riccati equation, the close loop system is stable.

The worst case control scheme is applied to an unstable linear system with unknown system parameter subject to perfect partial measurement. The example illustrates the superior performance of the worst case controller coupled with the MGO over the LQR coupled with MGEKO. Furthermore, this

work also applies the worst case control scheme to an air-breathing HFV with full state measurement and subject to large aerodynamic uncertainties, such as 50% loss in thrust, 50% drop in lift and 25% increase in drag. The worst case control scheme demonstrates faster tracking performance and better transient performance than the SOS/NDI algorithm presented in [45].

As discussed in the current work, the optimality conditions are difficult to solve in close form solution to find the worst-case parameters. Numerical methods must be utilized to solve the optimality conditions. Hence, finding efficient numerical methods to solve the optimality conditions is important. Secondly, the stability condition requires five assumptions, which includes the existence of solution to the controller and observer Riccati equations. However, the existence of solution is difficult to ascertain at the initial time. One area of possible future work is to determine the range of initial error weightings that can guarantee the existence of solution to both Riccati equations given initial parameter and state estimates, and thereby ensure stability of the unknown linear system at initial time. Lastly, the stability properties of the worst case controller was proved using a Lyapunov function. One can also prove the close loop stability by using the value function proposed in this work and ensure that it satisfies the Hamilton-Jacobi-Isaacs equation.

Bibliography

- [1] G. Grübel, "Uncertainty and control-some activities at DFVLR", Ackermann J. (eds) *Uncertainty and Control. Lecture Notes in Control and Information Sciences*, Vol. 70. pp. 1-47, Springer, Berlin, Heidelberg, 1985.
- [2] K. Zhou and J. C. Doyle, *Essentials of Robust Control*, Upper Saddle River, NJ, USA: Prentice-Hall, 1998.
- [3] K. Zhou, J. C. Doyle, and K. Glover, *Robust and Optimal Control*, Upper Saddle River, NJ, USA: Prentice-Hall, 1996.
- [4] D. C. McFarlane and K. Glover, *Robust Controller Design Using Normalized Coprime Factor Plant Descriptions*. New York, NY, USA: Springer-Verlag, 1990.
- [5] J. C. Doyle, K. Glover, P. P. Khargonekar and B. A. Francis, "State-space solutions to standard H_2 and H_∞ control problems," *IEEE Trans. Automat. Contr.*, Vol. 34, No. 8, pp. 831-847, Aug. 1989.
- [6] J. C. Doyle, "Analysis of feedback systems with structured uncertainty," *IEE Proc. D-Control Theory Appl.* Vol. 129, No. 6, pp. 242-250, Nov. 1982.
- [7] K. J. Åström and B. Wittenmark, *Adaptive Control*, Reading, MA, USA: Addison-Wesley, 1995.

- [8] M. Stefanovic and M. G. Safonov, "Safe adaptive switching control: Stability and convergence," *IEEE Trans. Automat. Contr.*, Vol. 53, No. 9, pp. 2012–2021, Oct. 2008.
- [9] H. P. Whitaker, J. Yamron, and A. Kezer, "Design of Model-Reference Adaptive Control Systems for Aircraft," MIT Instrumentation Laboratory, Cambridge, MA, USA, Report R-164, 1958.
- [10] R. L. Butchart and B. Shackcloth, "Synthesis of model reference adaptive control systems by Liapunov's second method," *Proc. IFAC Symp. on Adaptive Control*, Teddington, UK, 1965.
- [11] K. S. Narendra and A. M. Annaswamy, *Stable Adaptive Systems*, New York, USA: Dover, 2005.
- [12] D. J. Leith and W. E. Leithead. "Survey of Gain-Scheduling Analysis Design," *International Journal of Control*, Vol.73, pp. 1001-1025, 1999.
- [13] B.D.O. Anderson, *et al.* "Multiple Model Adaptive Control with Safe Switching," *International Journal of Adaptive Control and Signal Processing*, Vol.15, pp. 445-470, 2001.
- [14] M. Kuipers and P. Ioannou, "Multiple model adaptive control with mixing," *IEEE Trans. Automat. Contr.*, vol 55, No.8, pp. 1822-1836, Aug 2010.
- [15] A.A. Feldbaum, "Dual control theory, Part I", *Automation and Remote Control*, Vol. 21, No.9, pp. 874–880, Apr. 1961.
- [16] A.A. Feldbaum, "Dual control theory, Part II", *Automation and Remote Control*, Vol. 21, No.9, pp. 1033-1039, Nov. 1961.
- [17] E. Tse and Y. Bar-Shalom, "An actively adaptive control for linear systems with random parameters via the dual control approach," *IEEE Trans. Automat. Contr.*, Vol. 18, No. 2, pp. 109-117, Apr. 1973.
- [18] B. Xu, D. Gao, and S. Wang "Adaptive Neural Control based on HGO for Hypersonic Flight Vehicles." *Science China Information Sciences*, Vol. 54, pp. 511–520, 2011.

- [19] B. Xu, D. Wang, F. Sun, and Z. Shi, "Direct Neural Discrete Control of Hypersonic Flight Vehicle." *Nonlinear Dynamics*, Vol. 70, pp. 269–278, 2012.
- [20] G. Tadmor, " H_∞ in the time domain: The standard four blocks problem," Brown Univ., Providence, RI, Rep. LCDS/CCS 88-21, 1988.
- [21] Staff of the Flight Research Center, "Experience With The X-15 Adaptive Flight Control System", NASA TM X-6208, NASA, Washington D.C, March 1971.
- [22] S. G. Anavatti, F. Santoso and M. A. Garratt, "Progress in adaptive control systems: past, present, and future", *2015 International Conference on Advanced Mechatronics, Intelligent Manufacture, and Industrial Automation (ICAMIMIA)*, Surabaya, Indonesia, pp. 1-8, 2015.
- [23] K.J. Åström, U. Borisson, L. Ljung, and B. Wittenmark, "Theory and applications of self-tuning regulators," *Automatica*, Vol. 13, No. 5, pp. 457-476, 1977.
- [24] B. T. Polyak, P. S. Shcherbakov and M. V. Topunov, "Invariant Ellipsoids Approach to Robust Rejection of Persistent Disturbances," *IFAC Proceedings Volumes*, Vol. 41, No. 2, pp. 3976-3981, 2008.
- [25] D. Seo and M. R. Akella, "Non-certainty equivalent adaptive control for robot manipulator systems," *Systems and Control Letters*, Vol. 58, Issue 4, pp. 304-308, 2009.
- [26] J. Yoneyama, J. L. Speyer and C. H. Dillon, "Robust adaptive control problem for linear systems with unknown parameters," *Automatica*, Vol. 33, No. 10, pp. 1909-1916, 1997.
- [27] B. Sayyarodsari, J.P. How and A. Carrier, "Robust Adaptive Control of Linear Systems with Constant Uncertain Parameters," *Proceedings of the 1997 American Control Conference*, Albuquerque, NM, USA, Vol. 4. pp. 2376-2378, 1997.
- [28] D. J. N. Limebeer, B. D. O. Anderson, P. P. Khargonekar, and M. Green, "A game theoretic approach to H_∞ control for time varying systems," *SIAM J. Control and Optimiz.*, Vol. 30, No. 2, pp. 262-283, 1992.

- [29] I. Rhee and J. L. Speyer, "A Game Theoretic Approach to a Finite-Time Disturbance Attenuation Problem," *IEEE Transactions on Automatic Control*, Vol. 36, No. 9, pp.1021 -1032, 1991.
- [30] P. P. Khargonekar, K. M. Nagpal, and K. Poolla, " H_∞ control with transients," *SIAM J. Control and Optimiz.*, Vol. 29, No. 6, pp. 1373-1393, Nov. 1991.
- [31] K. Uchida and M. Fujita, "Finite horizon H_∞ control problem with terminal penalties," *IEEE Trans. Automat. Contr.*, Vol. 37, No. 11, pp. 1762-1767, Nov. 1992.
- [32] T. Başar and P. Bernhard, *H_∞ Optimal Control and Related Minimax Design Problems.*, Boston, MA, USA: Birkhauser, 1991.
- [33] G. Didinsky and T. Başar, "Design of minimax controllers for linear systems with nonzero initial conditions and under specified information structures," *29th IEEE Conference on Decision and Control*, Vol. 4, pp. 2413-2418, 1990.
- [34] G. Didinsky, T. Başar and P. Bernhard, "Structural properties of minimax controllers for a class of differential games arising in nonlinear H_∞ control," *Systems and Control Letters*, Vol. 21, No. 6, pp. 433-441, 1993.
- [35] G. E. Fruchter, J. L. Speyer, and S. Hong, "Game Theoretic Analysis of a Linear Compensator In the Presence Of Disturbances And Parameter Uncertainties". *Proceedings of the 31st IEEE Conference on Decision and Control*, Tucson, Arizona. Vol. 1 pp.949-954, Dec. 1992.
- [36] J.L. Speyer, G. Fruchter, and Y.-S. Hahn, "A Game Theoretic Approach to Dual Control", *Proceedings of the Seventh Yale Workshop on Adaptive and Learning Systems*, pp. 20-22, May, 1992.
- [37] G. Didinsky and T. Başar, "Minimax Adaptive Control of Uncertain Plants," *33rd IEEE Conference on Decision and Control*, Lake Buena Vista, FL, USA, 1994, pp. 2839-2846.

- [38] G. Didinsky, Z. Pan, and T. Başar. "Parameter identification for uncertain plants using H_∞ methods." *Automatica*, Vol. 31, No. 9, pp. 1227-1250, 1995.
- [39] D. F. Chichka and J. L. Speyer "An Adaptive controller based on disturbance attenuation," *IEEE Trans. Automat. Contr.*, Vol. 40, No. 7, pp. 1220 -1233, 1995.
- [40] J. Yoneyama, J. L. Speyer, and C. H. Dillon, "Robust adaptive control for linear systems with unknown parameters," *Automatica*, Vol. 33, No. 10, pp. 1909-1916, 1997.
- [41] C. H. Dillon and J. L. Speyer, "Design of robust adaptive longitudinal flight control", *Journal of Guidance, Control, and Dynamics*, Vol. 23, No. 2, pp. 325-331, Mar.-Apr. 2000.
- [42] L. Xie, and C. E. de Souza. "Robust H_∞ control for linear time-invariant systems with norm-bounded uncertainty in the input matrix." *Systems and Control Letters*, Vol. 14, No. 5, pp. 389-396, 1990.
- [43] W. Huang and J. L. Speyer, "Adaptive Control Based on Disturbance Attenuation and the Modified Gain Observer for Parameter Uncertain Linear Systems.", *Proceedings of the 2021 American Control Conference*, New Orleans, LA, USA, 2021.
- [44] W. Huang and J. L. Speyer, "Disturbance attenuation controller for parameter uncertain linear systems adaptive through a modified gain observer", *IEEE Transaction on Automatic Control*, submitted.
- [45] A. Ataei-Esfahani and Q. Wang, "Nonlinear Control Design of a Hypersonic Aircraft Using Sum-of-Squares Method," *2007 American Control Conference*, New York, NY, USA, pp. 5278-5283, 2007.
- [46] W. Huang and J. L. Speyer, "Hypersonic Cruise using a Disturbance Attenuation Controller Adaptive through a Nonlinear Modified Gain Observer", *AIAA Journal of Guidance, Control and Dynamics*, to be submitted.

- [47] T. L. Song and J. L. Speyer, "The modified gain extended Kalman filter and parameter identification in linear systems," *Automatica*, Vol. 22, No. 1, pp. 59-75, 1986.
- [48] T. L. Song and J. L. Speyer, "A stochastic analysis of a modified gain extended Kalman filter with applications to estimation with bearings only measurements," *IEEE Trans. Automat. Contr.*, Vol. 30, No. 10, pp. 940-949, Oct. 1985.
- [49] T. L. Song, "A continuous-time modified gain extended kalman filter," *Korea Institute of Control, Robotics and Systems*, Vol. 1, pp. 269-274, Oct. 1986.
- [50] J. L. Speyer and D. H. Jacobson, *Primer on Optimal Control Theory*, Philadelphia, PA, USA: SIAM, 2010.
- [51] J. L. Speyer and W. H. Chung, *Stochastic Processes, Estimation, and Control*, Philadelphia, PA, USA: SIAM, 2008.
- [52] C. Scherer, *Theory of Robust Control*, The Netherlands, Delft:Mechanical Engineering Systems and Control Group, Delft University of Technology, 2001.
- [53] W. M. Wonham, "On a matrix Riccati equation of stochastic control," *SIAM J. Contr. Optim.*, Vol. 6, No. 4, pp. 681-697, 1968.
- [54] W. Hahn, *Stabiity of Motion*, Berlin-Heidelberg, Germany: Springer-Verlag, 1967.
- [55] W. M. Wonham, "On pole assignment in multi-input controllable linear systems," *IEEE Trans. Automat. Contr.*, Vol. 12, No. 6, pp. 660-665, 1967.
- [56] T. A. Talay, *NASA History Division: Introduction to the Aerodynamics of Flight*, NASA, Langley Research Center, Washington, D.C, 1975.
- [57] J. D. Watts, "Flight Experience with Shock Inpingment and Interference Heating On the X-15-2 Research Airplane", NASA TM X-1669, NASA, Washington D.C, Oct. 1968.

- [58] I. Leyva, "The Relentless Pursuit of Hypersonic Flight", *Physics Today*, Vol. 70, No.11, pp 30-37, Nov 1, 2017.
- [59] Darpa: Falcon HTV-2 (April 15, 2012). Retrieved from http://www.darpa.mil/Our_Work/TTO/Programs/Falcon_HTV-2/Falcon_HTV-2.aspx
- [60] K. P. Groves, D. O. Sigthorsson, A. Serrani, S. Yurkovich, M. A. Bolender, and D. B. Doman, "Reference Command Tracking for a Linearized Model of an Air-Breathing Hypersonic Vehicle." *Proceedings of AIAA Guidance, Navigation, and Control Conference and Exhibit*, San Francisco, CA, USA, 2005.
- [61] C. Mu, C. Sun, W. Xu, "Fast sliding mode control on airbreathing hypersonic vehicles with transient response analysis." *Proceedings of the Institution of Mechanical Engineers, Part I, Journal of Systems and Control Engineering*, Vol. 230, No. 1, pp. 23–34, 2016.
- [62] D. O. Sigthorsson, *et. al.*, "Robust Linear Output Feedback Control of an Airbreathing Hypersonic Vehicle." *Journal of Guidance, Control, and Dynamics*, Vol. 31, No. 4, pp. 1052-1066, 2008.
- [63] Z. T. Dydek, A. Annaswamy, and E. Lavretsky. "Adaptive Control and the NASA X-15-3 Flight Revisited." *IEEE Control Systems Magazine*, Vol. 30, No. 3, 2010.
- [64] T. E. Gibson, L. G. Crespo, and A. M. Annaswamy, "Adaptive Control of Hypersonic Vehicles in the Presence of Modeling Uncertainties." *Proceedings of the 2009 American Control Conference*, St. Louis, Missouri, MO, USA, pp. 3178–3183, 2009.
- [65] G. Gao and J. Wang, "Observer-based fault-tolerant control for an air-breathing hypersonic vehicle model." *Nonlinear Dynamics*, Vol. 76, pp.409–430, 2014.
- [66] H. An, *et. al.*. "Low-complexity hypersonic flight control with asymmetric angle of attack constraint." *Nonlinear Dynamics*, 100, pp. 435–449, 2020.

- [67] J. T. Parker, A. Serrani, S. Yurkovich, M. A. Bolender, D. B. Doman, "Control-oriented modeling of an airbreathing hypersonic vehicle." *Journal of Guidance, Control and Dynamics*, Vol. 30, No. 3, pp. 856–869, 2007.
- [68] A. Ataei-Esfahani and Q. Wang, "Nonlinear Control of an Uncertain Hypersonic Aircraft Model Using Robust Sum-of-Squares Method." *IET Control Theory and Application*, Vol. 6, No. 2, pp.203–215, 2012
- [69] B. Xu and Z. Shi, "An overview on flight dynamics and control approaches for hypersonic vehicles." *Science China Information Science*, Vol. 58, pp. 1-19, 2015.
- [70] H. Xu, M. D. Mirmirani, and P. A. Ioannou, "Adaptive Sliding Mode Control Design for a Hypersonic Flight Vehicle," *Journal of Guidance, Control and Dynamics*, Vol. 27, No. 5, pp.829-838, Sep, 2004.
- [71] J. Sun, *et. al.*, "Robust chattering-free control for flexible air-breathing hypersonic vehicles in the presence of disturbances and measurement noises," *2018 Annual American Control Conference, Milwaukee, WI, USA*, pp. 2264-2269, 2018.
- [72] Q. Wang and R. F. Stengel, "Robust Nonlinear Control of a Hypersonic Aircraft," *Journal of Guidance, Control and Dynamics*, Vol. 23, No. 4, pp. 577–585, 2000.
- [73] J. D. S. et al., "Hypersonic vehicle simulation model: Winged-cone configuration," NASA Langley Research Center, Tech. Rep. NASA TM102610, November 1990.
- [74] C. I. Marrison and R. F. Stengel, "Design of robust control systems for a hypersonic aircraft," *Journal of Guidance, Control and Dynamics*, Vol. 21, No. 1, pp. 58–63, 1998.